Distribution Agreement

In presenting this thesis or dissertation as a partial fulfillment of the requirements for an advanced degree from Emory University, I hereby grant to Emory University and its agents the non-exclusive license to archive, make accessible, and display my thesis or dissertation in whole or in part in all forms of media, now or hereafter known, including display on the world wide web. I understand that I may select some access restrictions as part of the online submission of this thesis or dissertation. I retain all ownership rights to the copyright of the thesis or dissertation. I also retain the right to use in future works (such as articles or books) all or part of this thesis or dissertation.

Signature:

_____ _____

Brian M. Hays Date

Rotational Spectroscopy of O(^{1}D) Insertion Products

By

Brian M. Hays

Doctor of Philosophy

Chemistry

Susanna L. Widicus Weaver, Ph.D.

Advisor

Michael C. Heaven, Ph.D.

Committee Member

Tim Lian, Ph.D.

Committee Member

Accepted:

Lisa A. Tedesco, Ph.D.

Dean of the James T. Laney School of Graduate Studies

Date

Rotational Spectroscopy of O(^{1}D) Insertion Products

By

Brian M. Hays

B.S., Loyola University New Orleans, 2010

Advisor: Susanna L. Widicus Weaver, Ph.D.

An abstract of A dissertation submitted to the Faculty of the James T. Laney School of Graduate Studies of Emory University in partial fulfillment of the requirements for the degree of

Doctor of Philosophy

in Chemistry

2015

Abstract

Rotational Spectroscopy of O(^{1}D) Insertion Products
by Brian M. Hays

Aminomethanol ($HOCH_2NH_2$) is an important astrochemical molecule due to its proposed role in the formation of glycine, the simplest amino acid, in space. Astrochemical models have predicted aminomethanol formation in star-forming regions, but its detection in space has been precluded by its lack of a laboratory spectrum to guide astronomical searches. This molecule poses a challenge for laboratory spectroscopy because it is terrestrially unstable. The selective O(^{1}D) insertion reaction into a C-H bond of methylamine has been proposed to create the molecule. Calculations were carried out to predict the energetics of this formation pathway, to investigate other possible products, and to predict the pure rotational spectrum of aminomethanol. To search for aminomethanol's laboratory spectrum, a new spectrometer was developed to produce molecules in the gas phase using O(^{1}D) insertion reactions and then probe them using (sub)millimeter spectroscopy. The new experiment combined (sub)millimeter spectroscopy and a laser photolysis mixing supersonic expansion source. This experiment was first tested on the methanol and vinyl alcohol systems, produced from O(^{1}D) insertion into methane and ethylene, respectively. Also, new fast sweeping techniques were developed to greatly increase the spectral acquisition speed of direct absorption (sub)millimeter wave spectroscopy. The fast sweeping techniques were also used to create a new (sub)millimeter – microwave double resonance spectroscopy technique. All of these techniques were then combined to aid in the search for aminomethanol. The results of these experiments as well as the current results from searches for aminomethanol are presented here.

Rotational Spectroscopy of O(^{1}D) Insertion Products

By

Brian M. Hays

B.S., Loyola University New Orleans, 2010

Advisor: Susanna L. Widicus Weaver, Ph.D.

A dissertation submitted to the Faculty of the James T. Laney School of Graduate Studies of Emory University in partial fulfillment of the requirements for the degree of

Doctor of Philosophy

in Chemistry

2015

Acknowledgements

I would like to thank my advisor, Dr. Susanna Widicus Weaver, for always believing in me and for making this work possible. I greatly appreciate all of the opportunities she has given me. I thank my committee, Dr. Michael Heaven and Dr. Tim Lian, for their support, advice, and discussion through my time at Emory. I also thank Dr. Heaven for his material support for generously lending his equipment for use in my studies. Without this equipment, none of this work would have been possible. I also thank Dr. Steve Shipman, for his advice and collaboration, which brought about some great results. I thank Dr. Joelle Underwood for allowing allowing me to begin chemistry research and Dr. Thom Spence for giving me an opportunity to begin building instruments. I also thank Dr. Lynn Koplitz for getting me back into chemistry and Dr. Kurt Birdwhistell, may he rest in peace, for keeping me interested in chemistry.

My lab mates have been a source of support and friendship during my time at Emory. I thank all of them for their help and camaraderie through the years. Luyao Zou deserves special thanks for developing the new fast sweeping spectroscopy for pulsed sources with me, it was fun! I also thank my colleagues around the chemistry department for their helpful discussion. The time that I worked with Kyle Mascaritolo in the Heaven lab was particularly enlightening for future experiments. Particularly, I would like to thank Dr. Adrian Gardner and Dr. John Mancini for their helpful scientific discussions, and nonscientific discussions.

I would like to thank all of my friends for their support for all of these years (now over 20 years for some of them!) and for being great with me during my time working here. They all are the best friends anyone could ask for.

I would like to thank my family most of all, Lewis, Karen, Stefanie, and Mark. I thank them all for helping me through this and being there for me. I would not have been able to get to this point without their love.

Contents

Listing of Figures

List of Tables

1

Introduction

1.1 Background

Complex organics molecules (COMs) have been found throughout the interstellar medium and are often used as tracers of star formation. For astrochemistry, COMs are often described as molecules with 6 or more atoms that contain carbon, but can also contain hydrogen, oxygen, and nitrogen[1]. These COMs are predicted to form primarily on interstellar grain surfaces through photolysis driven radical-radical recombination reactions[2]. The chemistry of COMs is influenced primarily by methanol photolysis, where the radical products can then roam on the surface and recombine with other radicals to form organic molecules. This type of chemistry has been used to

explain the formation methyl formate, dimethyl ether, and glycolaldehyde in the interstellar medium[2]. A way to test this type of proposed chemistry would be to search for other molecules predicted by these types of reactions and compare the abundances to the predictions from the chemical models. Three such molecules are methanediol ($CH_2(OH)_2$), methoxymethanol (CH_3OCH_2OH), and aminomethanol ($HOCH_2NH_2$); their detection would validate these chemical models as predictive tools and also provide astrochemical information for important prebiotic processes. While these are excellent target molecules for astronomical searches, their detection in space is precluded by their lack of laboratory spectra.

The primary method of detecting COMs in space is through pure rotational spectroscopy, particularly in the (sub)millimeter spectral region[1]. Given the typical size of COMs and the temperatures of star forming regions, the peak line intensities for COMs are often in this region of the electromagnetic spectrum. This spectral region is also where COMs can be detected in emission from most interstellar sources. With several new telescopes (i.e., the Herschel Space Observatory, the Stratospheric Observatory for Infrared Astronomy, the Atacama Large Millimeter Array) operating with spectral coverage in the (sub)millimeter spectral region, laboratory spectroscopy needs to catch up with the demand of these observatories to enable the detection of new molecules.

The goal of the studies presented herein is to provide the spectroscopic tools to produce and characterize these types of molecules in the laboratory. This involved using a chemically-selective mechanism to produce aminomethanol, methanediol, and methoxymethanol. $O(^1D)$ insertion reactions into simple hydrocarbons were used to produce new molecules in sufficient quantity to probe them using pure rotational spectroscopy. The spectroscopic tools used in the (sub)millimeter were also updated to increase spectral acquisition speed.

1.1.1 Structure of the Dissertation

The work herein is divided into seven chapters. Chapter 2 focuses on the theoretical calculations performed for methanediol, methoxymethanol, and aminomethanol to investigate their formation using O(^{1}D) insertion reactions and their structures for rotational spectroscopy. Chapter 3 discusses the experimental setup for the O(^{1}D) insertion spectroscopic studies, with applications to a proof-of-concept experiment involving methanol formation from O(^{1}D) insertion into methane. Chapter 4 focuses on the formation of vinyl alcohol from O(^{1}D) insertion into ethylene, the updates made to the spectrometer, and the spectroscopy of vinyl alcohol. Chapters 5 and 6 discuss new (sub)millimeter fast sweeping techniques using absorption and double resonance spectroscopy. Chapter 7 combines the results from all of these studies so that they can be applied to study the insertion of O(^{1}D) into methylamine to form aminomethanol.

2

Theoretical Calculations of O(^{1}D) Insertion

2.1 Introduction

Models of astrochemistry in star-forming regions predict the formation of many complex organic molecules (COMs)[2]. These models predict that the molecules methanediol, methoxymethanol, and aminomethanol can be made in comparable abundances to other molecules detected in space through photo-driven surface reaction chemistry[2]. Also, these molecules are predicted interstellar precursors to biogenic molecules, such as sugars and amino acids[3]. Despite their astronomical and astrobiological importance, the observation of these molecules in space is precluded by their lack of laboratory rotational spectra. These molecules are metastable under laboratory con-

ditions so they need to be produced *in situ*, preferably in a manner which is highly selective for their formation. O(^{1}D) insertion reactions have been proposed as one possible mechanism to produce these molecules because O(^{1}D) insertion into the C-H bond of commercially available hydrocarbons is highly exothermic and facile.

The reaction of O(^{1}D) with small hydrocarbons has been studied extensively, both experimentally[4,5,6,7,8,9,10,11,12,13,14,15,16,17,18,19,20,21,22,23,24,25,26,27,28,29,30,31,32,33,34,35,36,37,38,39,40] and theoretically[42,43,44,45,46,47,48]. The insertion mechanism of O(^{1}D) into C-H bonds is predominantly favored. The insertion reaction is typically characterized by the large exothermicity of the reaction, releasing >100 kcal/mol of energy into the molecule. If this energy is not quenched, intramolecular vibrational energy redistribution (IVR) can lead to unimolecular dissociation of the products[5]. The specificity of the reaction into C-H bonds is well studied, but O(^{1}D) can also insert into H-H bonds[49], N-H bonds[50], and O-H bonds[5] in closed-shell molecules.

Methanediol forms readily in aqueous solutions of formaldehyde under terrestrial chemical conditions. The vapor above such mixtures can contain as much as 3% methanediol[51]; however, a gas-phase spectrum has not been reported. Methanediol is predicted to form in interstellar environments through the reaction between OH and CH_2OH radicals that form from water and methanol photolysis[2]. Previous theoretical studies show that methanediol is stable under typical interstellar cloud conditions[52], and is therefore likely to be present in high abundance in interstellar clouds if its predicted formation route is correct.

Similarly to methanediol, methoxymethanol forms terrestrially in aqueous solutions of formaldehyde where methanol has been added as a stabilizer[51]. In the interstellar medium, methoxymethanol is predicted to form from reactions between CH_2OH and CH_3O in ices[2]. These radicals both form from methanol photolysis within the ice. The detection of methoxymethanol would therefore place quantitative limits on the methanol photodissociation branching ratios under these conditions[53].

Aminomethanol forms in terrestrial chemistry in the first step of the reaction between ammonia and formaldehyde, but is highly reactive and goes on to form hexamethylenetetramine[54]. Hexamethylenetetramine is a major product of industrial chemistry with a large variety of uses ranging from its role in rubber and plastic production to use as an antibiotic[51]. Theoretical studies show aminomethanol to be stable in the gas phase under typical laboratory and interstellar conditions if subsequent reactions can be quenched[55]. Aminomethanol is predicted to form from radical-radical reactions between NH_2 and CH_2OH in interstellar ices[2]. These radicals form from the photolysis of ammonia and methanol, respectively. Aminomethanol has been predicted to be the interstellar precursor to glycine, which is thought to form from the gas-phase reaction between protonated aminomethanol and formic acid[3]. Aminomethanol is therefore a key prebiotic interstellar molecule.

Previous laboratory studies of methanediol, methoxymethanol, and aminomethanol are limited because of the reactivity of these molecules. Methanediol[6] and methoxymethanol[4] were studied in matrix isolation experiments using infrared spectroscopy to monitor the products of O(^{1}D) reactions with methanol and dimethyl ether, respectively. Methanediol was also formed in a gas-phase experiment investigating the reaction between O(^{1}D) and isotopically enriched methanol[5]. Aminomethanol was shown to form during thermal processing of interstellar ice analogues containing water, formaldehyde, and ammonia[56].

The proposed experiments would involve inserting O(^{1}D) into methanol, dimethyl ether, and methyl amine and quenching the excess energy to stabilize the insertion products. The products would then be observed using pure rotational spectroscopy. The energetics and other product channels of these reactions need to be investigated to determine their experimental viability as well as the other predicted products. Also, the spectroscopy would benefit greatly from accurate theoretical predictions of the structures for more precise moments of inertia. Therefore, the zero point en-

ergy correction would provide a much more accurate structure than the normally calculated equilibrium structure[57]. To meet these goals, minimization calculations were conducted to assess the product distribution from the insertion reactions. The minimum energy structures of the predicted C-H insertion products were then determined. Potential energy surfaces for the motions of each functional group were also determined to account for internal motion complicating the pure rotational spectra. Further calculations on the zero point vibrational correction were performed on aminomethanol in order to more accurately predict the pure rotational spectrum of this molecule. The bulk of the information contained in this chapter comes from Hays and Widicus Weaver, "Theoretical Examination of O(^{1}D) Insertion Reactions to Form Methanediol, Methoxymethanol, and Aminomethanol." *J. Phys. Chem. A.*, **2013**, *117*, 7142-7148[58].

2.2 Theoretical Methods

All calculations were performed using the Gaussian 09 Quantum Chemistry Package[59] and CFOUR[60] at the Cherry L. Emerson Center for Scientific Computation at Emory University. Each molecule geometry was optimized at the MP2 level of theory[61,62] using the aug-cc-pVTZ basis set[63]. Although reactions with O(^{3}P) can occur in the proposed experiments, it has been shown that abstraction is the dominant pathway for these reactions,[64] and triplet insertion products are highly unlikely. Therefore, only the insertion products in the singlet state were examined in this study. Initial guesses were made as to the minimum energy structure for each molecule. The dihedral angles related to the heavy atoms on each molecule were rotated in steps of 20 degrees to provide a series of first estimates for possible conformer structures. Each of these structures was then optimized to find a local energy minimum. The global minimum energy structure was then determined through comparison of the energies found for each conformer.

Once the global minimum energy structure was found for each molecule, the energetics of the insertion reaction leading to that product were examined. Calculations were performed along the minimum energy pathway for each insertion reaction, beginning with the starting material (i.e., O(^{1}D) + precursor) and ending with the global minimum energy insertion product structure. Some reactions were found to pass through an O(^{1}D) association product intermediate along the pathway to the insertion products. The geometries for stationary points found on the potential energy surface were optimized using the MP2/ aug-cc-pVTZ level of theory, and single point energies were calculated at the CCSD(T)/aug-cc-pVTZ level of theory[65,66,63]. The harmonic vibrational frequencies for the optimized structures along the singlet insertion path were found using the MP2/aug-cc-pVTZ level of theory and used to verify transition states.

In addition to exploring the reaction energetics, the resultant molecular parameters for the minimum energy geometry were used to predict spectra at 30 K with Pickett's CALPGM suite of programs[67] using a standard asymmetric top Hamiltonian in the Watson-A reduction. The rotational constants and electric dipole moment components used for the spectral predictions were taken from the MP2/aug-cc-pVTZ calculations. The dipole moments components were transformed to the principal axis system before they were included as input parameters for the spectral simulations.

The torsional barriers were estimated at the MP2/aug-cc-pVTZ level of theory using single point calculations, where the functional groups on each molecule were incrementally rotated about their dihedral angles and energies were determined for the geometry at each position. The torsional barriers were estimated as the difference between the maximum energy found in each of these calculations and the global energy minimum.

In addition, the zero point vibrational correction was found for the ground state of aminomethanol. The ground state structure was optimized for the equilibrium struc-

ture at the CCSD(T)/cc-pVTZ level of theory until the energy residuals were below 10^{-10} Hartree/Bohr. Vibrational second order perturbation (VPT2) were performed at the same level of theory using the CFOUR program package[57]. While VPT2 can be performed using Gaussian, CFOUR allowed for the separation of the calculations so they did not have to run sequentially in one job. This allowed for a coupled cluster level of theory to be used. These calculations took about 1.5 days per each of the points (in this case 36) to be run using 48 GB of ram and 24 parallel processors. The procedure is outlined elsewhere[68] and the scripts for use on the Emerson Center can be found in Appendix A.

2.3 Results

2.3.1 Insertion Product Energetics

The stationary points on the potential energy surface for the reactions of the parent molecules with O(^{1}D) are shown in Figures 2.1-2.3. The associated structural information are included in Appendix B. Each of the O(^{1}D) insertion reactions was found to be highly exothermic. The O(^{1}D) insertion reactions into C-H bonds follow a direct and barrierless insertion pathway, while the insertion reactions into N-H or O-H bonds proceed through an association channel before the final product is formed. The O(^{1}D) insertion reactions into the C-O and C-N bonds were also investigated, despite there being no previous experimental evidence for these insertion products.

In the reaction between O(^{1}D) and methanol, the formation of methanediol releases 155 kcal/mol of energy, while the formation of methyl hydroperoxide (CH_3OOH) releases 91.2 kcal/mol of energy. In the reaction between dimethyl ether and O(^{1}D), the formation of methoxymethanol releases 154 kcal/mol of energy, while the formation of dimethyl peroxide (CH_3OOCH_3) releases 94.0 kcal/mol of energy. In the reaction between O(^{1}D) and methyl amine, several products can form: aminomethanol forms from O(^{1}D) insertion into the C-H bond and releases 152 kcal/mol of energy;

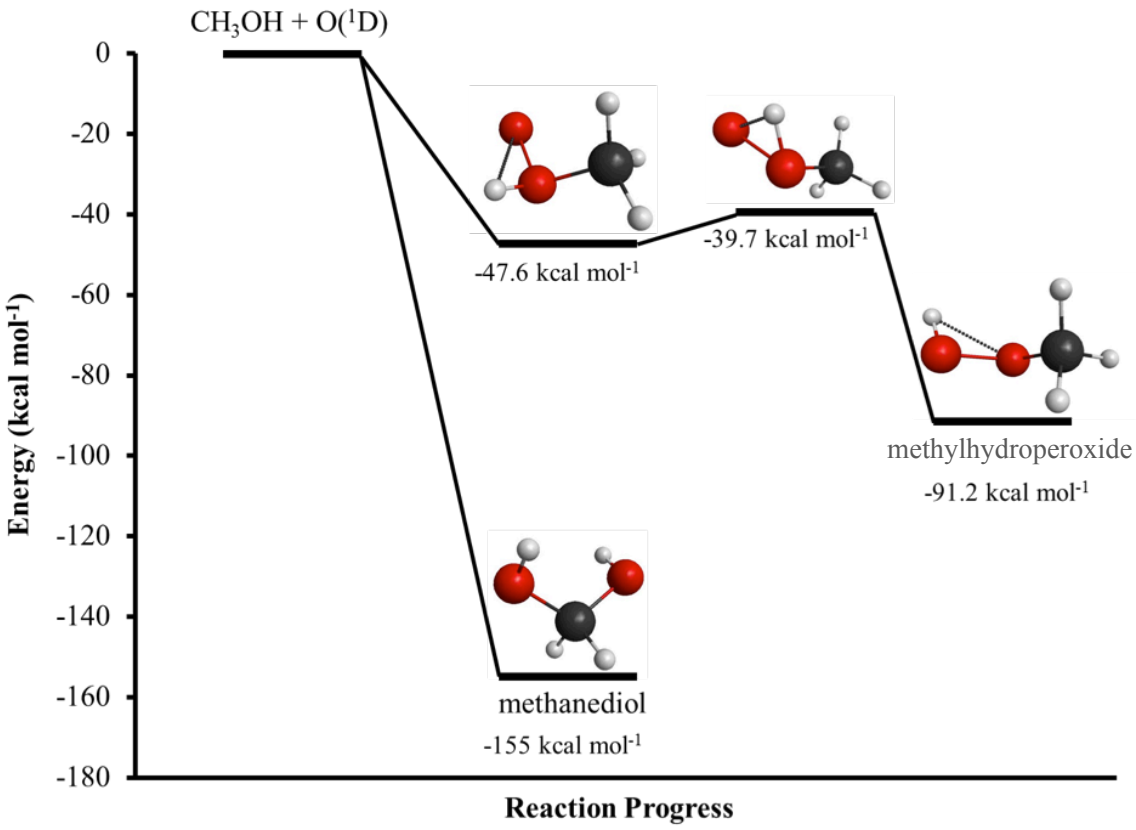

Figure 2.1: O(1D) Insertion into methanol to form methanediol and methylhydroperoxide.

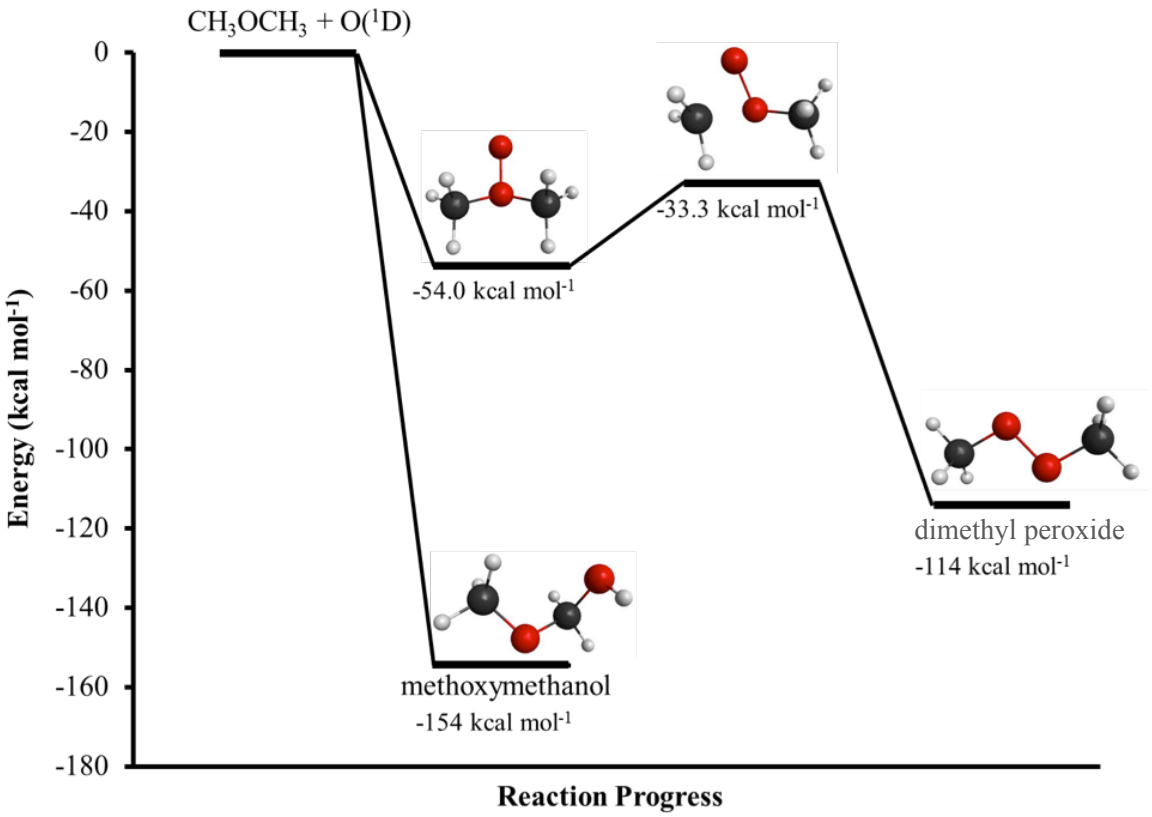

Figure 2.2: O(^{1}D) Insertion into dimethyl ether to form methoxymethanol and dimethyl peroxide.

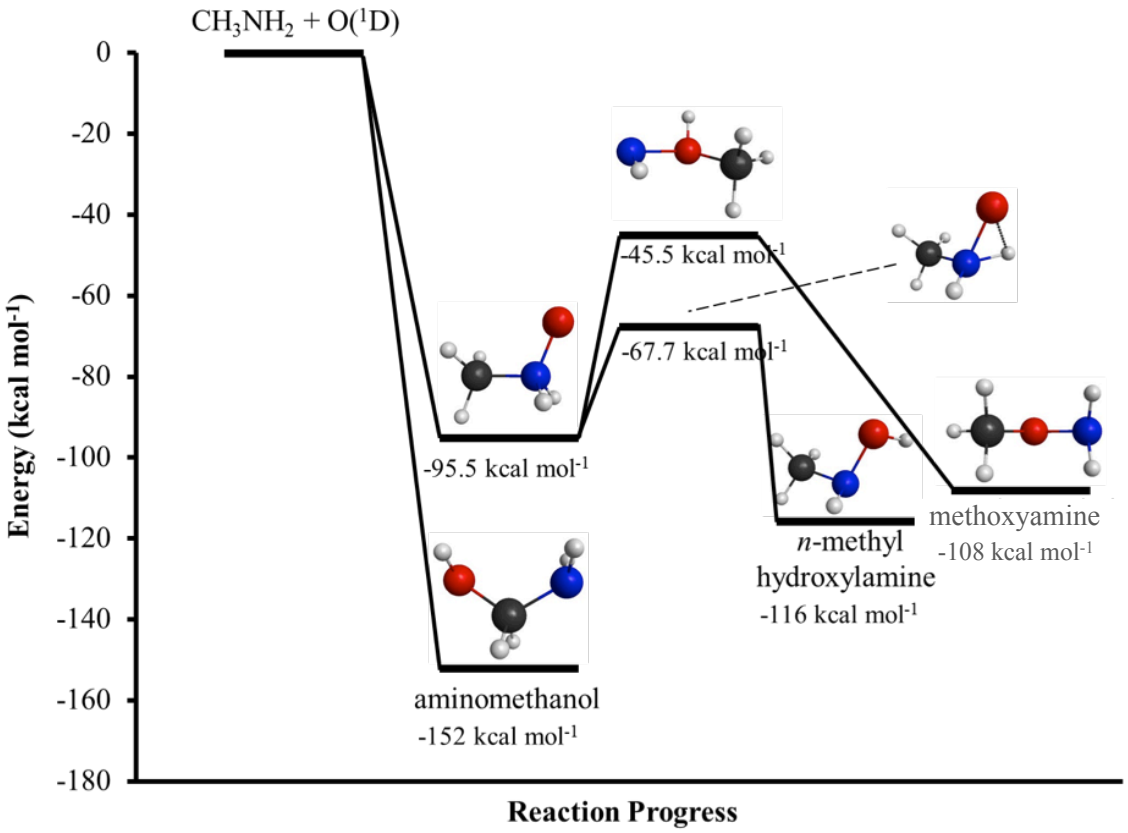

Figure 2.3: O(1D) Insertion into methyl amine to form aminomethanol, n-methylhydroxylamine and methoxyamine.

n-methylhydroxylamine (CH_3NHOH) forms from O(^{1}D) insertion into the N-H bond and releases 116 kcal/mol of energy; and methoxyamine (CH_3ONH_2) forms from O(^{1}D) insertion into the C-N bond and releases 108 kcal/mol of energy.

The geometries and associated energies determined in this work compare favorably to those reported by Huang et al.[5] for the O(^{1}D) + methanol reaction. Each of the energies determined for a stationary point in the current work are within 3 kcal/mol of the CCSD(T) results reported in the previous study. In the case of the O(^{1}D) + dimethyl ether reaction, the geometries determined in the current work agree well with those reported by Schalley et al.[69], but the energies differ by as much as 10 kcal/mol. However, this previous study used only DFT methods and a smaller basis set. The CCSD(T) energies reported in the current work should therefore be more reliable.

A difference of $\sim$ 20 kcal/mol was noticed between the single point energies determined from the MP2 and CCSD(T) calculations in the current work. Therefore, the multireference nature of these calculations was diagnosed through investigation of the T1 parameter[70] which was found to range from $\sim$0.005 to 0.02 for each of the stationary points in the CCSD(T) calculations. These systems are therefore predominantly single reference in character. The CCSD(T) calculations were therefore used for the energy comparisons shown in Figures 2.1 – 2.3.

2.3.2 Insertion Product Geometries

The optimized minimum energy geometries for the singlet states of methanediol, methoxymethanol, and aminomethanol are shown in Figure 2.4, and the corresponding structural information is given in Appendix B. The higher-energy conformers for each product are shown in Figure 2.5, and the corresponding structural information is also given in Appendix B. Each of the products is found to have multiple conformers that lie close in energy to the minimum energy geometry. Methanediol

has one conformer that is 2.64 kcal/mol higher in energy than the ground state. Methoxymethanol has two conformers that are 2.01 and 2.64 kcal/mol higher in energy than the ground state. Aminomethanol has three conformers that are 0.30, 0.73, and 4.33 kcal/mol higher in energy than the ground state. The ground state of n-methylhydroxylamine is 36.3 kcal/mol above the ground state of aminomethanol, and the next highest energy conformer of n-methylhydroxylamine is 39.8 kcal/mol above the ground state of aminomethanol. The reaction of O(^{1}D) with methanol could also yield methyl hydroperoxide, while the reaction of O(^{1}D) with dimethyl ether could also yield dimethyl peroxide. Neither of these products was explored in detail in the current work because their structures have already been determined through experiment[71,72,73] and theory[74].

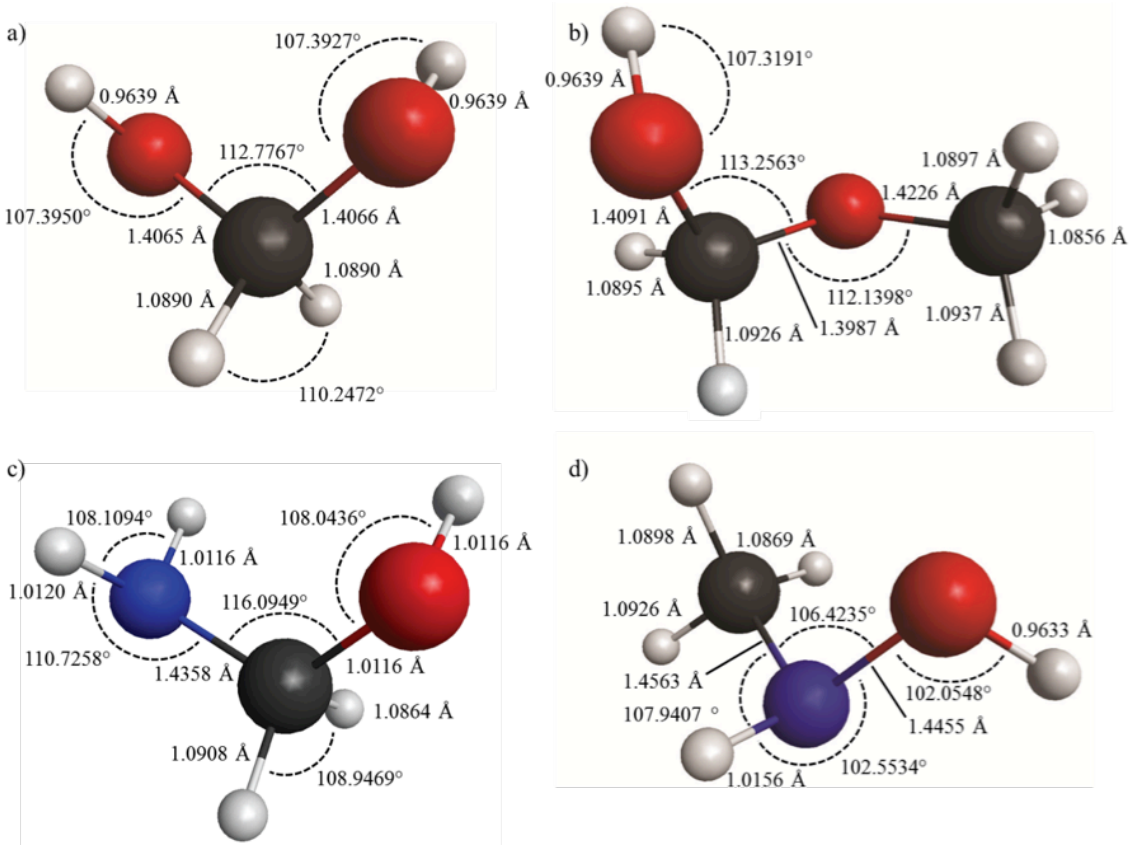

Figure 2.4: Ground state geometries of a) methanediol, b) methoxymethanol, c) aminomethanol, and d) n-methylhydroxylamine.

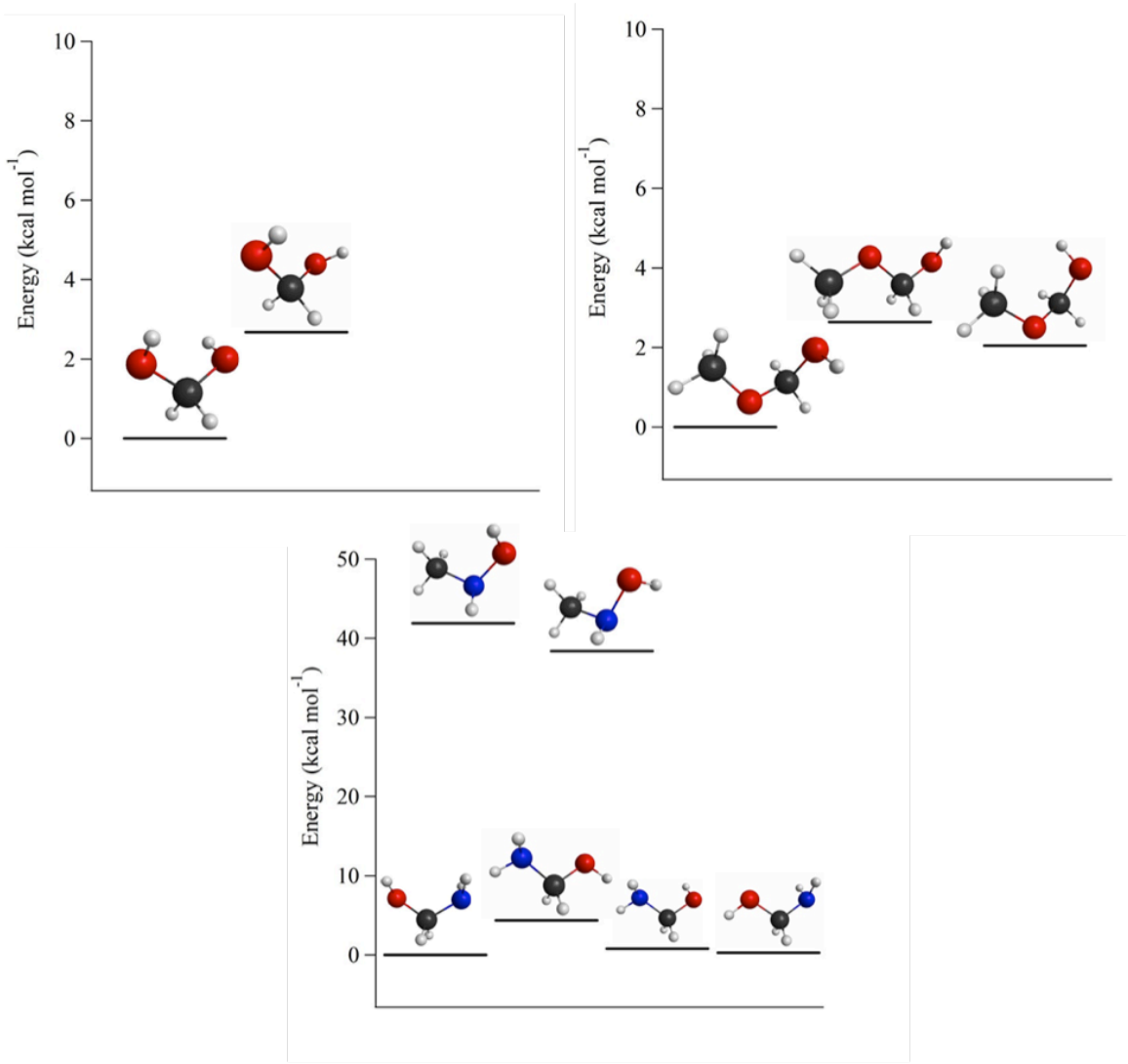

Figure 2.5: Conformers of methanediol, methoxymethanol, aminomethanol, and n-methylhydroxylamine.

Table 2.1: Spectral parameters determined from the *ab initio* calculations

Constant	methanediol	methoxymethanol	aminomethanol	n-methylhydroxylamine
A (GHz)	41.9128	17.1568	38.6930	39.1319
B (GHz)	10.1912	5.6238	9.5457	10.0320
C (GHz)	9.0330	4.8516	8.5868	8.7775
μ_A (D)	0.0089	0.2505	-0.3773	0.6631
μ_B (D)	0.0479	0.0890	-0.9132	-0.4439
μ_C (D)	0.0051	-0.1530	-1.3979	-0.0381

2.3.3 Prediction of Pure Rotational Spectra

The molecular parameters determined from the minimum energy geometries are given in Table 2.1. Only the rotational constants and components of the electric dipole moment are included, as the centrifugal distortion constants are presumed to be negligible compared to the uncertainties associated with the rotational constants. The information in Table 2.1 was used to predict the rotational spectrum for each molecule at a temperature of 30 K, which is appropriate for the conditions of the supersonic expansion that will be used for the experimental studies. The resultant spectral predictions generated using Pickett's CALPGM suite of programs[67] and assuming a standard asymmetric top Hamiltonian in the Watson-A reduction are shown in Figures 2.6-2.9.

An important consideration in the spectral study of small organic molecules is the potential for internal motion in the molecule, which can significantly complicate the spectrum. Therefore, the torsional barriers to internal motion of the functional groups for each product molecule were estimated by incrementally rotating the dihedral bond angles and performing single-point calculations at each step. The torsional potential energy surfaces determined from these calculations are presented in Appendix B. From these calculations, the hydroxyl wagging in methanediol was found to have a barrier of $\sim$1689 cm^{-1}. This is a reasonably high barrier, and spectral split-

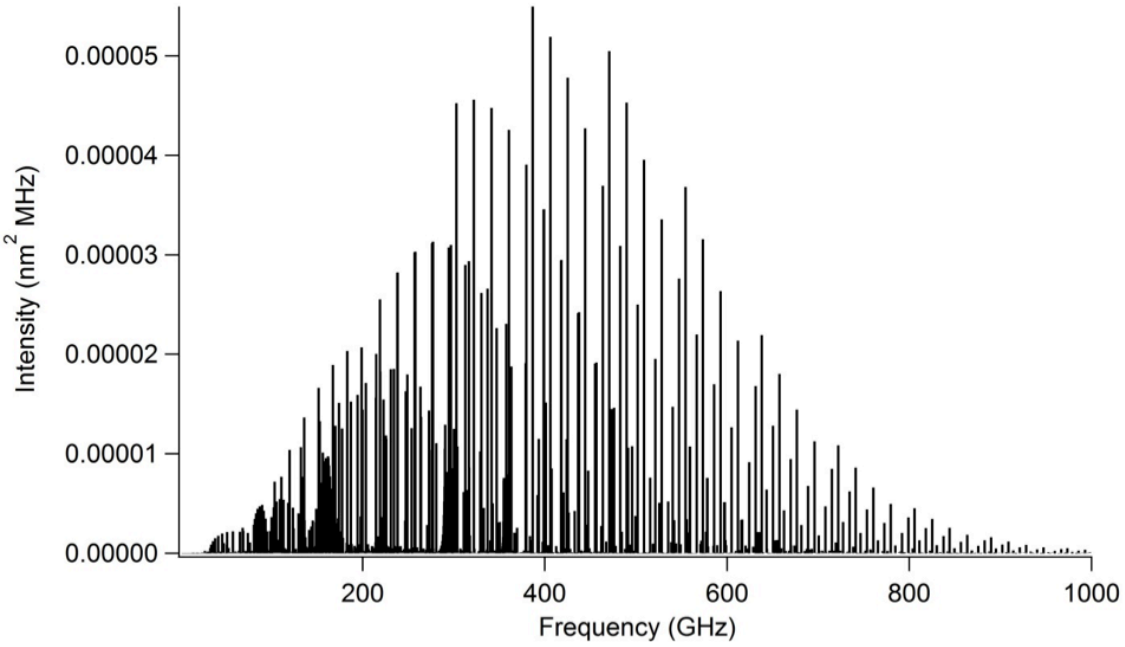

Figure 2.6: Prediction of the pure rotational spectrum of methanediol at 30 K.

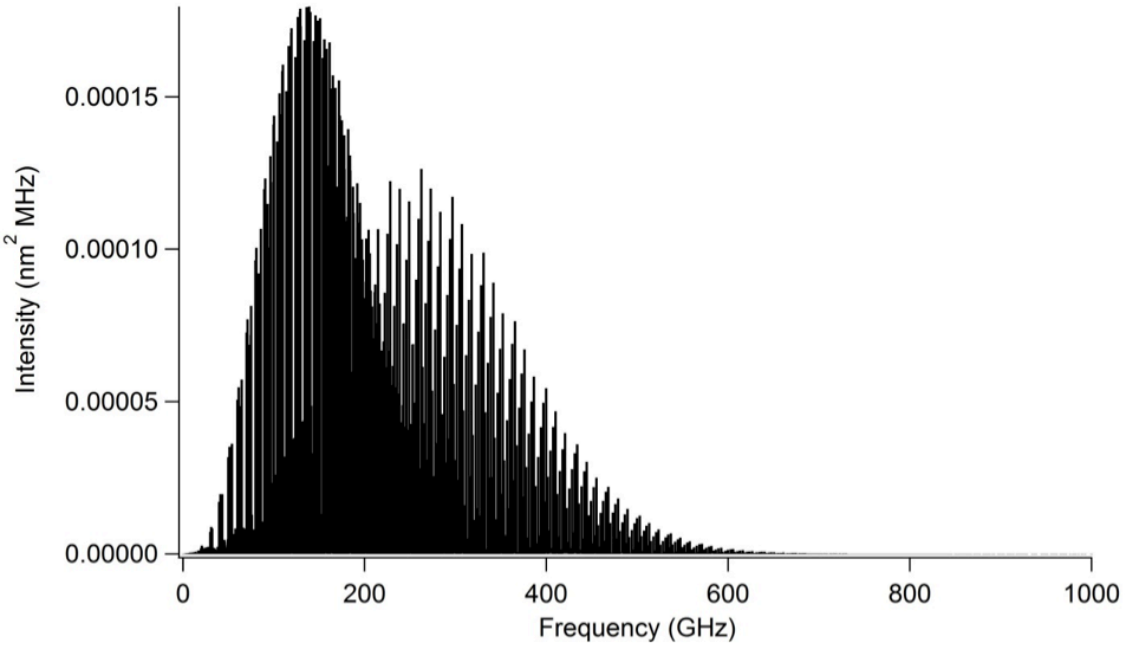

Figure 2.7: Prediction of the pure rotational spectrum of methoxymethanolat 30 K.

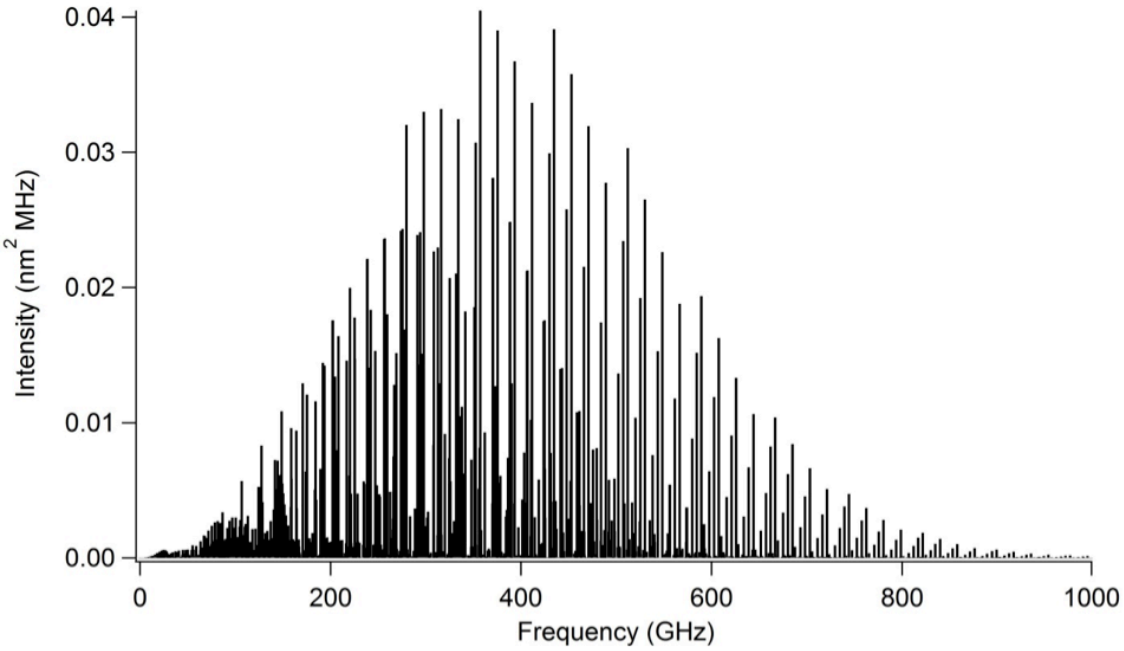

Figure 2.8: Prediction of the pure rotational spectrum of aminomethanol at 30 K.

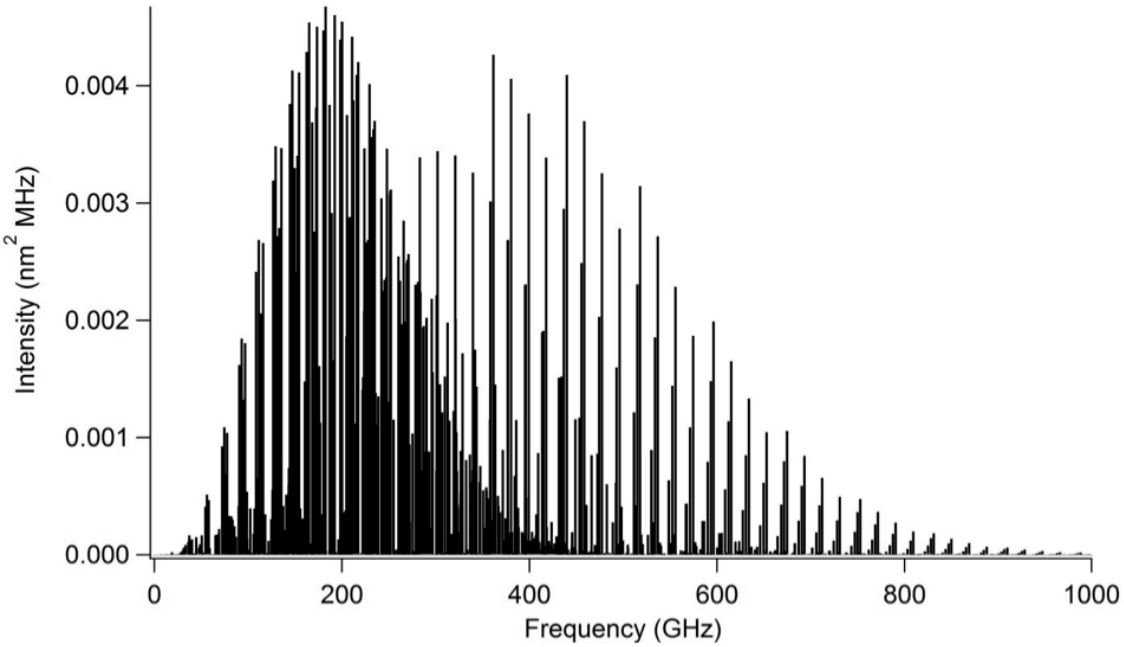

Figure 2.9: Prediction of the pure rotational spectrum of n-methlyhydroxylamine at 30 K.

ting resulting from this motion is expected to be minimal. For methoxymethanol, both the rotation of the methyl group and the wagging of the hydroxyl group were examined. The hydroxyl wag was found to have a barrier of ∼1697 cm^{-1}, which is again sufficiently high to result in negligible spectral splitting. However, the barrier to methyl rotation was found to be ∼669 cm^{-1}, which indicates that the methoxymethanol spectrum will display standard methyl rotor internal rotation splitting. In the case of aminomethanol, the wagging motions of the amine group and the hydroxyl group were examined. The barrier for the amine wag was found to be 2140 cm^{-1}, which is sufficiently high to preclude torsional spectral splitting. However, the barrier for the hydroxyl wag was found to be 684 cm^{-1}, which will result in torsional spectral splitting. The other molecule that might form from the reaction of methylamine with O(^{1}D) is n-methylhydroxylamine. The barrier to methyl rotation is ∼1384 cm^{-1} for this molecule, while the barrier for wagging of the hydroxyl rotor is ∼2405 cm^{-1}; no torsional splitting is expected to be observed in the resultant spectrum. The effects of internal motion for methoxymethanol and aminomethanol were not included in the spectral simulations shown in Figures 2.7 and 2.8, but are likely to be important factors in the spectral analyses for these molecules.

Of the molecules studied in this work, only n-methylhydroxylamine has experimentally measured spectral information for which a comparison can be made. A low-frequency rotational spectroscopic study of n-methylhydroxylamine has been reported[75]. The rotational constants determined in the present work agree with that study to within 200 MHz, which is well within the expected uncertainties based on the geometry optimizations presented here. Additionally, the experimentally determined barrier to methyl rotation in n-methylhydroxylamine in the first vibrational state is reported to be ∼120 cm^{-1} lower than what was found in the torsional barrier analysis presented above. Again, this is well within the expected uncertainties associated with the calculations.

Table 2.2: Spectral parameters determined from equilibrium structure of aminomethanol at the MP2/aug-cc-pVTZ level of theory and with the zpe correction for the structure at the CCSD(T)/cc-pVTZ level of theory.

Constant	MP2/aug-cc-pVTZ	CCSD(T)/cc-pVTZ (zpe correction)
A (GHz)	38.6930	38.3252
B (GHz)	9.5457	9.5296
C (GHz)	8.5868	8.5436
μ_A (D)	-0.3773	-0.2892
μ_B (D)	-0.9132	0.9736
μ_C (D)	-1.3979	-1.2811

2.3.4 Further Predictions of the Structure of Aminomethanol

Aminomethanol was chosen for additional, more detailed computational study for two reasons. The dipole moment is much higher than the other molecules, which makes its interstellar and laboratory detection much more feasible. Also, its prebiotic relevance to glycine formation[3] makes it extremely astrochemically interesting. Therefore, the CFOUR quantum chemistry package was used to find the zero point correction to the moments of inertia at a similar level of theory. This should lead to more accurate determination of the rotational constants for pure rotational studies.[57] The vibrational second order perturbation theory correction was applied to the equilibrium structure of aminomethanol, and refined spectral constants are shown in Table 4.1.

2.4 Conclusions

The energetics and products of the reactions of O(^{1}D) with methanol, dimethyl ether, and methyl amine have been examined computationally. The products of C-H insertion, methanediol, methoxymethanol, and aminomethanol, respectively, were found to be the most energetically favored products. The pure rotational spectra were also predicted from these calculated structures to aid experimental searches for these

molecules. While they all have prebiotic relevance, aminomethanol's dipole moment is the largest, making it more likely to be observable in space. For aminomethanol, the zero point energy correction to the equilibrium structure was also found at a high level of theory, providing a better approximation to what would be observed in a pure rotational spectroscopy experiment. While internal motion of the target molecules and possible other reaction products could complicate experiments, these results provide a foundation on which to base a pure rotational spectroscopic experiment that includes O(^{1}D) insertion to produce these molecules.

3

Experimental Design

3.1 Introduction

The molecules discussed in Chapter 2 (methanediol, methoxymethanol, and aminomethanol) are all astrochemically interesting molecules[2] that have not yet been identified in space due to the lack of laboratory spectral data. To produce them in the lab, $O(^1D)$ insertion reactions into small organic precursors were proposed to selectively form these molecules[58]. This method of production requires a new type of spectrometer that can produce these molecules *in situ*. A new spectrometer was designed to produce $O(^1D)$ in large abundance, to quench the products using a photolysis-supersonic expansion source adapted from the design of Lester and coworkers[76,77],

and to probe the cold molecules in the gas phase using pure rotational spectroscopy. To test this experimental design, methanol was produced from O(^{1}D) insertion into methane, and the system was optimized for performance before studying other less stable molecules. The text and figures found in this Chapter were adapted in part from Hays B. M., Wehres N., Alligood B. A., Roy A. L. M., Laas J. C. & Widicus Weaver S. L. "Rotational Spectral studies of O(^{1}D) insertion reactions with methane and ethylene: Methanol and vinyl alcohol in a supersonic expansion." *Chem. Phys. Lett.*, invited feature article, accepted, 2015[78].

3.1.1 The insertion of O(^{1}D) into Methane

One of the most thoroughly studied reactions of this type is the insertion of O(^{1}D) into methane. This insertion reaction is exothermic by ∼135 kcal/mol, producing highly vibrationally-excited methanol molecules that subsequently undergo unimolecular dissociation [8]. This reaction has been studied extensively through both experimental[7,8,9,10,11,12,13,14,15,16,17,18,19,20,21,22,23,24,25,26,27,28,29,30,31,32,33,34,35,36,37,38,39,40] and theoretical[42,43,44,45,46,47,48] methods. An energy diagram showing an overview of the insertion reaction and subsequent dissociation pathways is shown in Figure 3.1. Figure 3.1 shows that there are many possible dissociation channels stemming from the insertion of O(^{1}D) into methane, including both the primary methanol insertion product, and secondary products resulting from its subsequent unimolecular dissociation; the two lowest-energy insertion products are the primary CH_3OH product, and H_2CO resulting from one such dissociation channel.

3.2 Experimental Design and Methods

The experiments for production of methanol utilized a combination of millimeter spectroscopy with laser-initiated O(^{1}D) chemistry. Surprisingly, there are only a few examples of millimeter/submillimeter wave spectrometers that have been coupled to

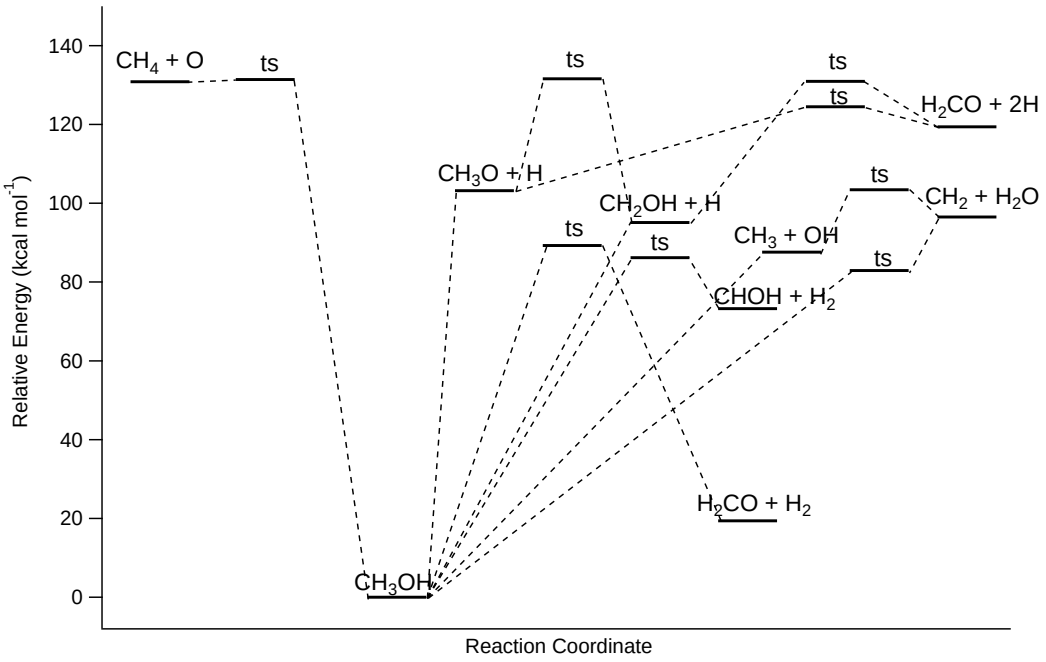

Figure 3.1: The energy diagram for the $O(^1D) + CH_4 \rightarrow CH_3OH$ reaction, based on theoretical investigations reported in the literature[46,47,48].

lasers[79,80,81,82,83]. A schematic diagram of the experimental setup is shown in Figure 3.2.

For the $CH_4 + O(^1D) \rightarrow CH_3OH$ experiments, samples were prepared by mixing argon (NexAir, ultra-high purity), methane (NexAir, 99%), ozone, and oxygen (NexAir, ultra-high purity) in varying concentrations. The ozone was produced using a Pacific Ozone L11 Ozone Generator, the output of which was diluted to $\sim$ 1% O_3 in O_2 at atmospheric pressure. The $Ar/O_3/O_2/CH_4$ gas mixture was delivered via a pulsed valve (Parker Hannifin, Series 9) into a 3 cm long, 1 mm inner diameter UV-grade fused silica capillary tube (Wilmad Glass) before it was supersonically expanded into the vacuum chamber. The fused silica tube was attached to the valve faceplate with epoxy (TorrSeal); the design of the source was based on that used by Lester and coworkers[76,77]. The valve was driven at a repetition rate of 56 Hz with an on duration of 2 – 4 ms. An effective pumping speed at the valve of $\sim$250 L s^{-1} was maintained using a rotary vane + roots blower pumping system. The chamber

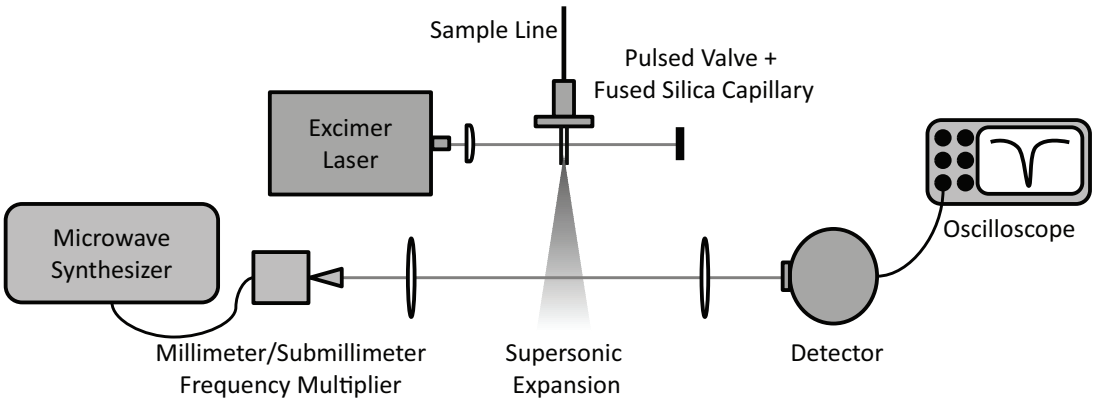

Figure 3.2: Schematic diagram of the experimental setup.

pressure varied depending on the backing pressure used for a given experiment, but was typically ∼60 mTorr.

No direct measurements of temperature or pressure were conducted in the capillary tube, but these quantities can be inferred from the experimental details. All studies were performed with the gas samples at room temperature; previous studies using this type of source determined that the gas temperature in the capillary tube dropped by 3 K[77]. Therefore, the gas in the capillary can be approximated to be at room temperature. Additionally, the total number density of a given reactant in the capillary tube can be determined from the backing pressure, the chamber pressure, and the gas mixing ratios.

The supersonic expansion was probed using (sub)millimeter light produced from a Schottky diode multiplier chain. The output of an analog signal generator (Agilent Technologies, E8257D PSG with options 1EA, UNU, 550, and UNT) was multiplied using a ×6 active multiplier chain (Virginia Diodes Inc., AMC-S268). The multiplier consists of a K_a band amplifier (Spacek Labs, SP3020-30-25B2) which is connected to a WR10 tripler (Virginia Diodes Inc.), the output of which is further amplified before a WR5.1 doubler (Virginia Diodes Inc.) that has an output frequency range of 140 – 220 GHz. The millimeter radiation was focused to a 17 mm × 25 mm spot size (measured at 175 GHz) that crossed the supersonic expansion at a distance of

$\sim$2 cm from the exit of the fused silica tube. For frequencies above 220 GHz, other VDI doublers and triplers were used, which can reach a maximum frequency of 1 THz with our current equipment. The radiation was then detected using an InSb hot electron bolometer (QMC Ltd., QFI/XBI) with $\sim$2 μs time response. The output of the detector was recorded by a digital oscilloscope (Tektronix, TDS1001B), which was used to average and record the time response of the signal. Spectra in the frequency domain were recorded with 60 kHz frequency spacing by determining the integrated intensity of the absorption signal from the time trace on the oscilloscope. A typical spectrum obtained in this study consists of up to 128 averages per data point. The time traces taken at each frequency point were fit to a linear regression from the first few and the last few time points; these fits were subtracted from the time traces to center the baselines of each time trace at zero, reducing the effects of random amplitude variation in the experiment. Unlike many (sub)millimeter spectroscopy experiments, the signal out of the synthesizer was not frequency modulated since signal averaging was performed by the oscilloscope. However, all spectra were power normalized using a power spectrum that was obtained using an amplitude modulated millimeter/submillimeter signal processed by a lock-in amplifier (Stanford Research Systems, SR830).

The production of $O(^1D)$ was initiated by the laser photolysis of O_3 in the fused silica tube. A KrF excimer laser (GAM LASER Inc., EX5 – 250 Hz) operating at 248 nm with a pulse width of 8 ns was used. The resultant $O(^1D)$ underwent collisions with other molecules in the fused silica tube, where methanol was formed from $O(^1D)$ insertion into methane. As shown by Lester and coworkers[76,77], initiating the laser-induced chemistry in the fused silica tube before the expansion helps to promote product formation and stabilization through collisions. Use of a UV-grade fused silica cylindrical lens to focus the laser light onto the tube was found to increase methanol product yield as compared to the use of a spherical lens for focusing the

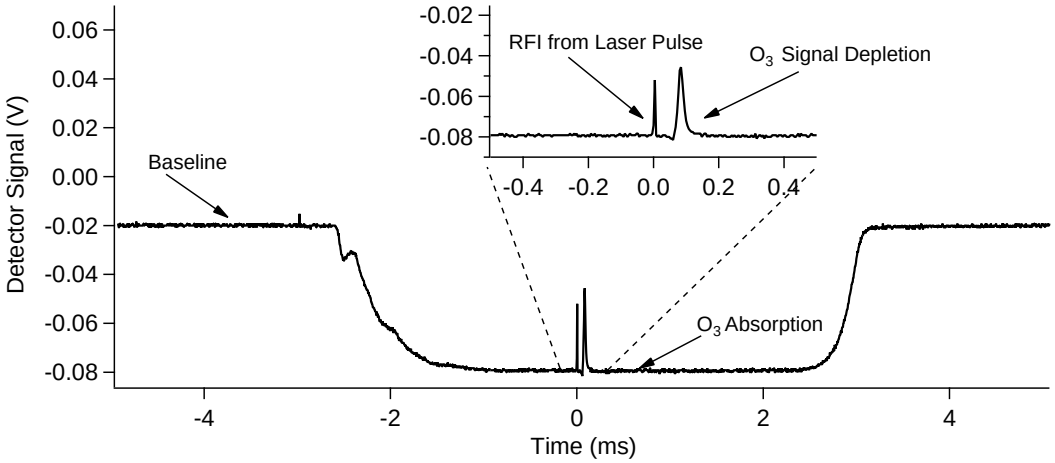

Figure 3.3: Time trace showing the O_3 absorption signal offset from the baseline, the RFI from the laser pulse, and the depletion of the O_3 signal.

laser light; this arrangement is the same as that used by Lester and coworkers in recent studies[84]. Additional benefits of using the cylindrical lens were an increase in product transit time through the millimeter beam, and a decrease in laser damage to the fused silica tube. The laser power was 8.6 mJ per pulse, which was then focused by the cylindrical lens to a spot that was 2 mm $\times$ 1.5 cm. The laser was timed to fire immediately after the O_3 signal reached its maximum value.

3.3 Results and Discussion

3.3.1 Analysis Methods

The spectroscopic information was collected by monitoring the detector signal as a function of time as the molecular absorber moved through the (sub)millimeter beam. This time trace was recorded at each frequency step, and an absorption spectrum in frequency space was constructed by plotting the integrated absorption signal from the time trace for each frequency setting. The time traces were used to monitor product formation or reactant depletion, while the spectra were used to quantify the reactant and product densities and temperatures. An example of a time trace is given in Figure 3.3, which shows the detector response of the system as a function of time when set to

the center frequency of an O_3 line. Here the baseline signal is seen in the beginning of the trace, followed by the absorption dip when O_3 is pulsed into the vacuum chamber. The spike in the middle of the trace is the radio frequency interference (RFI) from the laser pulse. On a timescale of $\sim$50 μs after the laser pulse, the O_3 absorption signal is depleted. This depletion lasts for $\sim$70 μs, and then the O_3 absorption returns until the end of the valve pulse. At this point, the detector signal reverts back to the baseline value. The signal depletion observed for O_3 primarily corresponds to the production of $O(^1D)$. O_3 photolysis at 248 nm gives $\sim$90% $O(^1D)$[85].

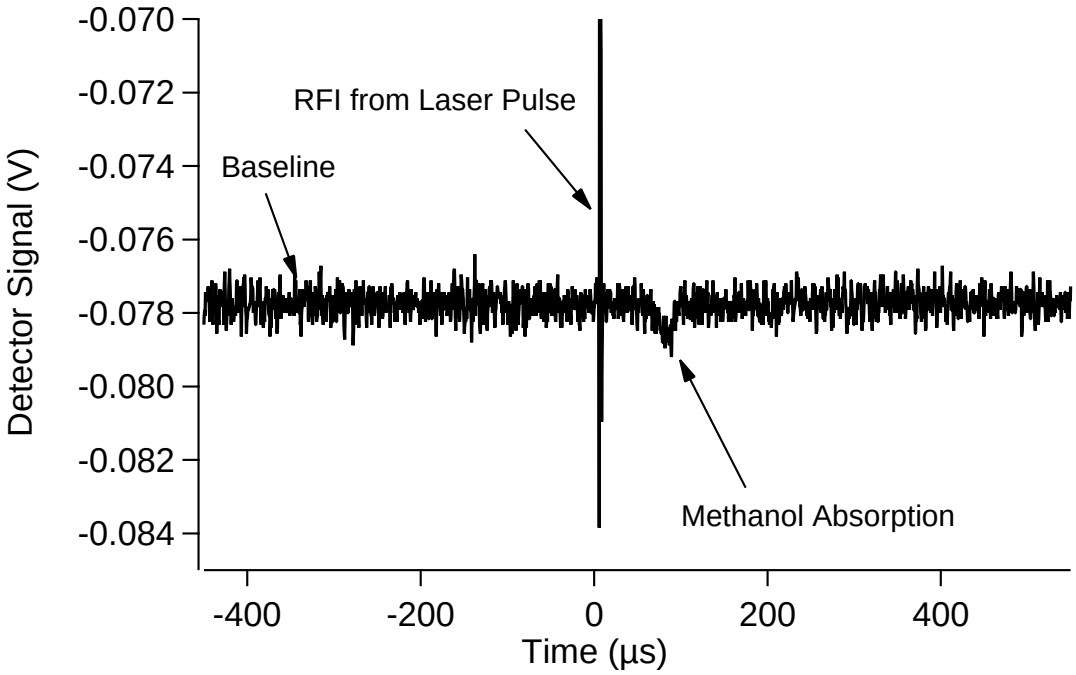

Figure 3.4: Time trace showing the methanol absorption signal offset from the baseline following the RFI from the laser pulse.

Figure 3.4 shows the time trace of the detector response as a function of time when set to the center frequency of a methanol line. Here the signal stays at baseline for the majority of the acquisition. The only two deviations from baseline are the RFI associated with the laser pulse, and the absorption dip corresponding to methanol production.

While the time traces are helpful in monitoring reactant depletion or product for-

mation, a quantitative analysis of the results relies upon spectral acquisition so that temperature and density can be determined. Frequency spectra were collected by recording a time trace at each frequency setting as the millimeter/submillimeter system was stepped at 60 kHz intervals; the integrated intensity of the absorption signal was then determined so that a plot of intensity versus frequency could be constructed. All frequency spectra were power normalized to account for changes in intensity due to the power response of the frequency multipliers. Ozone, methanol, and formaldehyde all have absorption lines in the frequency span of one multiplier setup (140 – 220 GHz). Multiple lines could thus be monitored without changing multiplier chains, enabling the density and temperature of these molecules in the expansion to be determined quantitatively through a standard Boltzmann analysis. This method has been shown[86] to be a reliable approach for quantitative interpretation of millimeter/submillimeter spectral data when a supersonic expansion source is used; the procedure used for the spectral analysis is also described in this reference. Briefly, the integrated intensities of each spectral line are determined through a Gaussian fit. The function $ln\Big[(\int_{-\infty}^{\infty} I_b dv)(k/(h^2\nu B g_u))\Big]$ can be plotted versus $E_l + h\nu$, and a linear regression analysis yields a slope inversely proportional to T_{rot} and an intercept equal to $ln(N_T/Q(T_{rot}))$. Here, $\int_{-\infty}^{\infty} I_b dv$ is the integrated intensity of the spectral line, h is Planck's constant, k is Boltzmann's constant, c is the speed of light, B is the Einstein B-coefficient for the transition, g_u is the upper state degeneracy, ν is

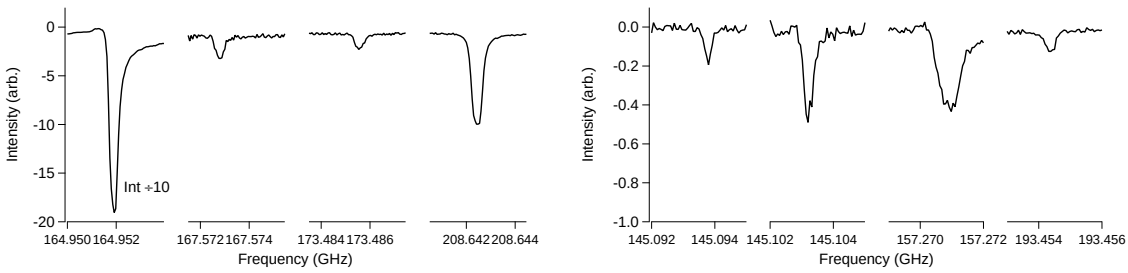

Figure 3.5: Ozone (left) and methanol (right) spectral lines observed. The lowest frequency ozone line has been rescaled so that all lines are visible in this spectrum.

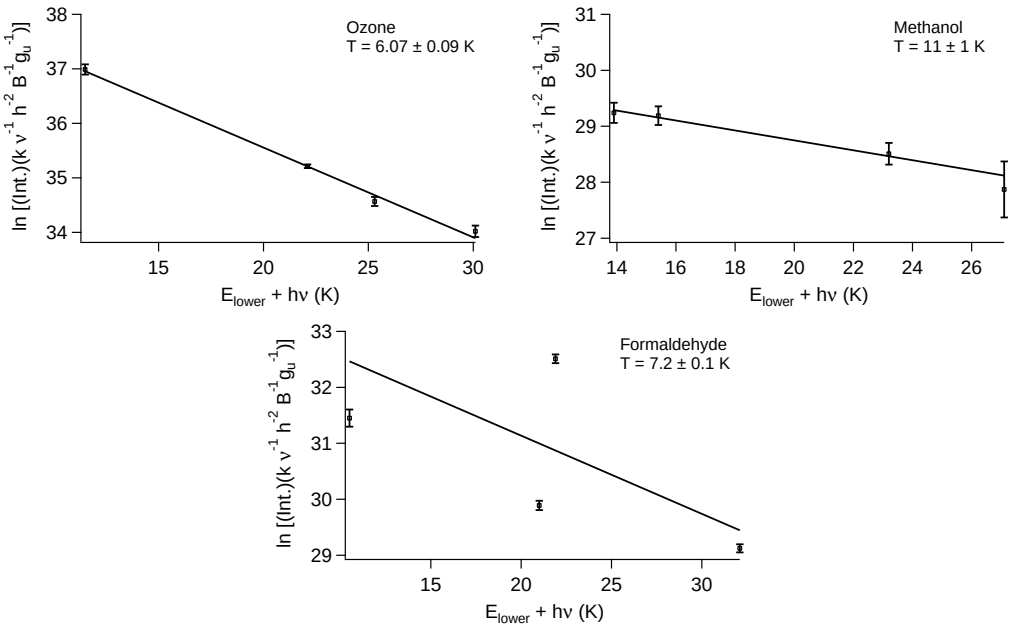

Figure 3.6: Boltzmann diagrams for ozone, methanol, and formaldehyde, where "Int." is the integrated intensity determined through a Gaussian fit to the line shape. The error bars reflect 3σ values.

the transition frequency, N_T is the column density, $Q(T_{rot})$ is the rotational partition function, and T_{rot} is the rotational temperature. Absolute column densities cannot be obtained using this method unless the intensities are calibrated. Therefore, in this experiment, all column densities are scaled to percentages relative to ozone. An example of typical ozone and methanol spectra are shown in Figure 3.5; these spectra were collected during the same experiment, under the same conditions. The associated Boltzmann diagrams for these two spectra, as well as one for formaldehyde from the same experiment, are shown in Figure 3.6.

As seen in Figure 3.6, the Boltzmann diagrams for ozone and methanol had high correlation coefficients, indicating that these species were in thermal equilibrium. However, the Boltzmann diagrams for formaldehyde displayed low correlation coefficients, indicating that formaldehyde may not be in thermal equilibrium. This is not surprising, given the multiple pathways to formaldehyde formation at different energies shown in Figure 3.1 and discussed in Section 7.1. Therefore, while the trends for formaldehyde can be expected to yield qualitative information about the effects of ex-

perimental conditions on its formation and stabilization, the results for formaldehyde are only semi-quantitative.

In addition to scaling the densities to values relative to ozone, it is also helpful to scale these values by the photodissociation efficiency for ozone. This approach accounts for any shot-to-shot fluctuations in the laser output power, and enables proper scaling for the amount of $O(^1D)$ available in the reaction mixture. This percentage was determined by integrating across the depletion signal of the absorption feature in an ozone time trace like that shown in Figure 3.3.

3.3.2 Methanol Production as a Function of Backing Pressure

The first experimental parameter that was investigated was the effect of backing pressure on the amount of products formed. The backing pressure was varied between trials, while the overall gas mixing ratio was held constant at O_2+O_3:Ar:CH_4 fractions of 0.25:0.65:0.10. Experimental conditions limited the range of pressures that could be tested, and therefore limited the optimization of this parameter. The signals of the methanol and formaldehyde products were too weak to be detected by our methods at backing pressures of less than 400 Torr. Additionally, the ozone generator could not be operated with a sample line pressure greater than 900 Torr. Given that this factor of two in backing pressure is close to the experimental uncertainty on the product measurements, no clear trend can be discerned from the pressure trials. These results hint that the backing pressure does not significantly affect the production efficiency for methanol or formaldehyde over the tested pressure range. It should be noted that a lack of pressure dependence might also indicate zero-order kinetics for this reaction, where surface interactions within the tube would be the only influence on product formation. It is not possible to test this scenario with the current experimental setup, as the fused silica tube diameter would need to be changed to test surface interactions. Regardless, while product signal enhancement

may be observed at even higher pressures, this cannot be tested using the current experimental setup, as significant modifications to the experimental design would be required. Given the current pressure limitations, all subsequent experiments were conducted at 850 Torr.

3.3.3 Methanol production as a function of laser photolysis position

The production of methanol was also tested as a function of laser photolysis position. Here, a spherical lens was used to focus the laser spot instead of the usual cylindrical lens, and the position of the lens and laser were adjusted to change the position of the laser beam on the fused silica tube. These measurements were conducted at 850 Torr backing pressure with a gas mixing ratio O_2+O_3:Ar:CH_4 of 0.25:0.65:0.10. The resultant methanol and formaldehyde densities were determined through the Boltzmann analysis method described in Section 3.3.1, and the percentage relative to ozone was determined by taking the ratio of the density determined for the product

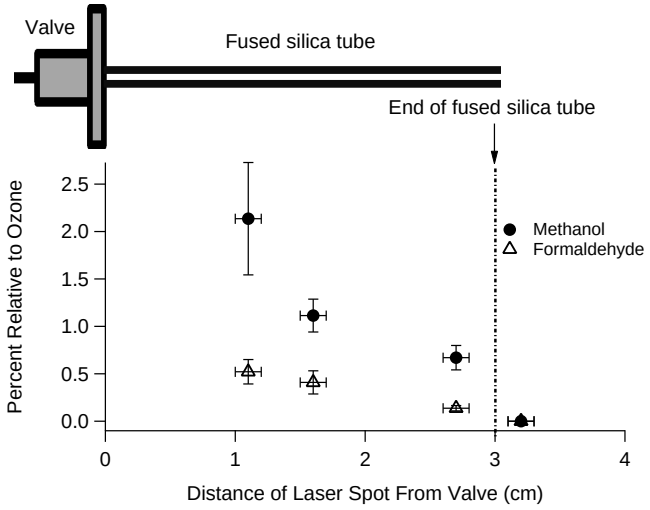

Figure 3.7: Percentage of product relative to ozone as a function of the distance between the valve faceplate and the laser spot. A schematic of the valve (not drawn to scale) and fused silica tube is shown at the top of the plot for reference. Each point has been scaled by the photodissociation efficiency for ozone determined from the time trace as described in Section 3.3.1 above. The y error bars reflect 3σ values; the x error bars reflect the size of the laser spot.

to that of ozone determined for each trial. Each of these values was also scaled by the photodissociation efficiency. The results are shown in Figure 3.7. There is a clear increase in product signal when the laser beam is positioned at the beginning of the fused silica tube (i.e., closer to the pulsed valve), which is consistent with the findings of Lester and coworkers[77] using a similar source design. This increase in product signal is more significant for methanol than for formaldehyde, indicating that additional residence time for the gas mixture in the fused silica tube increases the methanol production, while it has a lesser effect on formaldehyde production. It should be noted that there is no methanol detected when the laser spot is positioned on the beginning of the supersonic expansion (i.e., just past the end of the fused silica tube). Very weak formaldehyde signal was detected when the laser was in this position. However, the Boltzmann diagram indicated that the sample was not at thermal equilibrium, and no reliable value for the column density could be determined at this position. Fortunately since methanol production is enhanced by use of the fused silica tube, quantitative information for formaldehyde production with the laser spot focused outside of the tube is not required for guiding future experiments.

3.3.4 Additional Reaction Products Observed

The main goals of the $CH_4 + O(^1D) \rightarrow CH_3OH$ experiment were to confirm and optimize the production of methanol. However, Figure 3.1 indicates that there are several other possible products that could arise from this insertion reaction. While many of these products do have rotational spectral information (i.e., CH_3OH, H_2CO, CH_3O), some of these products do not have any available spectral information in the target frequency range (i.e., CHOH, CH_2OH). In addition, each of the pathways shown in Figure 3.1 may undergo further reactions to produce species that are not shown in this diagram. Fortunately, the structure-specificity of rotational spectroscopy enables us to search for all molecules with known rotational spectra. Once sufficient

spectral coverage is obtained, identification of new molecules can also occur through comparison with predicted spectra based on computational studies. The molecules analyzed in the current work were identified via their rotational spectroscopic signatures, through identification of two or more lines as given in the Cologne Database for Molecular Spectroscopy (CDMS)[87] and the Jet Propulsion Laboratory (JPL) Spectral Line Catalog[67].

The laser induced products methanol, formaldehyde, methoxy, carbon monoxide, water, $O_2(^1\Delta)$, HO_2, and hydrogen peroxide were detected in this experiment. None of these products are observed in the absence of laser photolysis of ozone. Methanol is the targeted insertion reaction product, and is produced with the highest abundance of any product. This is to be expected in an optimized experiment, as direct insertion is expected to be the primary formation route for this molecule. The direct product of laser photolysis of ozone at 248 nm, $O_2(^1\Delta)$, is also detected, despite its weak magnetic moment allowed transitions. $O_2(^1\Delta)$ is directly proportional to the amount of $O(^1D)$ that was formed from photolysis.

Formaldehyde is observed in the next highest abundance as compared to methanol; it can form through several methanol dissociation channels as shown in Figure 3.1. Formaldehyde can be observed under most photolysis conditions in this experiment, inside or just beyond the fused silica tube. CH_3O lines are only observed when the laser spot is positioned near the exit of the tube, and no lines of CH_3O are observed when the laser spot is positioned at the beginning of the tube (i.e., near the pulsed valve). These results indicate that CH_3O does form as a result of the insertion reaction, but that the presence of the fused silica tube promotes its further reaction by allowing for an increased number of collisions and longer reaction timescales. In support of this finding, HO_2 is only observed when the photolysis occurs in the fused silica tube. The HO_2 radical could be forming from reaction of either CH_3O or CH_2OH with O_2; this is consistent with the lack of CH_3O detection when collisions

are maximized (i.e., when the fused silica tube is in use). However, it is also possible that HO_2 is forming from the reaction of OH with O_3. We conclude from these findings that the use of the fused silica tube is driving either formation or collisional stabilization (or both) for CH_3OH, while further reactions involving the methanol dissociation products lead to other product formation, including H_2CO and HO_2. Searches were also conducted for lines from ethanol (CH_3CH_2OH) and dimethyl ether (CH_3OCH_3), which are expected to form from radical-radical recombination reactions of methanol dissociation products, but neither of these species were detected.

In addition to the above major product channels, several additional reaction products were observed in the methane experiment. Hydrogen peroxide was detected, although the spectra were quite weak. H_2O_2 can form through hydrogen abstraction channels involving O_2, or through the third-body assisted reaction of hydroxyl radicals. Regardless of its formation pathway, the presence of H_2O_2 implies that the chemistry of this system proceeds several steps past the scheme shown in Figure 3.1.

3.4 Conclusions

A new spectrometer was built to test using the production mechanism of $O(^1D)$ insertion reactions into methane to produce the insertion product methanol. Methanol was observed as a laser induced product of $O(^1D)$ insertion into methane using (sub)millimeter absorption spectroscopy. The photolysis occurred in a fused silica tube, which helped to stabilize the products through collisions. Other products were formed in the tube that were either the result of unimolecular decomposition (i.e. formaldehyde, methoxy, and water) or from further reactions in the tube (i.e. HO_2, hydrogen peroxide, and CO). The formation of methanol using this setup proves the insertion mechanism can be used to produce target molecules in high enough abundance to be detected using millimeter/submillimeter spectroscopy.

4

Vinyl Alcohol

4.1 Introduction

The successful benchmarking of the experiment studying O(^{1}D) insertion into methane to form methanol lays the groundwork to study less stable molecules. The first target molecule was vinyl alcohol. Production of this molecule occurs through O(^{1}D) insertion into ethylene. Such studies would validate the use of this setup for study of more unstable molecules, while also extending the spectral coverage for vinyl alcohol to guide astronomical searches. To aid this study, several improvements were made to the experiment to reduce acquisition time, to enable more spectral averaging, and to allow reactive chemical mixtures to be used.

The text and figures in this Chapter were adapted in part from Hays B. M., Wehres N., Alligood B. A., Roy A. L. M., Laas J. C. & Widicus Weaver S. L. "Rotational Spectral studies of O(^{1}D) insertion reactions with methane and ethylene: Methanol and vinyl alcohol in a supersonic expansion." *Chem. Phys. Lett.*, invited feature article, accepted, 2015[78].

4.1.1 Background

The reaction with O(^{1}D) and ethylene has previously been investigated in a few experimental studies[88,89,90], and the singlet surface of the structural isomers of vinyl alcohol were investigated computationally[91] in the context of the O(^{3}P) addition to ethylene undergoing an intersystem crossing. To our knowledge, no theoretical studies have examined the singlet surface for this reaction in more detail. As such, an energy diagram has not been included such as the one shown for methanol in the previous Chapter. Based on the information that is available from Nguyen et al.[91], the vinyl alcohol isomers show many tautomerization channels to acetaldehyde and ethylene oxide, as well as decomposition channels from these products, with the end products being carbon monoxide, methane, ketene, formaldehyde, and several radicals. The main channel for the reaction between ethylene + O(^{1}D) was found to be the C-H insertion channel to form highly excited vinyl alcohol[88,89] with some possible contribution from abstraction reactions[89]. It has also been predicted that the O(^{1}D) + ethylene reaction could lead to ethylene oxide through a barrierless reaction channel[90].

Vinyl alcohol can be produced by phototautomerization of acetaldehyde[92], making it an important contributor in atmospheric chemistry[93]. Vinyl alcohol has been previously characterized in the microwave regime using pyrolysis sources[94,95]; this included spectral coverage up to 50 GHz and J=25. A similar source was used for a millimeter-wave gas-phase study[96], with spectral coverage up to 120 GHz and J=10[96]. Vinyl

alcohol has two conformers that have been studied: syn-vinyl alcohol[96,94] and anti-vinyl alcohol[95]. In these two conformers, the hydroxyl group either points away from or toward the plane of the molecule, respectively.

A tentative astronomical detection of vinyl alcohol has also been reported in Sgr B2(N)[97]. However, this detection has not been confirmed at higher frequencies[98,99]. Higher-frequency spectroscopic measurements that extend beyond the work of Saito[96] would aid future astronomical searches for this molecule.

4.2 Experiemental Methods

The basic experimental design is the same as the setup described in Chapter 3 and shown in Figure 3.2, except several improvements and additions were needed for this study. A National Instruments PCI-5124 digitizer card was used to record the signal instead of an oscilloscope. This decreased the downtime for saving data to the computer and allowed for much more flexibility in the programmed scanning routine developed for this experiment. The digitizer was typically operating at 10 MSa s^{-1}, with a maximum rate of 200 MSa s^{-1}. The typical acquisition time lasted 250 μs, with the signal from the laser-initiated products lasting $\sim$50 μs. The data were acquired in the same fashion as described in Chapter 3, where a time trace was collected at each frequency and averaged for 20 to 500 averages per frequency point before moving on the next frequency. The laser used to initiate photolysis was a GAM Laser EX10 – 200 Hz, which offered roughly double the output power of the laser used in the methane/methanol studies. The additional power increased the amount of photolysis products, but was not critical to the success of experiment.

An additional experimental improvement involved a new pulsed valve setup for the mixing of ozone and ethylene. These gases readily react upon contact, which required that the gas mixing was minimized until the laser photolysis region. Therefore, a new source was constructed to overcome this challenge. As shown in Figure 4.1, two

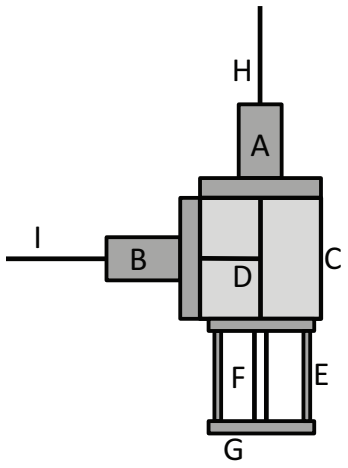

Figure 4.1: Schematic of the mixing source, comprised of : A) ozone pulsed valve; B) reactant (i.e., ethylene) + argon pulsed valve; C) mixing block; D) gas channels; E) support to hold metal plates holding fused silica tube in place, F) fused silica tube, G) output coupler and mounting plate, H) ozone gas line; I) reactant + argon gas line.

pulsed valves (Parker Hannifan, Series 9) were attached to adjacent sides of a 3.8 cm Plexiglass cube, which served as a gas mixing block. Two 1 mm wide channels were drilled into the mixing block so that they intersected the pinholes on the faceplates of the pulsed valves. One of these channels passed entirely through the mixing block, while the second channel intersected the first channel in the center of the mixing block. The 1 mm diameter fused silica tube was attached to the output channel of the plexiglass cube and held in place by a stainless steel plate that attached to the plexiglass cube with support rods. This plate had a 1 mm pinhole and served as an output coupler for the supersonic expansion. The laser spot was focused near the output of the silica tube. The ethylene and argon mixture behind the pulsed valve was held at $\sim$ 1 atm and contained 10% ethylene. The oxygen and ozone mixture ($\sim$ 1% ozone) was held at 900 Torr behind the other pulsed valve.

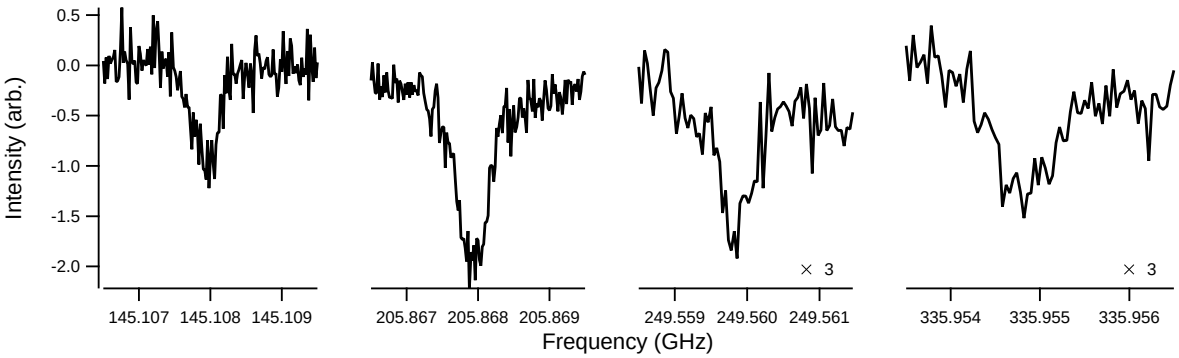

Figure 4.2: Example syn-vinyl alcohol spectra. The intensities of the spectra in the highest two frequency ranges have been multiplied by a factor of 3.

4.3 Results and Discussion

4.3.1 Vinyl Alcohol Spectroscopy

Performance of the mixing source was verified by monitoring the depletion of ozone in the absence of laser photolysis. Ozone depletion could be observed even in the new mixing source, but the source did allow for sufficient ozone and ethylene to pass to the laser photolysis region. Additionally, the mixing source added length to the transit time of reactants through the pulsed valve system. This increased the duration of molecular signal in the (sub)millimeter beam from 2 ms to 5 ms.

Production of vinyl alcohol was facile. Example vinyl alcohol spectra are shown in Figure 4.2. Surprisingly, the optimum laser position for production of vinyl alcohol was near the end of the fused silica tube. This is the opposite result from what was obtained for methanol, where production was optimized when the laser beam was positioned near the pulsed valve. This result indicates that either collisional stabilization is not required for vinyl alcohol production, or that vinyl alcohol undergoes additional reactions in the fused silica tube that lower its overall abundance in the supersonic expansion.

The search for vinyl alcohol was guided by the previous microwave[94] and millimeter wave[96] studies, and the information contained in the Cologne Database for Molecular

Spectroscopy (CDMS)[87]. Spectral predictions based on these previous studies were used to guide spectral searches at frequencies above 140 GHz. Searches focused on the syn conformer of vinyl alcohol because it is the lowest energy conformer. Anti-vinyl alcohol was also observed, but only after significant spectral averaging. As such, only a few of the strongest lines for anti-vinyl alcohol could be measured. The spectral lines measured for this conformer are not included in the spectral analysis presented below.

A total of 49 new transitions of syn-vinyl alcohol were detected between the range of 140 and 450 GHz, including transitions up to J=10. Because the expansion temperature is so cold, the vinyl alcohol line intensities drop dramatically at frequencies above 450 GHz, and no additional lines could be observed. For transitions below 220 GHz, the spectral resolution and associated frequency uncertainty was 20 kHz, while transitions above 220 GHz had a spectral resolution and associated frequency uncertainty of 40 kHz. The new vinyl alcohol lines match very well with spectra predicted based on previous analyses.

The new measurements were combined with previous datasets[100,94,96] using the information from the CDMS catalog[87]. The fit was performed using the CALPGM program suite[101] with a standard asymmetric top Hamiltonian in the Watson A reduction. The molecular parameters determined from the refined fit are presented in Table 4.1. The fit file is included in Appendix C. The results match well with those from the CDMS catalog, and offer an order of magnitude improvement in precision for several of the molecular parameters as compared to the previously published work.

4.3.2 Additional Reaction Products Observed

In the ethylene + O(^{1}D) experiment, detection of vinyl alcohol was facile. Additional molecules that were detected include formaldehyde, methanol, methoxy, ketene, ethanol, acetaldehyde, HO_2, hydrogen peroxide, carbon monoxide, and water. Unsuc-

Table 4.1: Spectral parameters determined for syn-vinyl alcohol compared to the previous study of Rodler and Bauder[94] and the information in the CDMS catalog[87]. The assignments from the current work were combined with the lower-frequency assignments of Rodler and Bauder[94] and Saito[96] to give the results presented here.

Parameter	Previous Work[94]	CDMS[87]	This work	Units
A	59660.80(2)	59660.7737(124)	59660.78243(199)	MHz
B	10561.665(3)	10561.60537(212)	10561.60521(49)	MHz
C	8965.786(3)	8965.84207(186)	8965.84204(44)	MHz
Δ_J	7.71(2)	7.4901(167)	7.49749(278)	kHz
Δ_{JK}	-61.6(4)	-60.002(277)	-59.876(38)	kHz
Δ_K	917(1)	914.05(82)	914.853(129)	kHz
δ_J	-1.664(2)	-1.66533(127)	-1.665723(297)	kHz
δ_K	28.97(5)	-0.115791(156)	-0.115784(67)	kHz
Φ_K	–	-0.0297(87)	–	
J_{max}	24	24	24	
K_{max}	19	19	19	
# Lines	36	62	111	
Total Fit rms	64.0	41.1	47.8	kHz

Note: One σ errors are listed in parentheses in units of last significant figure.

cessful searches were conducted for several additional likely products; most notably absent was ethylene oxide, a structural isomer of vinyl alcohol and acetaldehyde. Formaldehyde was the most abundant product by several orders of magnitude. This was most likely due to the fast reaction of $O_2(^1\Delta)$ with ethylene, which produces a four member ring before breaking apart into two formaldehyde molecules. This assumption is reinforced by the lack of detection of $O_2(^1\Delta)$ when ethylene was present in the reaction mixture. The detection of acetaldehyde, which is a stable tautomer of vinyl alcohol, implies that some of the vinyl alcohol is inefficiently quenched in the fused silica tube and isomerizes. The identification of acetaldehyde but the non-detection of ethylene oxide implies that the vinyl alcohol product had sufficient energy to overcome the barrier to isomerization to acetaldehyde, but lost enough energy through collisions that it did not also isomerize to ethylene oxide.

The detection of ethanol implies the addition of hydrogens to vinyl alcohol or a sample impurity. The rest of the products that were detected can be attributed to either decomposition (i.e., ketene, carbon monoxide, and water), further reaction in the tube (i.e., methoxy and methanol), or further reactions with oxygen or ozone (i.e., hydrogen peroxide and HO_2). Some of this chemistry is very similar to what was seen with the methane experiments, especially regarding the formation of HO_2. The oxygen in the backing gas probably plays a large role in the chemistry. Additional products were anticipated but could not be detected this experiment. OH is expected to form as a decomposition product, but is beyond the detection range of the spectrometer. Other products, such as acetylene and ethylene, have no dipole moment and therefore no pure rotational spectrum, while others, such as the vinyl radical, could not be detected due to the lack of information about its pure rotational spectrum.

4.4 Conclusions

The reaction of ethylene and $O(^1D)$ was investigated using an improved version of the apparatus described in Chapter 3. Vinyl alcohol was observed as a primary product along with several other products from decomposition and further reaction in the fused silica tube. The spectral assignment of vinyl alcohol was extended up to 450 GHz, confirming the spectral predictions of earlier studies and providing improved spectral assignments to guide astronomical observations. The production of vinyl alcohol also demonstrates that an unstable molecule can be produced using this experimental approach, enabling studies of other unstable molecular targets.

5

Fast Sweeping Direct Absorption Experiments

5.1 Background

Many challenges were presented by the previously described experiments, but the speed of acquisition has been the biggest hurdle to overcome. New experimental approaches were therefore sought to increase the speed of acquisition for these experiments, which resulted in the development of a new technique for (sub)millimeter spectroscopy. In this Chapter, previous techniques of broadband (sub)millimeter spectroscopy will be reviewed, followed by a detailed description of the new (sub)millimeter

spectrometer.

Traditional (sub)millimeter spectrometers have used simple direct absorption techniques. In these experiments, a narrowband frequency source is stepped across a broad frequency range one frequency point at a time. The standard mode of operation for these instruments involves frequency modulating the center frequency so that the signal output of the spectrometer can be detected via phase-sensitive detection using a lock-in amplifier, enhancing the signal-to-noise of the resultant spectrum. The main drawback of this approach is that only 1-10 frequency points can be taken in a second with spacings ranging from 10 to 100 kHz between frequency points. This means that while these spectrometers are very sensitive, it will take an extremely long time to scan over the entire (sub)millimeter spectrum; the spectral range covers 50 GHz to 1 THz for the experiments presented here. This leads to a spectral search problem, especially for previously unstudied molecules where spectral predictions have high uncertainties.

A few groups have taken experimental steps to circumvent the these challenges. To scan large bandwidths in the microwave region, Chirped Pulse - Fourier Transform Microwave (CP-FTMW) spectroscopy was developed by Pate and co-workers[102]. Here, tens of GHz of a broadband spectrum can be taken in < 40 μs. The basic principle of this spectrometer is that a broadband linear frequency sweep polarizes a gas sample in about 1 μs, and a free induction decay (FID) is detected for up to 40 μs after excitation. The FID is then Fourier transformed to produce a broadband frequency spectrum. Along with the broadband spectroscopy, this technique relies on digital technology that is highly repeatable, stable, and fast. This allows for trillions of averages to be taken in a relatively short time span. This spectroscopy technique has been expanded into the (sub)millimeter region using frequency multiplication techniques and/or a heterodyne receiver on the backend to bring the FID back down to the microwave region, where digital electronics and amplifiers work best for detecting these

kind of signals[103,104,105,106,107]. The significant drawback of these spectrometers is the lack of commercial high power millimeter wave amplifiers for efficient excitation, and the high cost of a (sub)millimeter wave heterodyne receiver. To get around some of these issues, a high number of averages are taken ($> 10^9$) to compensate for the low power. The FIDs are much shorter for millimeter wave CP than for microwave CP, and therefore it is much easier to take many averages.

Another existing method for broadband (sub)millimeter wave spectroscopy involves the Fast Scan Submillimeter Spectroscopy Technique (FASSST) technique developed by de Lucia and coworkers[108,109,110,111]. This spectrometer was originally based on Backward Wave Oscillators (BWOs) that were capable of fast frequency sweeps across a 100 GHz wide range in the (sub)millimeter regime. This technique initially required Fabry-Perot (FP) cavity interference fringes to be used as a means for frequency calibration of the non-linear sweep due to drift in the system because of the use of analog technology[108,109]. The setup has since been updated to digital technology, where reproducible sweeps that are linear could be generated using a Direct Digital Synthesis (DDS) based frequency synthesizer, the output of which was then doubled using an active multiplier chain[110]. This eliminated the need for a FP cavity and allowed linearly scaled frequency calibration. The most recent iteration of FASSST uses all solid state components and a modulation scheme to decrease instrument size[111]. This instrument also replaces the HEB with a heterodyne receiver to maintain all phase information, and a lock-in amplifier for phase-sensitive detection of the modulation signal.

While both the FASSST and CP-FTmmW spectrometers are reliable instruments for (sub)millimeter spectroscopy, they both require significant financial investment. Therefore, a new instrument was devised that only required equipment that was readily attainable. Components from an existing CP-FTMW experiment were combined with the lab's existing spectroscopy experiment to make an experiment that is similar

in concept to the FASSST experiment, but with major differences in operation and detection. This new technique is overviewed below.

5.2 Experimental Design

The experiment incorporates several materials from a pre-existing CP-FTMW spectrometer and from the experiment that was described in Chapter 4[78]. An experimental schematic is shown in Figure 5.1. The output of an analog signal generator (Agilent Technologies, E8257D PSG with options 1EA, UNU, 550, and UNT) mixes with the output of an arbitrary waveform generator (AWG, Agilient M8190A). The synthesizer output was at 8050 MHz, while the AWG produced a linear frequency sweep from 3958.33 – 4125 MHz in 1.5 ms. The output of the AWG was passed through a band pass filter (0 – 5 GHz) to filter out any higher harmonics. The upper sideband from the double balanced mixer (Miteq DM0520LW1) passed through a band pass filter (9.1 – 14.2 GHz) and then through a preamplifier (Phase One Microwave SL-182010) before being frequency doubled (Wright Technologies ATX26-220). The output from the doubler was appropriately attenuated before going into the active multiplier chain (AMC). The AMC used in this experiment consists of a K_a band amplifier (Spacek Labs, SP3020-30-25B2) which is connected to a WR10 tripler (Virginia Diodes Inc.), the output of which is further amplified before a WR5.1 doubler (Virginia Diodes Inc.) that has a nominal output frequency range of 140 – 220 GHz. The radiation was coupled into a flow cell, propagated the length of the cell, and then was focused and detected using an InSb hot electron bolometer (QMC Ltd., QFI/XBI) with $\sim$2 μs time response. The flow cell is a two meter long PVC tube that can be evacuated to <10 mTorr, but was held at 50 mTorr by introducing methanol vapor from a flask of liquid methanol (Fisher Scientific 99.9%, no further purification); the pressure of methanol in the flow cell was controlled by a needle valve between the sample and the cell. The output of the detector was amplified using a low noise amplifier, and

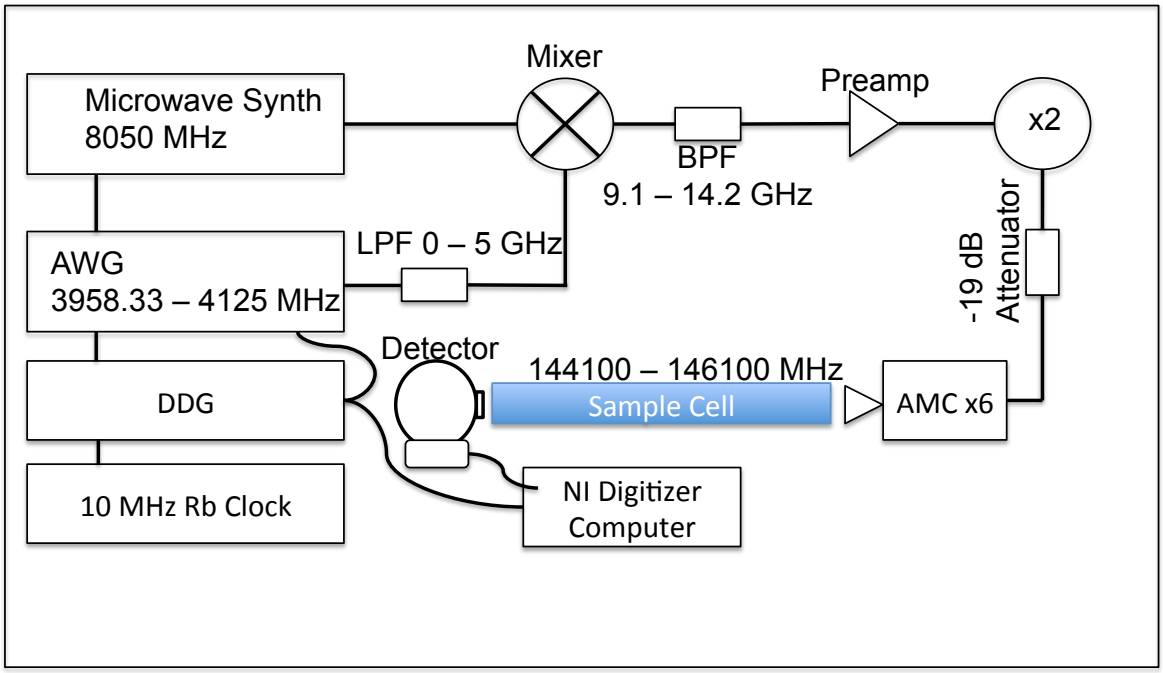

Figure 5.1: Schematic of the fast sweeping direct absorption experiment

then recorded using a National Instruments PCI-5124 digitizer card. The digitizer card recorded 13,000 points, about 12,000 of which were the chirped pulse acquisition and the rest of which were background, all recorded at a rate of 8 MSa/s. The timing of the AWG and the digitizer were controlled by a digital delay generator (Stanford Research Systems, DG645) pulsing at a rate of 600 Hz. The synthesizer, delay generator, and AWG were all locked to the same 10 MHz Rb clock for timing and phase stability. The synthesizer and digitizer were controlled using a custom scanning routine that could save any number of averages taken; however, all of the spectra shown here were taken with 1 million averages. The typical acquisition time took $\sim$ 1 hour.

5.3 Results

5.3.1 Experimental Data

The range of 144,100 – 146,100 MHz was chosen because this range coincided with a large number of methanol transitions reported in the JPL catalog[67]. The spectrometer

was swept across this 2 GHz range in 1.5 ms. This rate gave a good balance between sweeping through a molecular transition with reasonable resolution without losing signal due to the bolometer response time. Figure 5.2 shows the bolometer response from these sweeps. The large voltage drop-offs on each sweep are associated with the turn on and turn off of the AWG. Is should be noted that the signal does not begin exactly at 0 time; this is due to the response delay of the bolometer. A zoomed-in version of this spectrum is shown in Figure 5.3, revealing several methanol transitions. The signal-to-noise ratio (SNR) of this spectrum is around 10,000 for the most intense methanol transition.

As seen in in Figures 5.2 and 5.3, the baseline of this experiment has large scale amplitude variation likely due to the frequency dependent response of the bolometer and/or the frequency dependent power output of the AMC. The effects of standing waves from the optical setup of the AMC, lenses, flow cell, and detector are also present, but give rise to small scale variations compared to the large amplitude power fluctuations. The large amplitude variation leads to difficulties fitting and subtracting the baseline.

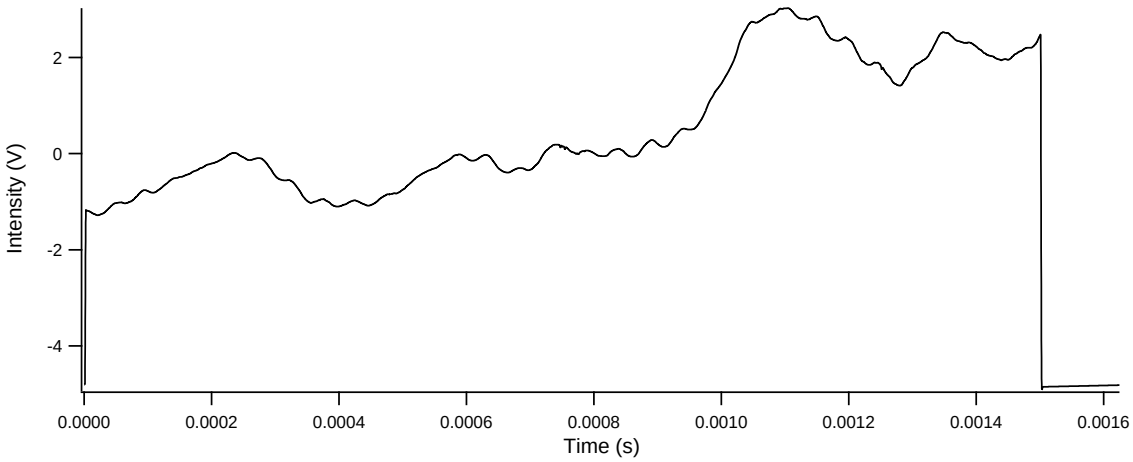

Figure 5.2: Response of the bolometer shown as a function of time when the setup is swept over 2 GHz in 1.5 ms.

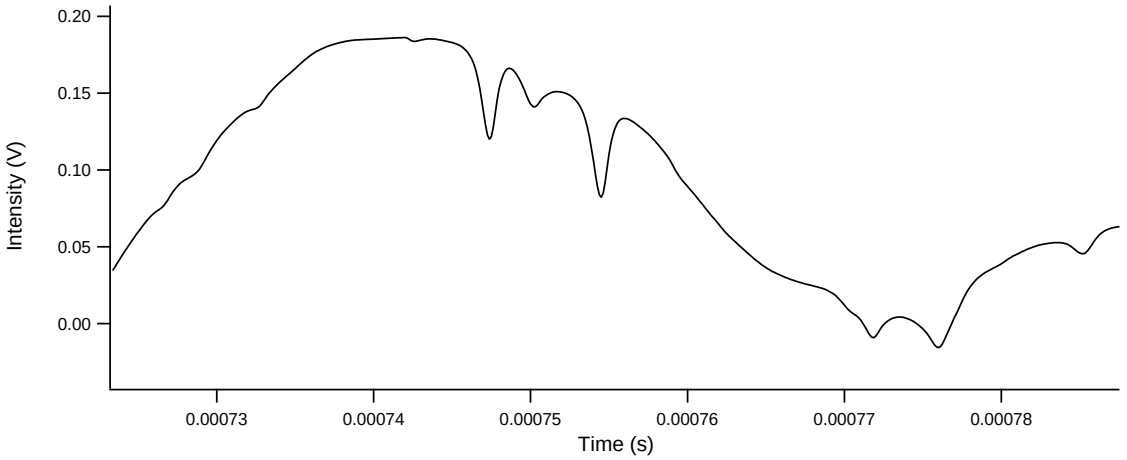

Figure 5.3: A zoomed in portion of the bolometer response in the range where methanol transitions are resonant with the incoming radiation.

5.3.2 Data Analysis and Baseline subtraction

The frequency sweep from the AWG scales linearly with time. A linear correction factor was therefore applied to the time spacing as recorded by the digitizer to convert the spectrum to frequency space. A scalar factor of 2.125 μs had to be included to account for the bolometer response time. The response time correction was verified by comparing the observed transitions against the known line centers for several methanol transitions. The resultant spectrum had a frequency spacing of 170 kHz, with 125 ns time resolution.

The removal of the baseline is paramount to fully utilizing this broadband spectroscopic technique. The first choice for baseline removal was to take the same sweep with no sample present in the flow cell. The removal of methanol from the flow cell brought the pressure down to <10 mTorr, which unfortunately had a very large effect on the spectral baseline. The large scale amplitude variation and the smaller scale standing waves changed significantly, and the baseline subtraction yielded what is shown in Figure 5.4. The methanol transitions are now visible to the eye (i.e., as shown as sharp downward absorption dips) but the spectrum now has a sinusoidal baseline that makes analysis difficult and precludes detection of weaker transitions.

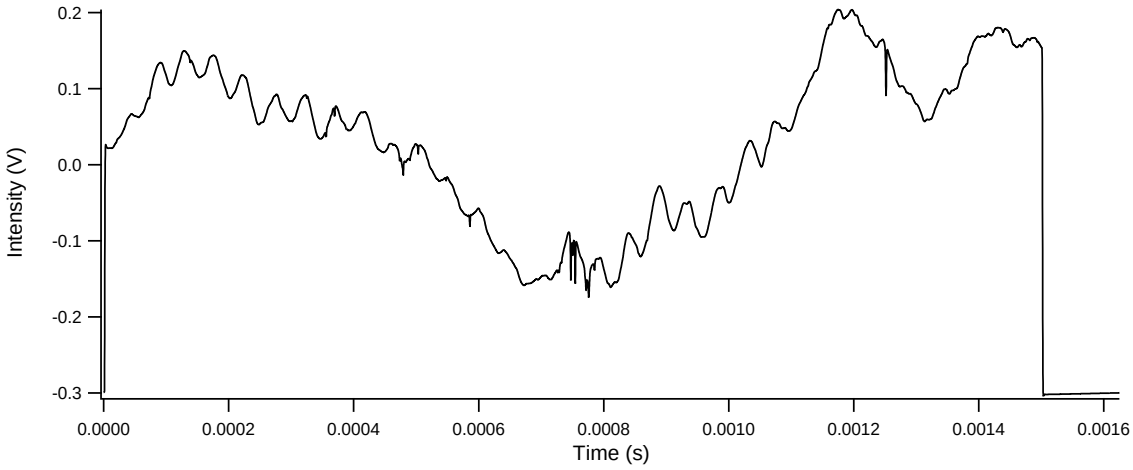

Figure 5.4: The baseline subtracted time response of the detector.

The large changes were likely due to changes in the pressure, which changes the standing waves in the spectrometer. The refractive index of the sample chamber also changes with pressure, which could also affect the spectrum.

Several other attempts were made to fit the baseline using various techniques. Numerical filters were applied to the Fourier transform of the spectrum, where the low frequency noise and the high frequency noise could be filtered against each other. However, the deviation of the spectral line intensity from the baseline could not be filtered out using low, high, and notch pass filters. An example of the low pass filtered baseline in Figure 5.5 shows the primary reason these filters did not work. The amplitude associated with absorption lines could not be removed from the filtered spectra, leaving the filtered subtracted spectrum with a flat baseline but with pseudo second derivative lineshapes. Splines were also used to try to fit the spectral baselines, but this could not be effectively done without masking out the transitions. The masking defeated the purpose of using this method to look for new transitions of molecules without prior knowledge of their frequencies.

The most useful method of data analysis involved taking the second derivative of the data set. It was found that faster sweep rates yielded the best SNR when this derivative method was used. A processed spectrum is shown in Figure 5.6, where

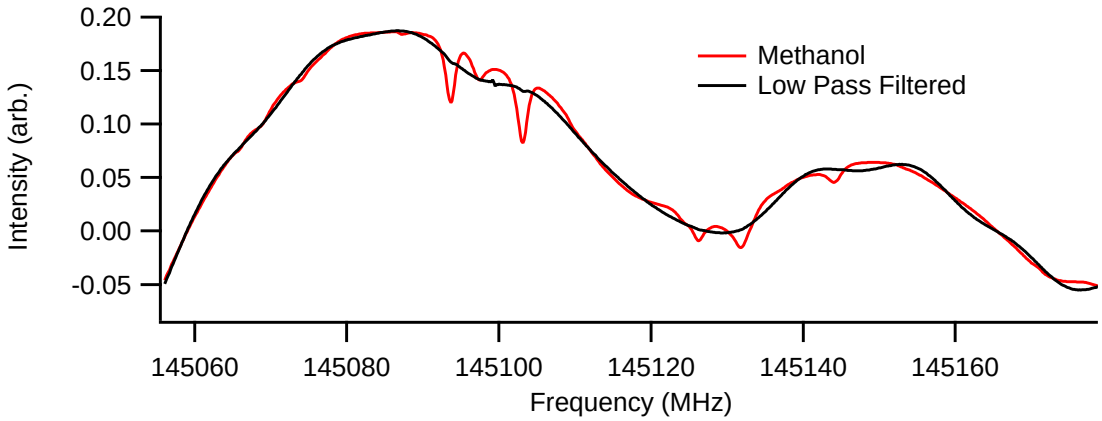

Figure 5.5: The frequency calibrated spectrum with the filtered spectrum shown for comparison.

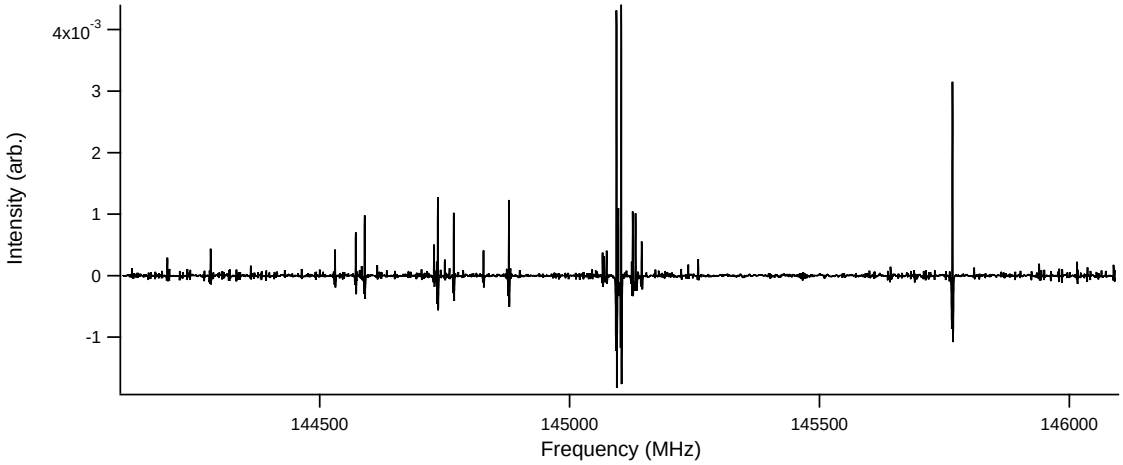

Figure 5.6: Frequency calibrated spectrum of methanol using second derivative of the dataset.

several methanol transitions are clearly visible. The baseline amplitude variation is drastically reduced and the spectrum is easily observed. The 2nd derivative spectrum was taken of the background subtracted data as shown in Figure 5.4, to remove the effect of spurs arising from the frequency sweep. Unfortunately, over an order of magnitude in SNR is lost when the second derivatives are taken, but the spectrum is now much more usable for analysis.

5.3.3 Comparison to Previous Techniques

The fast sweeping technique was compared against a typical spectrum taken with a lock-in amplifier. This second data set was taken with an analog frequency synthesizer

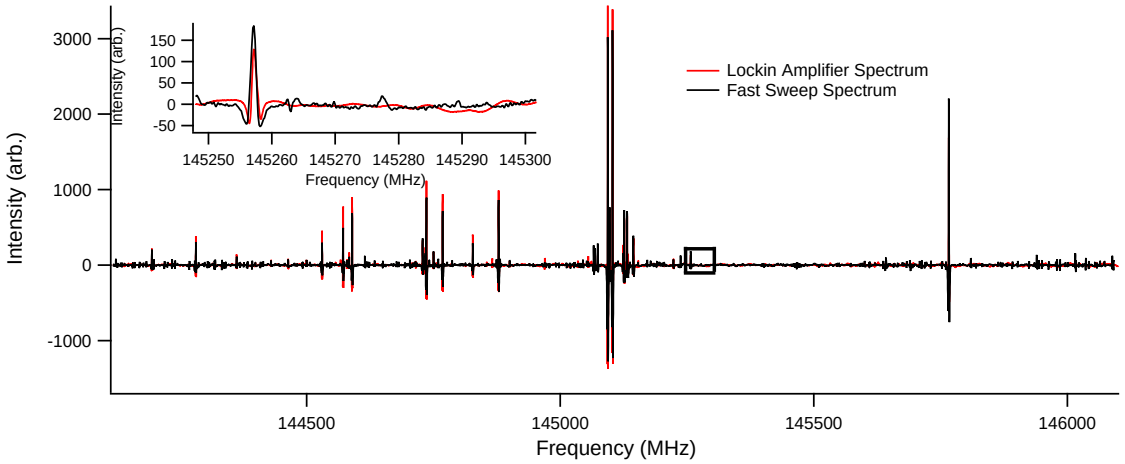

Figure 5.7: The second derivative of the fast sweep spectrum compared to the lock-in amplifier spectrum. The data sets were rescaled to fit on the same intensity scale.

whose output was multiplied with the AMC described above. The output of the synthesizer was frequency modulated at a 15 kHz rate. The light was detected by the same detector as described above, the output of which was processed by a lock-in amplifier, and the phase-sensitive, second derivative, amplified signal was recorded in a scanning routine that controlled the synthesizer and the lock-in amplifier. The signal was integrated for 100 ms per frequency point with a 30 kHz frequency point spacing taken over the same range as above. The spectrum took twice as long to take as the 1,000,000 average spectrum taken with the linear frequency sweep. The two spectra are compared in Figure 5.7. While the SNR for the raw sweep spectrum is higher, the SNR for the second derivative spectrum is an order of magnitude lower than for the spectrum taken with the lock-in.

A whole spectral scan can be taken in a fraction of a second with the fast scanning routine, but the SNR in just one scan is very poor. The ability to average many times is the most important advantage of this experiment. Analogous to CP-FTMW, the ability to average a large amount of spectra is what gives this experiment an advantage in sensitivity.

5.4 Conclusions

A new spectrometer has been developed that utilizes an AWG to produce linear frequency sweeps which are multiplied to the (sub)millimeter spectral range where the direct absorption spectra are recorded as a function of time. Methanol was examined over a 2 GHz range to show the functionality of the spectrometer in taking fast and sensitive data. While this frequency range was the focus of these benchmarking experiments, any frequency range could be accessed using the AMCs. The ability for rapid spectral acquisition compared to other techniques offers a huge advantage in the search for new spectral transitions. However, this spectrometer is still in development and several issues need to be resolved. The baseline subtraction needs to improved so that the full dynamic range of these spectra can be used. The time domain spurs need to be removed to increase signal-to-noise in these spectra. Also, the spectrometer needs to be adapted to pulsed valve experiments so that it can be used to search for exotic products, such as those discussed in Chapter 2.

6

Fast Sweeping Double Resonance

6.1 Introduction

Double resonance spectroscopy has been used for many high resolution experiments to extend the measurements of an experimental system to new frequency ranges and higher resolution. Microwave sources are typically used as a double resonance source, either as the transition pump or probe. When extended higher in frequency to the millimeter wave regime, new but less powerful light sources need to be used. A common scheme for double resonance using millimeter wave sources involves using a Fourier Transform Microwave (FTMW) spectrometer to probe a known microwave transition while pumping the transition using a scanning millimeter wave beam[112,113].

This technique is often used to extend the frequency range of these spectrometers by determining the connection between the upper state of a given microwave transition and a higher frequency transition. Currently, there are no spectrometers that use millimeter wave direct absorption spectroscopy to do double resonance spectroscopy with connecting microwave transitions. A new spectrometer has therefore been designed that combines chirped pulse technology with millimeter wave direct absorption experiments. The millimeter wave transition is probed using standard millimeter wave direct absorption spectroscopy, while a connecting state is pumped using a microwave source, where the detected signal comes from the millimeter wave absorption instead of the microwave. This technique would be helpful when a millimeter wave transition can be found but cannot be easily assigned, and therefore a microwave transition could be used to determine connecting states to aid in spectral assignment.

6.2 Experimental Design

A schematic of the experiment is shown in Figure 6.1. The fast sweep millimeter wave - microwave double resonance experiment involves combining an existing pulsed valve source and millimeter wave direct absorption spectrometer with a chirped pulse microwave spectrometer. The output of an analog signal generator (Agilent Technologies, E8257D PSG with options 1EA, UNU, 550, and UNT) was multiplied using an active multiplier chain (AMC). The AMC used in this experiment consists of a K_a band amplifier (Spacek Labs, SP3020-30-25B2) which is connected to a WR10 tripler (Virginia Diodes Inc.), the output of which is further amplified before a WR5.1 doubler (Virginia Diodes Inc.) that has an output frequency range of 140 – 220 GHz. The use of additional multipliers can extend this range to 50 GHz – 1 THz. The radiation was coupled into the vacuum chamber using a teflon lens mounted on a vacuum flange; this lens served to collimate the incoming radiation. The radiation was then focused using a second lens to a spot that lies $\sim$2 cm below the output of a pulsed

valve that drives a supersonic expansion. The radiation was focused into an output coupler which included a teflon lens $\sim$ 10 cm past the pulsed valve. This lens focused the radiation into a PVC tube that acted to guide the radiation. The radiation exited the chamber through a teflon lens mounted on a vacuum flange. The radiation was detected using an InSb hot electron bolometer (QMC Ltd., QFI/XBI) with $\sim$2 μs time response. The output coupler was covered with several layers of Eccosorb with 1 1/2 cm diameter openings in the middle; this allowed millimeter wave radiation to pass through to the detector but filtered out most of the microwave radiation.

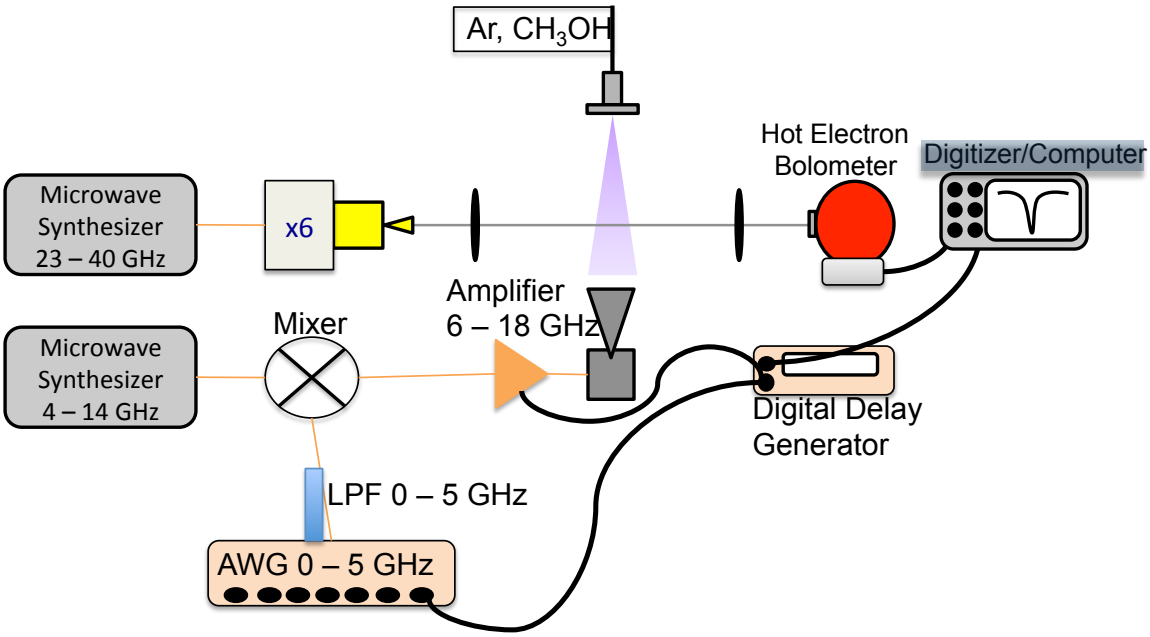

Figure 6.1: Schematic of the fast sweeping double resonance experiment.

The microwave double resonance signal was produced using the same model analog signal generator mentioned above, operated as a local oscillator (LO) whose output was from 4,625 – 13,900 MHz, which was mixed through a double balanced mixer (Miteq DM0520LW1) with an arbitrary waveform generator (AWG, Agilient M8190A), whose output was low passed from 0 – 5 GHz to prevent mixing with higher harmonics. A 50 MHz linear frequency sweep from 4,075 – 4,125 MHz over 25 μs was mixed with the synthesizer output. The lower sideband from the mixer was

bandpass filtered and then amplified using a 10 Watt solid state amplifier (Microwave Power L0618-40-T256) where the radiation was fed into the chamber and transmitted perpendicular to the millimeter and molecular beam. The feed horn was wrapped in thick Eccosorb that extended by over an inch past the end of the feed horn to prevent any stray microwave radiation from entering the millimeter wave output coupler. The feed horn was positioned so that most of the radiation would interact with the molecules in the supersonic expansion while minimizing the microwave radiation that reflected off of the pulsed valve and back into the millimeter wave output coupler.

The bolometer output was amplified using a low noise amplifier and was recorded using a National Instruments PCI-5124 digitizer card recording at 50 MSa/s. The timing of the AWG, amplifier, pulsed valve, and digitizer were controlled by a digital delay generator (Stanford Research Systems, DG645) pulsing at a rate of 50 Hz. The pulsed valve was opened for 2 ms per pulse. The amplifier was triggered 2 μs before and 2 μs after the AWG to prevent the mixing of the amplifier turn on/off signal with the microwave frequency sweep.

Several experiments were conducted to verify the functionality of this setup. First, methanol transitions were probed using a single pulsed valve to verify that the double resonance signal could be detected. Additional measurements of ozone were used to verify performance. This detection scheme was then applied to formaldehyde as a laser induced product of O(^{1}D) insertion reactions. This experiment therefore involved the use of the mixing source described in Chapter 4. Methylamine was used instead of ethylene as the precursor hydrocarbon, but the gas mixing, laser, and photolysis setup were the same as described in Chapter 4.

6.3 Results

6.3.1 Methanol double resonance

Jet cooled methanol was used as a first test case for this double resonance scheme. A schematic of the double resonance transitions is shown in the left side of Figure 6.2, where the upper state of the millimeter wave transition is pumped from the microwave transition. The right side of Figure 6.2 shows a time trace of methanol. Here, the millimeter wave radiation was fixed to the center frequency of the methanol transition and monitored in time as the pulsed valve opened and closed. As the methanol moves through the millimeter wave beam, the light is absorbed and this absorption is reflected as a voltage drop from the detector. Between 2 and 3 ms, the AWG was swept for only 25 μs with the frequency sweep centered on the methanol microwave transition. The double resonance signal is easily seen in this plot as the very narrow downward dip; detail is shown in the inset. This mostly downward dip means that when the microwave sweep was resonant with the methanol transition, the millimeter wave absorption increased. The total sweep bandwidth is about 50 MHz and the transition that results takes up at least half of that bandwidth.

This acquisition approach was then used to collect broadband double resonance spectra. The microwave synthesizer was stepped at 50 MHz intervals to produce

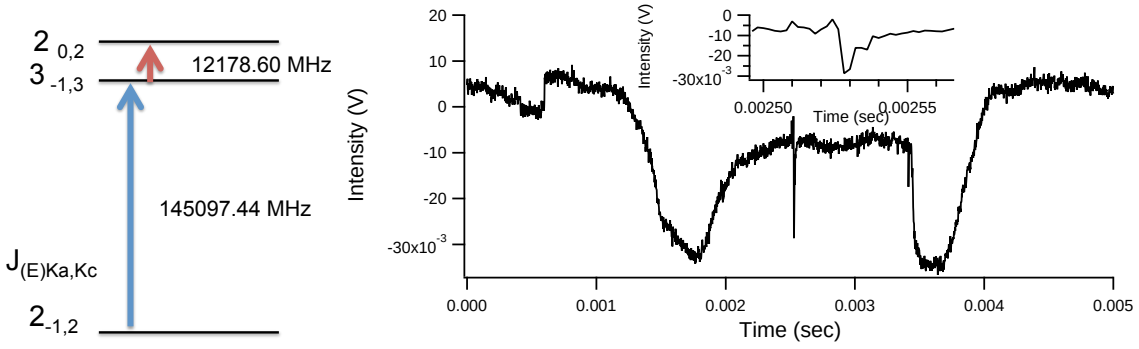

Figure 6.2: (Left) Transitions used for double resonance in the methanol system, not to scale. (Right) Time scan with of the pulsed valve opening for methanol. The inset shows there detail of the methanol double resonance signal.

amplified signals from 8500 – 13500 MHz, which covered the range that included the methanol double resonance. The time sweep over the double resonance signal for each LO frequency was recorded using the digitizer. The timing of the start of the AWG sweep was used to calibrate the start of the frequency sweep, with an additional scalar added to account for time delay from the bolometer response. A linear frequency calibration was applied to the spectra and cross-checked against the expected peak. This was done for each LO setting, and the sweeps were laid out as a segmented spectrum.

The total fast sweep double resonance spectrum is shown in Figure 6.3. The upward spikes are due to frequency-dependent microwave bleedthrough making it through the millimeter wave output coupler to the bolometer. While the bolometer is not optimized to detect microwave light, the detector still showed microwave response, and the signal would overload the preamp without the Eccosorb being present. The regular upward spikes seen in the spectrum are due to the response of the amplifier at the turn-on point for each sweep. The single downward signal seen in Figures 6.3 and 6.4 is due to the methanol double resonance. The only other possible source of downward spikes would be through overloading the bolometer with microwave

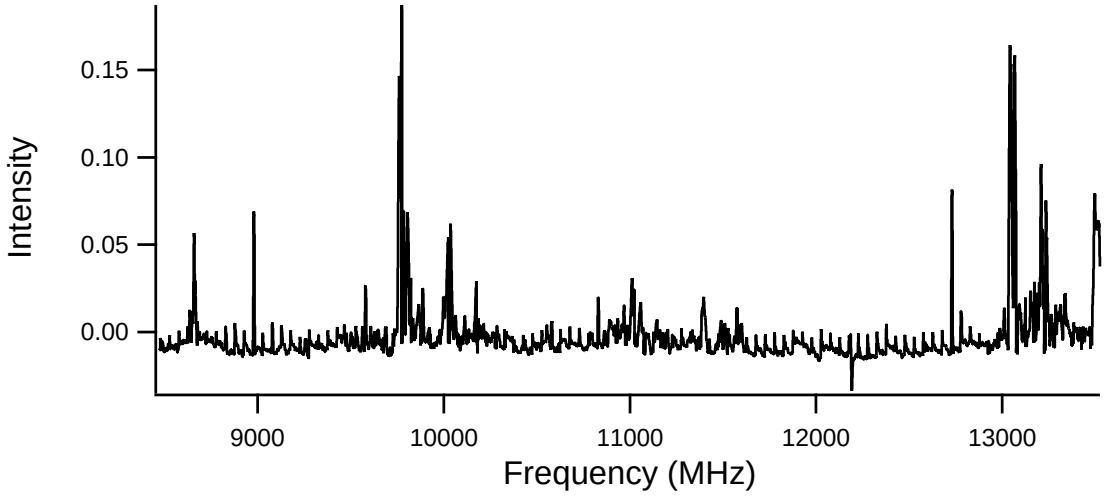

Figure 6.3: Segmented, frequency calibrated double resonance spectrum of methanol.

radiation due to inefficient Eccosorb shielding.

A background spectrum was acquired by tuning the microwave frequency to a setting that is not resonant with the methanol signal. The background subtracted spectrum is shown Figure 6.4, where the regular spikes and microwave bleedthrough have been subtracted out successfully while the double resonance signal remains. The microwave double resonance largely points in a negative direction, but has a portion that points in a positive direction. The line is roughly 20 MHz wide, which is much wider than the normal line width for these pressures and frequencies. This is likely due to power broadening from the high intensity (10 W) microwave signal. The negative direction of the methanol DR signal implies that the absorption increases for the millimeter wave transition.

Using the fast sweep instead of single frequency acquisition for the DR signal decreases the time it takes to record a full band spectrum. The entire 5 GHz range shown in Figure 6.3 was acquired in roughly thirty minutes. If the spectrum was taken using single frequency points, it would have required several hours of acquisition time.

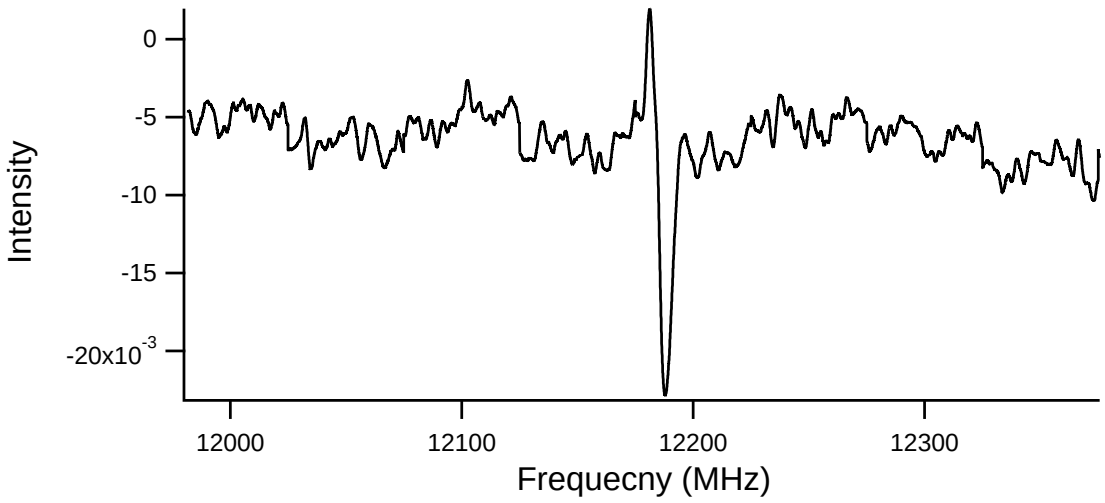

Figure 6.4: Segmented, frequency calibrated double resonance spectrum of methanol with background subtraction, highlighting the methanol double resonance signal.

6.3.2 Ozone double resonance

The double resonance spectrum of ozone was used as another test of what this detection technique can accomplish. A similar double resonance scheme was used for ozone as for methanol. The probed energy scheme is shown in Figure 6.5 where the upper level of the millimeter wave transition is the lower level of the microwave pump transition.

Figure 6.6 shows the ozone double resonance spectrum, including the off resonance background spectrum and background subtracted spectrum for comparison. The analysis approach used for this experiment was the same as for the methanol experiment described in Section 6.3.1. The background subtraction is again very effective in reducing the effects of microwave bleedthrough. The large amplitude variation observed in the background subtracted spectrum is likely due to the changing intensity of the ozone line from variations in the pulsed valve. This particular ozone transition is the most intense transition within the range of the spectrometer, therefore any variation in intensity is accentuated. The double resonance transition first modulates in a positive direction and then deeply in a negative direction, but with more negative intensity than the methanol transition.

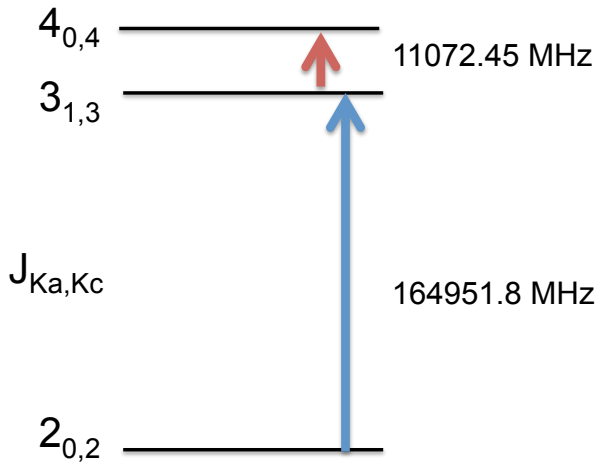

Figure 6.5: Transitions used for double resonance in the ozone system, not to scale.

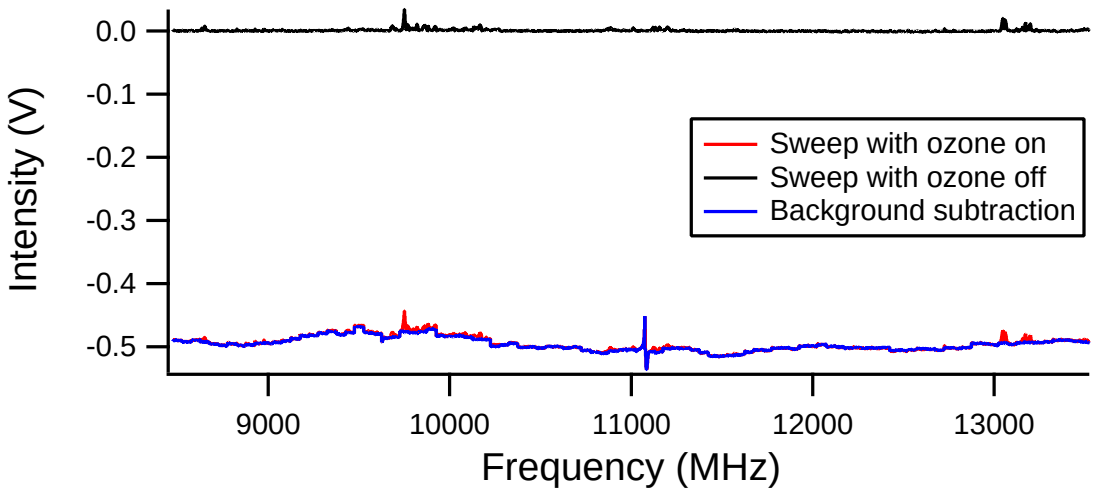

Figure 6.6: Segmented frequency calibrated double resonance spectrum of ozone with the black trace showing the spectrum with the off resonance millimeter wave frequency, red the millimeter wave on resonance with ozone, and blue showing the two spectra subtracted from each other.

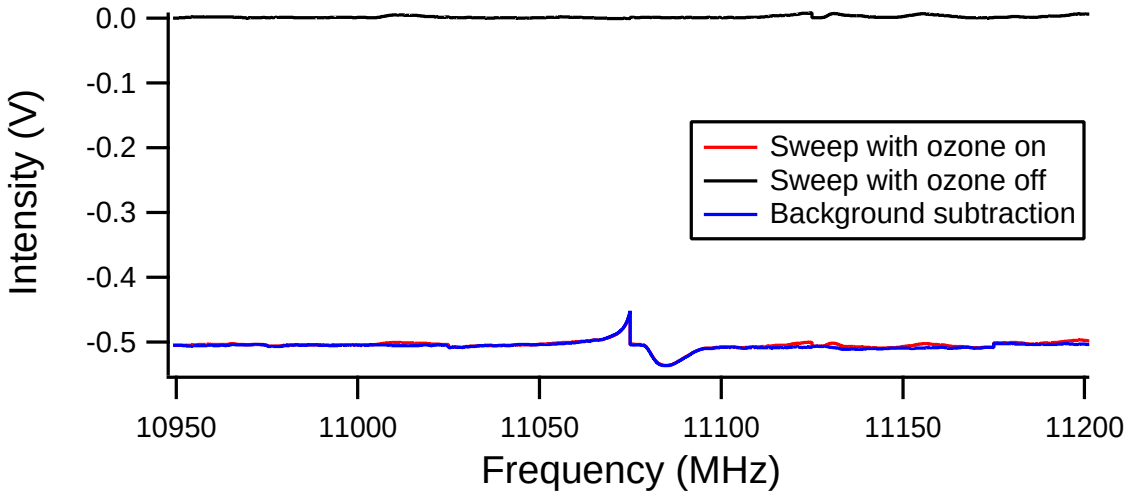

Figure 6.7: Segmented frequency calibrated double resonance spectrum of ozone with the black trace showing the spectrum with the off resonance millimeter wave frequency, red the millimeter wave on resonance with ozone, and blue showing the two spectra subtracted from each other, zoomed in on the double resonance signal.

A closer look at the transition is given in Figure 6.7. The double resonance signal straddled two different sweep segments and shows strange behavior. At the end of the lower frequency sweep, ozone starts to show resonance with the absorption of the millimeter transition by a decrease in signal. However, at the start of the next frequency sweep, the millimeter wave transition flattens out and then dips down,

indicating an increase in the absorption of the millimeter line. This line shape makes it hard to decipher which energy level would be tied to the microwave transition if this were a blind scan over an unknown molecule.

6.3.3 Formaldehyde double resonance

To further test this setup, an additional experiment was conducted focusing on a laser induced product was conducted. Formaldehyde was produced using laser photolysis of a mixture of methylamine and ozone at 248 nm in the experimental design described in Chapter 4. The formaldehyde double resonance scheme is shown in Figure 6.8. The photo-produced formaldehyde signal lasts for about 50 μs, which is enough time to use the frequency sweeps described earlier. The mixture was photolyzed in the fused silica tube before expansion, and that a cylindrical lens was used to focus the laser, which allowed the width of the rectangular laser pulse to be focused in such a way that the spot remained $\sim 1/2''$ long. This resulted in a longer transit time for formaldehyde through the millimeter wave beam.

The double resonance spectrum of formaldehyde is shown in Figure 6.9. The background spectrum was taken by turning the laser off while keeping the millimeter signal on resonance. The large spikes near the center of the scan are from random RFI from

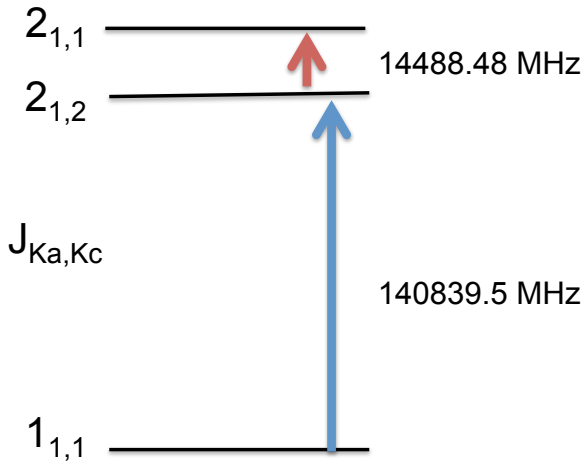

Figure 6.8: Transitions used for double resonance in the formaldehyde system, not to scale.

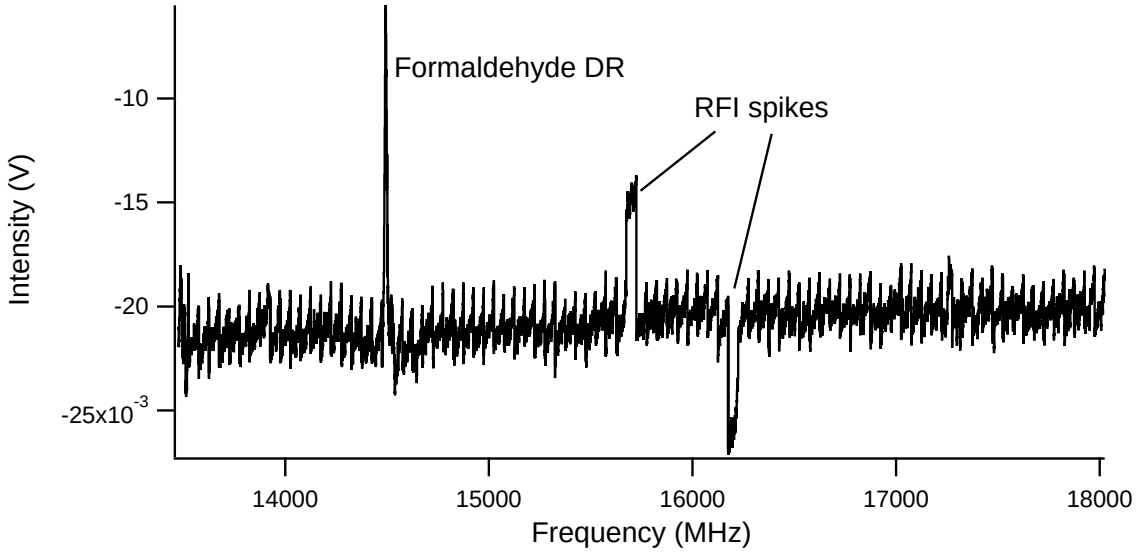

Figure 6.9: Background subtracted fast sweep double resonance spectrum of formaldehyde .

the laser interfering with the detector, which affects a whole frequency sweep. Better shielding around the detector and the detector's power supply usually decreases the affects of the RFI. The double resonance signal is clearly seen and points in a positive direction. This contrasts with the ozone and methanol double resonance spectra which have intensity in both directions. With metahnol, formaldehyde, and ozone probed using similar double resonance schemes, where the upper state of the millimeter wave transition is the lower state of the microwave transition, but yielding different lines shapes implies that the energy level scheme may not dictate the sign of the double resonance signal. Instead, the sign of the double resonance signal seems molecule dependent. Additional measurements are needed to further examine this signal response to determine whether there are any trends that can be used during spectral assignment.

6.4 Conclusions

A new double resonance scheme was used to connect direct absorption millimeter wave transitions with lower frequency microwave transitions while using fast sweep

technology. The fast sweeps from the microwave source allow for double resonance spectra to be taken extraordinarily quickly, taking only 30 minutes to complete an experiment that used to take several hours. The use of high power solid state amplifiers appears to power broaden the double resonance spectral lines, while the lines also have severe asymmetry that cannot be fit to a Gaussian profile. This technique is expected to be applied to millimeter wave spectra that are difficult to assign, where determining connecting microwave transitions will aid this process. The combination of this technique with laser-induced chemistry demonstrates how this technique can be applied to transient signals.

7

Methylamine + O(^{1}D)

7.1 Introduction

Aminomethanol ($HOCH_2NH_2$) is a molecule of significant astrophysical relevance due to the astrobiolgical implications of its chemistry. Its gas phase reaction with formic acid has been proposed as a pathway to form glycine, the simplest amino acid and a fundamental building block of life[3]. The importance of aminomethanol has led to it being studied in astrochemical models to test its formation in star forming regions[2] and in interstellar ice analogs[56]. While it is predicted to be stable in an interstellar environment[55], it has not been found in the interstellar medium due to a lack of a laboratory pure rotational spectrum to guide its astronomical detection. This is due

to its terrestrial instability. Therefore, I propose to produce this molecule using the O(^{1}D) insertion reaction into methylamine (CH_3NH_2) as theoretically proposed in Chapter 2. The instrument described in Chapters 3 and 4 was used to search for its pure rotational spectrum, with additional improvements that were explored in Chapter 5. The initial results from these experiments are presented here.

7.2 Experimental

To produce and probe aminomethanol, the O(^{1}D) insertion into methylamine was undertaken using the same spectroscopic setups as described in Chapters 3 and 4. This required the combination of ozone and methylamine, millimeter wave spectroscopy, and laser photolysis.

The photolysis setup used in Chapters 3 and 4 was utilized to produce O(^{1}D) in this mixture. The single valve photolysis source was first used to produce O(^{1}D). However, ozone and methylamine readily react and produce a black liquid behind the pulsed valve that would clog the valve, coat the silica tube with an absorptive contaminant, and reduce the concentrations of the reactants before laser photolysis. Therefore, the dual pulsed valve mixing source as shown in Figure 4.1 and described in Section 4.2 was used. This allowed for the reactants to interact for only a short period of time before entering the fused silica tube for laser photolysis. Behind one valve was a mixture of argon (Nexair, ultra high purity) and methylamine (AirGas, 99%), held at or just below atmospheric pressure with methylamine making up 10% of the mixture. Behind the other pulsed was oxygen (Nexair, ultra high purity) and ozone held at 900 Torr with the mixture containing ∼1% ozone. The ozone was produced using a Pacific L11 Ozone generator. The pulsed valves were timed to open simultaneously, releasing gas into the mixing block where the gases mixed briefly and passed through the fused silica capillary tube, before supersonically expanding out into the vacuum chamber. The valves were driven at 50 Hz with a 2 ms open time

duration. The gas pulse had a length of >4 ms as it crossed the (sub)millimeter radiation. The chamber pressure was maintained between 50 – 70 mTorr.

O(^{1}D) was produced by laser photolysis of ozone using the same setup as described in Chapter 4. The output of the laser was focused using a cylindrical lens. The half of the fused silica tube closest to the output into the chamber was illuminated by the laser. The products from the laser initiated reactions would transit the spectroscopic setup for ~ 50 μs, which is important for the fast sweep method used in this experiment (described below).

The spectroscopic setup and acquisition are the same as described in Chapter 3. The spectral resolution ranged from 0.03 to 0.06 MHz. Most spectra were averaged 128 times and analyzed the same way as described Chapter 3. Some later experiments used a fast sweeping method similar to those described in Chapter 5 and described below. The digitizer described in Chapter 4 was integrated into the experiment for the fast sweeping method, but was also used for the point-by-point scanning routine in conjunction with the fast sweeping method.

7.2.1 Fast Sweeping Spectroscopy in a Pulsed Experiment

For the fast sweeping experiment described in Chapter 5, the detector normalizes the baseline to 0 V because radiation is constantly being detected. However, the pulsed valve/pulsed laser experiment is much lower duty cycle than that experiment. In the pulsed experiments, the radiation free background of the detector is normalized to 0 V, while the background when radiation is present is much higher. This reduces the dynamic range of any molecular signals, so that only the strongest molecular signals could be detected. To circumvent this issue, continuous radiation is directed towards the detector with the fast sweeping signals superimposed onto the continuous light beam. This allowed the detection of pulsed molecular signals using fast sweeping to be applied in this experiment.

The signal generator that is used in the traditional direct absorption spectroscopic setup was also used to generate the necessary fast linear frequency sweeps. This was accomplished by using frequency modulation to impose a frequency sweep on the input radiation signal. This approach used a triangle wave modulation, rather than the sine waves typically used in frequency modulation, so that the frequency sweep would be linear. This had some advantages over the arbitrary waveform generator (AWG) method of producing linear frequency sweeps. One was that radiation would be CW into the experiment and would not cause the detector to undergo large changes in the baseline. Also, this method forgoes the use of an AWG, which greatly reduces the cost of the experiment.

The spectroscopic setup is the same as in Chapter 3. The modulation settings from the signal generator were 10 kHz rate with +/- 500 kHz deviation for a triangle wave instead of a sine wave. When this signal was multiplied by the active multiplier chain, the total bandwidth was +/- 3 MHz from the center frequency. The radiation is detected by the bolometer whose output is amplified and recorded by a National Instruments digitizer. The bolometer has $\sim$ 2 μs time response, which must be included in the frequency calibration. Each linear frequency sweep lasts 50 μs, so the timing needs to be adjusted so that one frequency sweep overlaps the entire laser induced signal. The spectra were recorded at 10 MSa/s with acquisitions lasting 250 μs. A sweep rate of 6 MHz/50 μs was a good compromise between sweeping quickly and maintaining signal intensity. A total of 2,500 points were collected for each scan, which resulted in 0.015 MHz frequency resolution for the fast sweeping method. A total of 100 – 1,000 averages were acquired for each scan. A new scan was taken every 6 MHz, and the data were combined at the end of scanning to make one contiguous spectrum. The timing of the pulsed valves, laser, and digitzer were controlled by a digital delay generator, which was also locked to the same 10 MHz Rb clock as the signal generator. This was important for precise timing and coherent averaging.

An example of the fast sweeping method for pulsed spectroscopy is shown in Figure 7.1. The top spectrum shows a single frequency time trace centered on a formaldehyde line center. The time trace follows laser produced formaldehyde as it moves through the spectroscopic beam. The laser RFI spike has been removed. The absorption signal results in a nearly -200 mV negative deviation from baseline. The middle trace shows the fast sweep method as it sweeps through the same formaldehyde transition, which requires precise timing so that the sweep and molecular signal overlap. The sweep is centered on the formaldehyde transition and deviates 3 MHz above and below the line center. The downward slope of the first sweep is due to the frequency dependent response of the detector and power variation from the spectroscopic source. The bottom trace shows the electronic modulation output from the signal generator, with the voltages scaled to the frequency output. The upward slope of this trace indicated that the linear frequency is actually moving higher in frequency. The detector signal

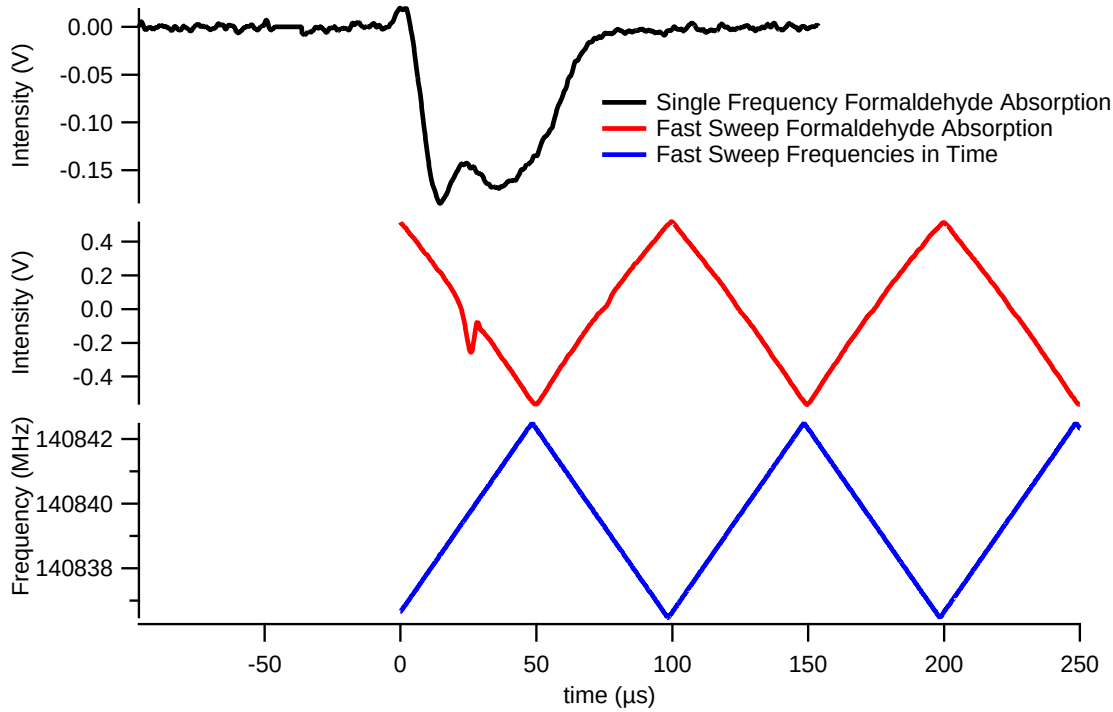

Figure 7.1: The single frequency time scan over formaldehyde (top), 5 fast frequency sweeps centered on the formaldehyde line (middle), graphical representation of the frequency sweeps in real time (bottom).

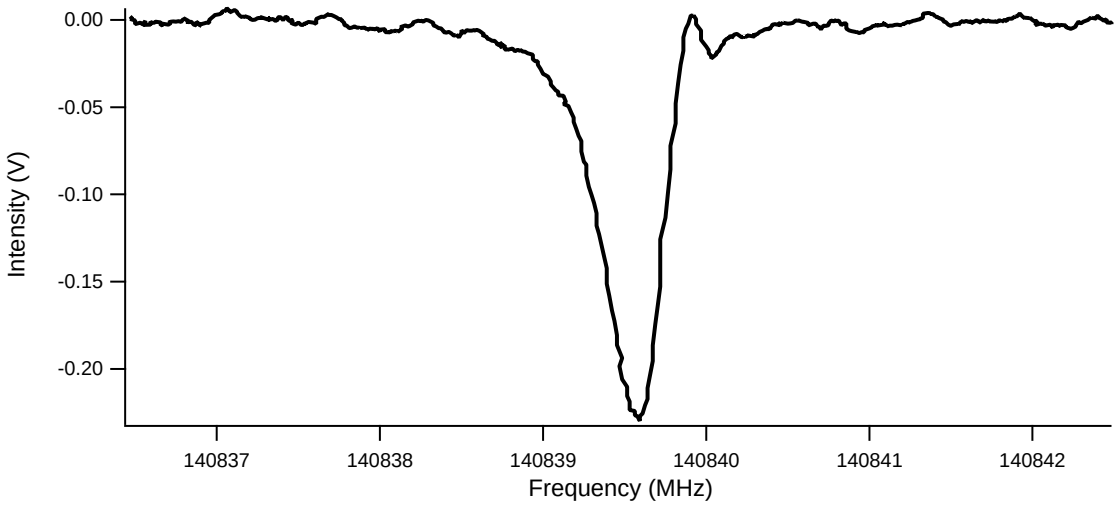

Figure 7.2: The frequency calibrated and baseline subtracted data from the middle and bottom trace of Figure 7.1.

is not sensitive to the direction of the sweep, so this electronic signal is recorded to determine if the first sweep is downward or upward in frequency.

Five linear frequency sweeps were detected per setting so that a signal and background spectrum could be taken simultaneously. Five sweeps were collected to ensure sufficient separation between the signal and background sweeps. The first sweep was set to always contain the molecular signal while the fifth sweep contained only background. To produce flat baselines, the first and fifth sweeps are subtracted from one another. This was performed on the data from Figure 7.1 as shown in Figure 7.2 for formaldehyde. The unusual lineshape is common for formaldehyde in this experiment. This method of baseline correction works very well for the pulsed experiment as opposed to the experiment in Chapter 5, where background subtraction was not effective. This is likely due to the baselines being taken immediately after each sample acquisition, with gas and pressure settings being roughly the same for each sweep. However, only baselines that swept the frequency in the same direction as the signal acquisition could be used for baseline subtraction. Background subtraction from the opposite direction resulted in more amplitude variation than from baselines sweeping the same direction. This simultaneous sample and background acquisition makes the

data analysis from the pulsed experiment very straightforward.

7.2.2 Scanning using artificially enlarged bandwidth

In another attempt to increase scanning speed in the single frequency acquisition experiment, the bandwidth of the microwave pulse was artificially increased to search for weak transitions, enabling larger step sizes to be used. The triangle modulation was used from the signal generator but was run at a 100 kHz rate with only 75 kHz deviation. This led to a 900 kHz wide sweep after multiplication that would be integrated in time and detected as one frequency point. The routine was stepped at 400 kHz step sizes so that > 2 points could overlap over a given transition. The key to this scanning method is that the signal generator and the delay generator, which controls the timing of the valves, laser and digitizer, are *not* tied to the same 10 MHz Rb clock. This allows for averages that lead to a blurring of the signal bandwidth. This method allowed for a ~ 5 times increase in scanning speed, but required reacquiring observed transitions using the standard point-by-point scanning method. This approach is much slower than the fast sweep scanning method, but is usable for signals that are < 30 μs long that would not be suitable for acquisition with the fast sweeping method. While this method of scanning was useful for much of this experiment, the fast sweep scanning method surpassed it easily in terms of acquisition speed. Therefore, spectra from this technique will not be shown or discussed further.

7.3 Results

7.3.1 point-by-point acquisition vs. fast sweep acquisition

Spectral acquisition using the fast sweep technique is much more rapid than point-by-point technique used in Chapters 3 and 4. The step size in the fast sweep experiment is 6 MHz, whereas the step size for the point-by-point technique is only 0.06 MHz. If the same number of averages are taken using each method, the fast sweep is 100

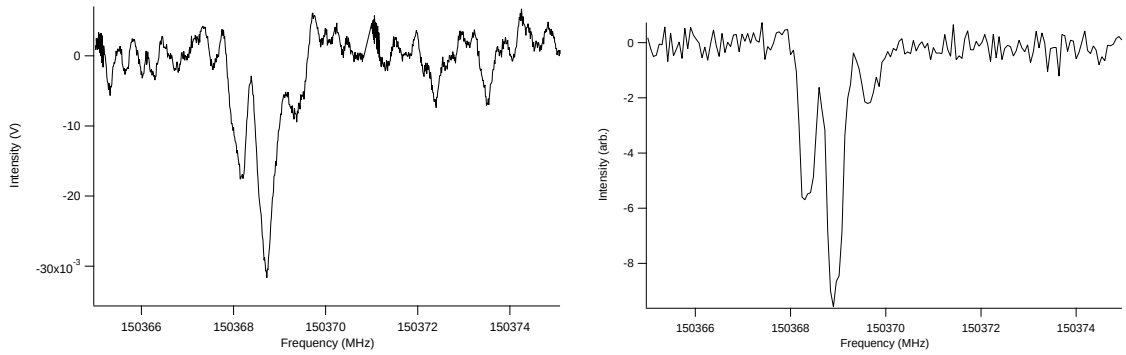

Figure 7.3: Fast sweep over hyperfine transitions of an unknown carrier (left) and single point acquisition over same unknown carrier (right).

times faster. However, the fast sweep method has a loss of SNR compared to the point-by-point acquisition. Figure 7.3 shows the two methods compared side by side over a laser induced transition from an unknown carrier in the methylamine + O(^{1}D) experiment. These acquisitions each involved 100 averages. The SNR for the fast sweep acquisition (left) is 13 and the SNR for the point-by-point acquisition (right) is 27. The fast sweep spectrum took $\sim$ 5 s for acquisition while the point-by-point spectrum took almost 6 minutes to acquire. The factor of 2 in the SNR can be reduced by increasing averaging for the fast sweep routine, which would still result in an increase in spectral acquisition speed as compared to point-by-point acquisition.

The fast scanning method does have some pitfalls for this experiment. While the fast scanning method is much more rapid than the single point acquisition, it is susceptible to false positives. When the laser fires, an RFI spike is detected by the bolometer. However, sometimes this RFI severely affects the power supply for the bolometer, which can overload the signal from the detector for up to 100 μs after the laser fires. This is seen sometimes as the same shape as a strong spectral line in the fast sweep routine, despite being a false positive. More shielding around the power supply for the detector seems to help, but this does not always block the severe RFI. Also, a signal occasionally appears in some of the fast sweeps as spikes that are at regular intervals and intensity. While these are easy to identify in a spectrum,

they occasionally overlap with and obscure real spectral lines. These spikes appear to come from the signal generator, but the cause has not yet been pinpointed. To get around this issue, different equipment would have to be used to produce the fast linear sweeps. An AWG would have to be reprogramed for use as a CW signal generator with timing and phase stability. Also, a Direct Digital Synthesis (DDS) chip could be used to produce similar linear frequency sweeps as the AWG. Both of these devices have been used to generate linear frequency sweeps in the microwave for chirped pulse spectroscopy[102,114], but the DDS would be much cheaper to implement.

To get around both of the above issues with the fast sweep routine without adding new equipment, point-by-point acquisition is performed on each suspected transition found in the fast sweeping scan. This confirms that a line is real and also gives a frequency calibration to check against in the fast sweep routine. However, performing single point confirmation scans over transitions is still time consuming. While 10 GHz can be covered in 3 hours with the fast sweeping routine, it takes about the same amount of time to confirm the spectral lines found in a sweep. For a denser spectrum, this could take even longer. This still leads to an increase in overall scanning speed, but does slow down the effective rate of taking a fast sweep spectrum.

7.3.2 Products Detected

Over the course of the methylamine + O(^{1}D) experiment, several products have been detected in the search for aminomethanol. These products are listed in Table 7.1. These molecules were identified through comparison with the information found in the JPL[67] and CDMS[87] spectral databases. The largest molecule found was formamide ($HCONH_2$), while NO was the smallest molecule found. No potential energy surface has been constructed to explore all of the decomposition products of aminomethanol, n-methlyhydroxylamine, or methoxyamine, but experience from previous experiments described in Chapters 3 and 4 can help to explain the products observed.

Table 7.1: Products observed, expected, and searched for in the methylamine + O(^{1}D) experiment

Observed	Expected	Not Detected
$O_2(^1\Delta)$	CO	CN
NO	H_2O	HONO
HNO	NH_3	NCO
HCN	OH	NH_2OH
HNC		H_2CNOH
HO_2		CH_3NHOH
NO_2		HOCN
H_2CO		NH_2CN
HOOH		HO_3
H_2CN		
HCNO		
HNCO		
CH_3O		
CH_2NH		
CH_3OH		
$HCONH_2$		

The theoretical work of Feldmann et al.[55] explores the formation of aminomethanol from formaldehyde and ammonia and its subsequent decomposition to water and methylenimine (CH_2NH). Assuming that aminomethanol is being formed in the insertion of O(^{1}D) into methylamine, both of these channels could act as decomposition channels. Indeed, both formaldehyde and methylenimine are found. Formaldehyde and methylenimine have some of the strongest spectral transitions amongst the laser induced products. A sample spectrum of methylenimine is shown in Figure 7.4, with the hyperfine pattern obviously visible. Ammonia and water were not detected in the experiment due to their transitions lying outside the range of the spectrometer.

Both OH and CH_2NH_2 radicals are expected from the dissociation of aminomethanol. Neither of these products are detected in the experiment, but their chemistry likely affects the other detected products. Other detected products are unlikely to form from the direct dissociation of aminomethanol. Instead, further reactions involving the dissociation products must be invoked to explain this chemistry. The chemistry of CH_2NH_2 with O_2 has been explored by Rissanen et al.[115], which predicts several

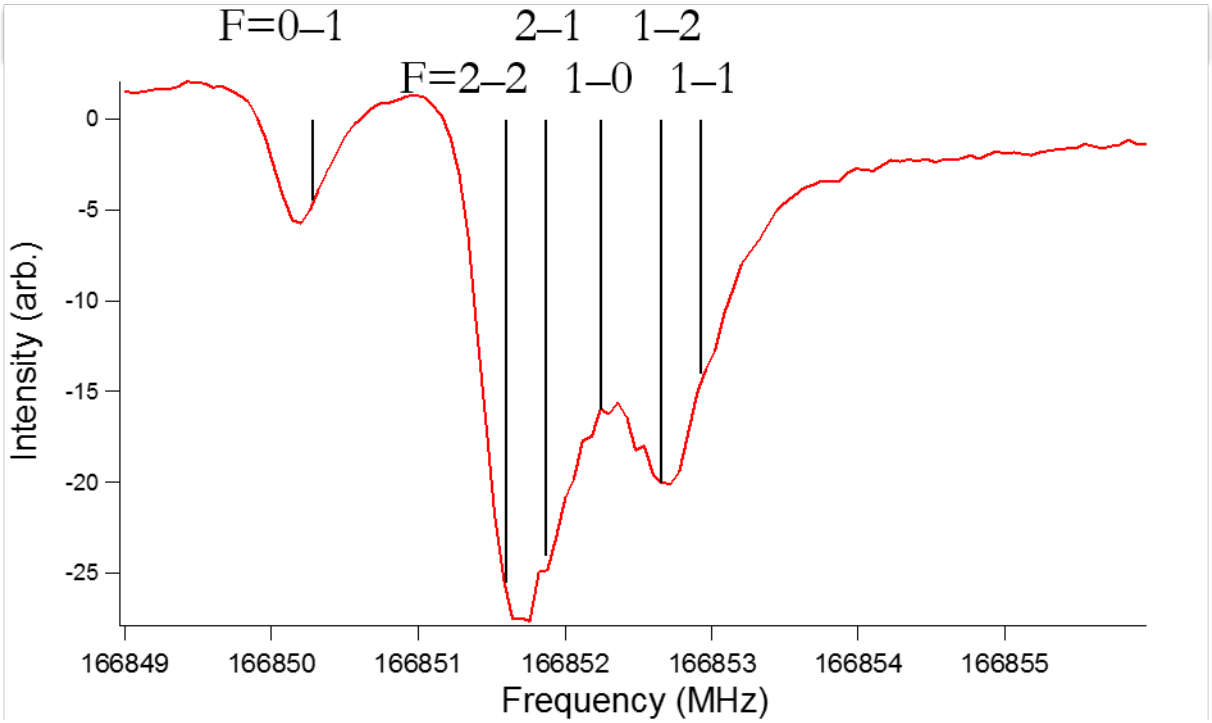

Figure 7.4: The $J_{Ka,Kc}$ $1_{1,0} - 1_{0,1}$ transition of methylenimine, with an overlaid stick spectrum indicating where predicted hyperfine transitions should occur.

channels forming in this reaction. One of these channels was predicted to be oxygen hydrogen abstraction leading to HO_2 and methylenimine formation, as well as formamide and OH formation. All of these molecules except OH were detected in the experiment, while OH was not detected due to its transitions occurring outside of the spectral range of the instrument. The smaller, less saturated molecules shown in Table 7.1 were likely formed from successive hydrogen abstraction reactions involving O_2, HO_2, and OH. More quenching of the insertion reaction could reduce formation of these molecules. Also, using a method to produce O(^{1}D) without so much excess oxygen might lead to fewer of these products forming. The most interesting chemistry amongst these products was the formation of HNO and NO. The HNO absorption peaks $\sim$ 10 μs before and $\sim$ 10 μs after the rest of the laser induced products, with NO absorbing where the HNO absorption decreased. The reason for this behavior has not yet been explained.

The products that were not detected in this experiment were likely the result of having transitions that lie outside of the explored frequency range. Alternatively, these products could have been formed in too low of abundance to be detected. While the HNCO and HCNO isomers were detected, their other well predicted structural isomer, HOCN, was not. The products HNO, NO, and NO_2 were all detected but HONO was not. A search for the structural isomer of formamide, formaldoxime (CH_2NOH), was conducted based off of previous microwave spectroscopy[116], but no transitions were detected. A search for the other structural isomer of formamide, nitrosomethane (CH_3NO), was not attempted due to previous spectroscopy predicting large internal motion[117,118], which complicates the spectral extrapolation. A search was also conducted for the direct product expected to form from the reaction of O(^{1}D) and methylamine, n-methylhydroxylamine. The previous microwave measurements[75] were fit, and a spectral prediction extrapolated to the millimeter region, but no conclusive transitions were found. Two transitions of unknown carrier(s) were found that were close to a predicted n-methylhydroxylamine transition as shown in Figure 7.5, but none of the other predicted transitions for this molecule had any observed transitions near them. A search was not conducted for the other product from direct reaction with methylamine and O(^{1}D), methoxyamine, because of internal motion complicating the prediction of its spectrum[71].

7.4 Search for Aminomethanol

The spectral predictions of aminomethanol from Chapter 2 were used to guide a spectral search. Initial experiments focused on some J=2-3 transitions in the 140-150 GHz range along with several other low J transitions. The J=2-3 transitions should be better predicted than higher J transitions that would be observed in other frequency regions. This frequency range is also an optimal range to use in the spectrometer, as it involves the overlap of high spectral power and optimum detector response.

Scanning commenced with the point-by-point scanning routine, which only covered the first 8 GHz of this range over the course of a year of laboratory effort. After the development of the fast sweeping technique, the range from 140 to 167 GHz was covered in just two days.

Transitions from unknown carriers were difficult to find at first, given the limitation in spectral acquisition speed. Figure 7.5 shows the first lines from unknown carrier(s) found in the experiment. The most intense lines found so far are shown in Figure 7.6. The hyperfine pattern shown in Figure 7.6 is indicative of a carrier that contains nitrogen. Another transition that showed similar hyperfine splitting and strength was found after the use of the fast scanning routine. This feature is shown in Figure 7.3 and in Figure 7.7 on the far left. The spectrum in Figure 7.7 contains another transition from an unknown carrier as well as a formaldehyde transition. This illustrates the utility in using the fast sweep technique: lines searches can be conducted over a broad frequency range relatively quickly.

The unidentified spectral lines collected from these blind searches are shown Table 7.2. The lines were compared to the spectral prediction given in Chapter 2, and the spectral fitting program SPFIT[101] was used to try to fit these spectra to an asymmetric top Hamiltonian. However, none of the fits yielded conclusive results. There is a

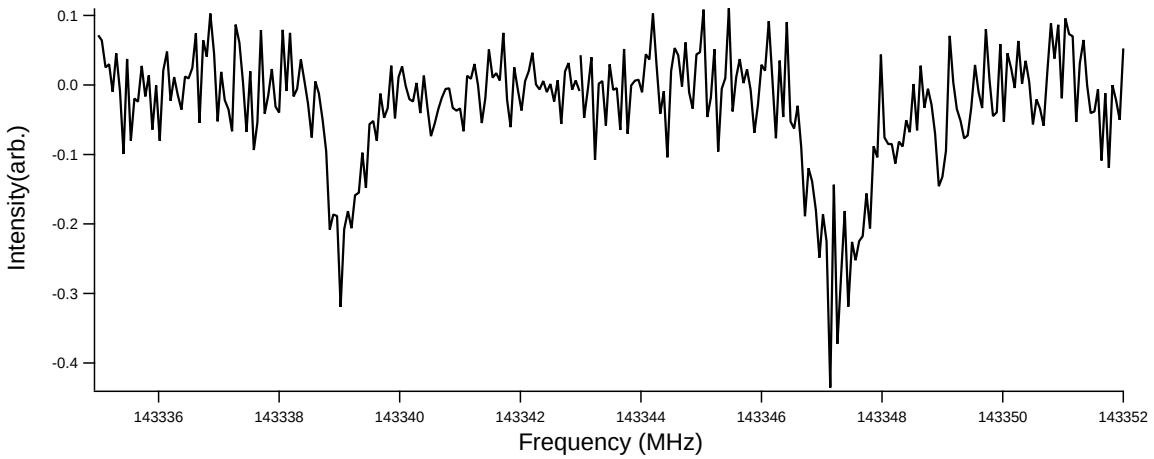

Figure 7.5: Two transitions of unknown carrier occurring near the frequency of an expected n-methylhydroxylamine line.

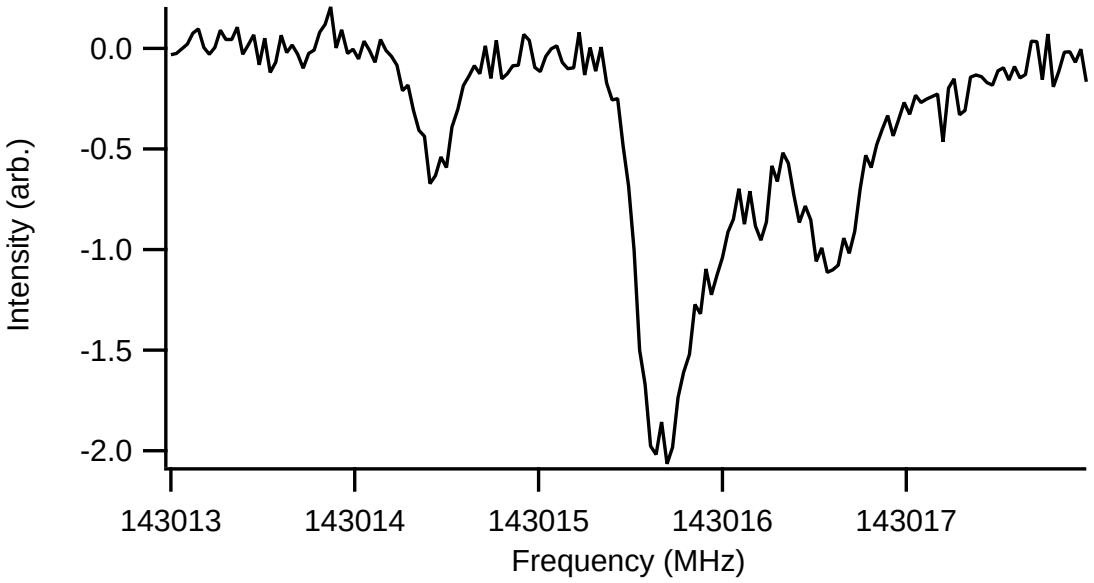

Figure 7.6: Hyperfine split line from an unknown carrier.

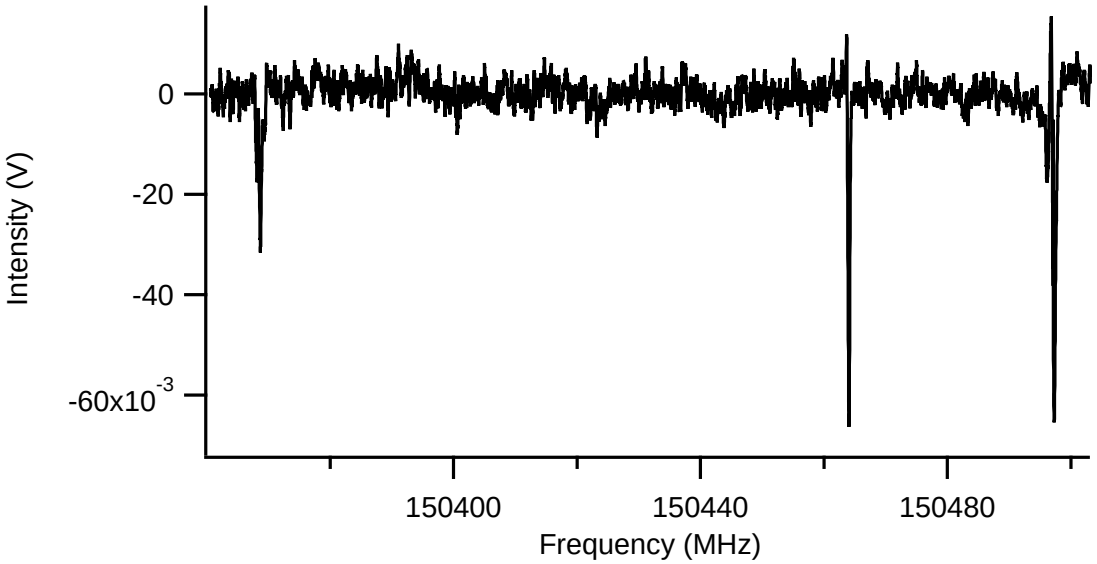

Figure 7.7: Fast sweep spectrum of the O(^{1}D) and methylmaine laser induced chemistry. The far right transition is formaldehyde, with the other two large transitions arising from unknown carrier(s). The rightmost transition is the same as shown in Figure 7.3

high barrier pathway that may form aminomethanol from ozone and methylamine[119]; therefore, transitions from laser-induced and non-laser-induced (dark) chemistry are included in the Table. Several lines were detected near 146 GHz, which is encouraging because this is the location of a strong Q branch for aminomethanol. However, no

Table 7.2: Transitions from unknown carriers found in the experiment of methylamine + O(^{1}D). The line in the middle indicates the cutoff between transitions being found by the single point acquisition scans (above) or the fast sweep scan (below).

Transition (MHz)	Hyperfine	Dark Product	Comments
143015	yes		Strong
143339.1			weak
143347.3	maybe		weak
146635.6			weak
146757.2			weak
146813.2			weak
146837.4			weak
146893.7			weak
143573	maybe		wide, weak
151747.6			
147217	yes	maybe	
141386.5		yes	
142174.3		yes	
142228.5		yes	
145240	yes	yes	many lines
145605	yes	yes	
145480.6			possibly vinlyamine
145685	maybe	yes	wide separation
148514	yes	yes	
150369	yes		Strong
150464.2			close to formaldehyde
161730.9		yes	
166286.5			
166440.9		yes	

pattern could be discerned from the lines that were found and attempts at assignment yielded no conclusive results. Additionally, the strong lines mentioned above are possibly from the same carrier. However, the spacing of these lines indicates that they may not arise from aminomethanol, as does the lack of a detection of similar strong lines at appropriate frequency spacings. None of the other combinations of lines have yet yielded a successful fit to aminomethanol.

Based on the products that have been identified from the reaction between O(^{1}D) and methylamine, aminomethanol is likely forming in this experiment. The energetics compared to previous experiments and from the theoretical work also indicate that

it should be stabilized in this experiment. The work of Feldmann at al.[55] is the only work to date that examines aminomethanol decomposition, and as discussed above, there are two channels for decomposition. Both of these channels were found to be exothermic in their calculations, with a 40.9 kcal/mol barrier to the ammonia and formaldehyde channel and a 55.1 kcal/mol for the methylenimine and water channel. The insertion of O(^{1}D) into methylamine was predicted to release 152 kcal/mol which is more than enough energy to surpass these barriers and lead to unimolecular dissociation unless the excess energy in aminomethanol is quenched. In the ethylene + O(^{1}D) experiment discussed in Chapter 4, vinyl alcohol has an exothermic dissociation pathway leading to acetaldehyde with a 56.9 kcal/mol energy barrier[91]; nonetheless, vinyl alcohol was detected. However, vinyl alcohol was the dominant product in that experiment, showing that it could effectively be quenched despite the accessible dissociation channels. This implies that for aminomethanol, the water + methlyenimine pathway may not be a significant channel for dissociation but the other channel might be significant. Additional quenching may still be a necessity in the methylamine + O(^{1}D) reaction to form aminomethanol. There are many additional experimental parameters that can be explored to further pursue aminomethanol experimentally in further experiments.

7.5 Conclusions and Outlook

The O(^{1}D) insertion reaction into methylamine was studied, and searches for the pure rotational spectrum of aminomethanol were conducted. The spectrometer used to searched for aminomethanol was a (sub)millimeter spectrometer that incorporated a new fast sweeping technique. While transitions belonging to aminomethanol may have already been found, no assignment of a spectrum has yet been possible. Many transitions from known and unknown carriers were found, but no identification of a new molecule has yet been made. The recently implemented fast sweeping technique

has greatly increased the speed of spectral acquisition and will likely lead to the assignment of new molecular spectra, and hopefully identification of aminomethanol.

The work discussed in this dissertation has built up to performing the experiments to search for the astronomically and astrobioloigcally relevant molecule aminomethanol. The theoretical work described in Chapter 2 laid the foundation for what to expect from O(^{1}D) insertion into methylamine, specifically what products are possible in that system and also to predict its pure rotational spectrum. The experimental design was presented in Chapter 3, where a mixture containing backing gas, ozone and methane was photolyzed using an excimer laser to produce the O(^{1}D), which reacted with methane to produce methanol. This experiment was successful and hinged on the important pulsed valve photolysis source that produced the reactive mixture in a fused silica tube before supersonic expansion in a vacuum chamber, where the mixture can be probed using (sub)millimeter spectroscopy. The experiment was extended in the ethylene + O(^{1}D) experiment to probe vinyl alcohol, as described in Chapter 4. A new mixing source that included two pulsed valves was developed to allow study of products resulting from of a reactive gas mixture. The detection of vinyl alcohol also confirmed that unstable molecules could be produced using this experimental approach.

One of the issues found in the early experiments was that the spectral acquisition speed was extremely slow. New methods were therefore developed to increase the spectral acquisition for (sub)millimeter spectroscopy. As described in Chapter 5, fast linear frequency sweeps were used to take broadband spectra of methanol. Averaging was used to increase the sensitivity of this instrument. The same fast frequency sweep was also applied to millimeter - microwave double resonance experiments, where the microwave signal was swept in time and the response was recorded on a millimeter wave transition, which greatly decreased the time it takes to acquire double resonance spectra. The experiment described in the above Chapter combined all of these ideas

and techniques to search for aminomethanol. The insertion of O(^{1}D) into methylamine, the implementation of a (sub)millimeter spectrometer that incorporated the laser induced production of O(^{1}D), the identification of insertion products, and the applications of fast linear frequency sweeps all led to the design of a new unique spectrometer that can be applied to searches for unstable molecules such as aminomethanol.

A

Appendix A

A.1 Scripts for use of the VPT2 program in CFOUR on the Emerson Center Computing Cluster

The scripts here are for performing ZPE corrections to molecules using second order vibrational perturbation theory (VPT2) using the CFOUR program[60] on the Emerson Center for Scientific Computing at Emory. The method here is adapted from this website[68] and from kind input from Dr. Sven Thorwirth. The impetus for high level ZPE corrections was driven by the work of Puzzarini et al.[57]. Using CFOUR instead of GAUSSIAN allows the use of CCSD(T) methods and also allows for the program to be manually run in a parallel computing environment. That is, it allows the user

to break apart the job into smaller chunks so that accurate anharmonic force fields can be built without running out of computing time, and for several jobs to be run amongst several clusters. The methods described here were tested on the system described in a study by Gauss and Stanton[120] and compared against the results from this paper. The files that were used here can also be found in the Emerson Center directories under: spark/swidicu/bmhays/test/quar.

A.1.1 Procedure

The method described on the ACES website[68] is still what is used in the modern CFOUR program, except with ACES replaced with CFOUR and CUBIC replaced with VPT2 in the input files. The issue with using this method as it stands is that it creates an incredible amount of data, which can easily go beyond 30 GB, especially using triple zeta basis sets. 30 GB is the maximum for our current Emerson Center account, so something had to be done to remedy this situation. The solution involves submiting the secondary jobs through standard LoadLeveler scripts while the beginning and end jobs are performed in the group's main directories.

A GENBAS basis set file needs to be downloaded from the CFOUR website and stored in the home directory for the cluster that will be used. In the working directory, the following files will be needed: start.cmd, zcommand.cmd, final.cmd, and a molecular input file (denoted as C3H2_DZ.inp which was used in this case).

The molecular input file, C3H2_DZ.inp, is an example of a standard input file for CFOUR. The structural and computational parameters for this file were taken from Gauss and Stanton[120]. For practical purposes, the structure used should be optimized to 10^{-10} Bohr/Hartree level before attempting this method. The file is given below:

```
C3H2
H
C 1 r1
C 2 r2 1 a1
```

```
C 3 r2 2 a2 1 d180
H 4 r1 3 a1 2 d180

r1   =         1.092452799126381
r2   =         1.451489303832762
a1   =       148.484926695106935
a2   =        55.198374655186875
d180 =       180.000000000000000

*CFOUR(CALC=CCSD[T],BASIS=PVDZ,CONVERGENCE=10
CC_CONV=10,LINEQ_CONV=10,SCF_CONV=10
CC_PROG=ECC
SCF_DAMP=500
MEMORY=48
MEM_UNIT=GB
ANHARM=VPT2
VIB=EXACT
ANH_ALGORITHM=PARALLEL
INCORE=EVERYTHING
ABCDTYPE=AOBASIS)
```

The important points in the input file are the VPT2, EXACT, and PARALLEL lines. The rest of keywords can be found in the CFOUR manual online.

The start script is used to start the calculation. This involves submitting it through the LoadLeveler to take advantage of the parallel processing. The WORDIR and the initialdir need to be changed to the current working directory. All lines that begin with # are comments in bash but are followed by commands for the LoadLeveler. The PATH and GENBAS need to be pointed to the right location, which should be the home directory for the GENBAS and the C4 program folder for the PATH. The script is as follows:

```
#!/bin/ksh
# @ initialdir = /spark/swidicu/bmhays/test/quar
# @ requirements = (Arch == "R6000") && (OpSys == "AIX61")
# @ class = spark24p
# @ notify_user =
# @ group = swidicu
# @ error = error
# @ queue
```

```
#
INPF=input
WORKDIR=/spark/swidicu/bmhays/test/quar
TMPDIR=$WORKDIR/tmp1
BASISDIR=/spark/swidicu/bmhays
PATH=/libs/C4/bin:$PATH
mkdir $TMPDIR
cd $TMPDIR
rm *
cp $WORKDIR/C3H2_DZ.inp ZMAT
cp $BASISDIR/GENBAS GENBAS
xcfour > xcfour.out
for i in zmat*
do
cd ..
l=`echo $i | sed 's/zmat//'`
mkdir $l
cp $TMPDIR/$i $l/$i
sed s/xxx/$l/g < zcommand.cmd > zcommand.$l
cp zcommand.$l $l/.
rm zcommand.0*
cd $TMPDIR
done
cd ..
mkdir final
cp $TMPDIR/JOBARC $WORKDIR/final/JOBARC
cp $TMPDIR/JAINDX $WORKDIR/final/JAINDX
#
```

This script creates a new directory called tmp1, then moves the input file, which is now called ZMAT, and the GENBAS to the directory and the runs the xcfour program in the directory. A lot of files will be outputted upon completion, but the important files are the sequential zmat∗ files, JOBARC, and JAINDX. Those files are all needed for later steps in the calculation. In the working directory, there should be several folders starting with 001 and ending with the last zmat∗ number. Each of these folders should have a zmat∗ file corresponding to the name of the folder and a zcommand.cmd script. A final folder is also made, to which the JOBARC and JAINDX files are copied.

The original zcommand.cmd file lis formatted as such:

```
#!/bin/ksh
# @ initialdir = /spark/swidicu/bmhays/test/quar/xxx
# @ requirements = (Arch == "R6000") && (OpSys == "AIX61")
# @ class = spark24p
# @ notify_user =
# @ group = swidicu
# @ error = error
# @ queue
#
# list commands below to be executed
INPF=zmatxxx
OUTF=zmatxxx.out
. /libs/scripts/c4
#
```

The new zcommand.cmd files in each folder should have the xxx replaced with the folder and zmat∗ number. In the folder 001, there should be a file called zmat001 and a zcommand.cmd file with the xxx replaced with 001. Also, the initialdir needs to be the same as the working directory before running the start script with xxx at the end.

Each of the numbered zmats can be run like a normal LoadLeveler using the script in the folder with zmat∗ file. Running it using this script uses the Emerson Center's scratch disk to store unnecessary files until the job is done. When the job is finished, there should zmat∗.out, JOBARC.new, and JAINDX.new in the folder. These files files should remain in their folders.

Once all of the zmat∗ have been run using the zcommand.cmd, the final.cmd script can be run. This script is as follows:

```
#!/bin/ksh
# @ initialdir = /spark/swidicu/bmhays/test/quar
# @ requirements = (Arch == "R6000") && (OpSys == "AIX61")
# @ class = spark24p
# @ notify_user =
# @ group = swidicu
# @ error = error
# @ queue
#
```

```
INPF=input
WORKDIR=/spark/swidicu/bmhays/test/quar
BASISDIR=/spark/swidicu/bmhays
PATH=/libs/C4/bin:$PATH
cd $WORKDIR
for i in 0*
do
cd $i
cp $BASISDIR/GENBAS GENBAS
cp JOBARC.new JOBARC
cp JAINDX.new JAINDX
cp zmat$i ZMAT
xja2fja
rm GENBAS
rm JOBARC
rm JAINDX
cd ..
cp $i/FJOBARC final/fja.$i
done
cd final
cp $BASISDIR/GENBAS GENBAS
for k in fja.*
do
cp $k FJOBARC
xja2fja
xcubic >> out.out
done
cd ..
#
```

This script needs to be run in the working directory, with the WORKDIR and initialdir corrected to account for the real directory. This script runs CFOUR's xja2fa utility program to create FJOBARC files. These are moved to the final directory and renamed fja.$*$ for record keeping. Each fja.$*$ is run in the xja2fa program followed by the xcubic program. This is called cubic, but it does VPT2 as described in the CFOUR manual. The output is written to the out.out file, where the ZPE corrected structure, rotational constants, alpha values, etc. can be found. After the calculation is complete, the excess files generated should be deleted to save disk space.

B

Appendix B

B.1 Supplementary Information from Hays and Widicus Weaver, 2013

The torsional potential energy surfaces for methanediol, methoxymethanol, aminomethanol, and n-methylhydroxylamine are shown in Figures B.1 – B.4. The structural information for all of the molecules in this study is included in Tables B.1-B.25. These structures were optimized at the MP2/aug-cc-pVTZ level of theory. For structures associated with Figures 2.1 – 2.3, harmonic vibrational frequencies were found at the MP2/aug-cc-pVTZ level of theory, and are also reported here.

B.2 Torsional Potential Energy Surfaces

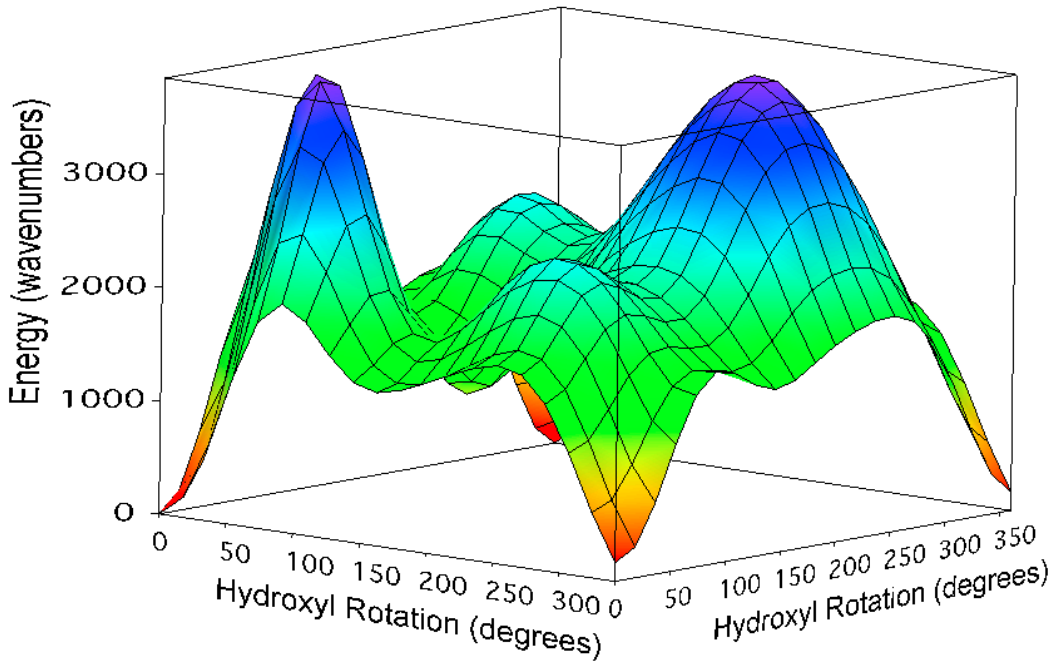

Figure B.1: The torsional potential energy surface of methanediol determined using single point calculations where the two hydroxyl groups were rotated by 20 degrees between each point.

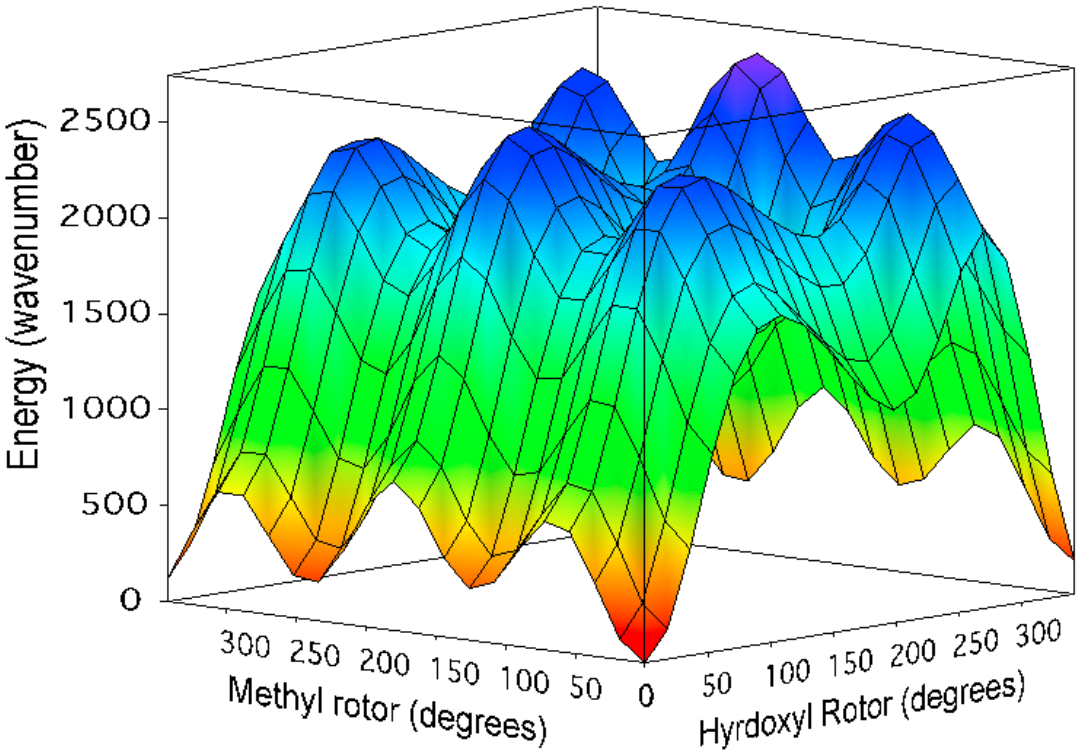

Figure B.2: The torsional potential energy surface of methoxymethanol determined using single point calculations where either the methyl group or the hydroxyl group was rotated by 20 degrees between each point.

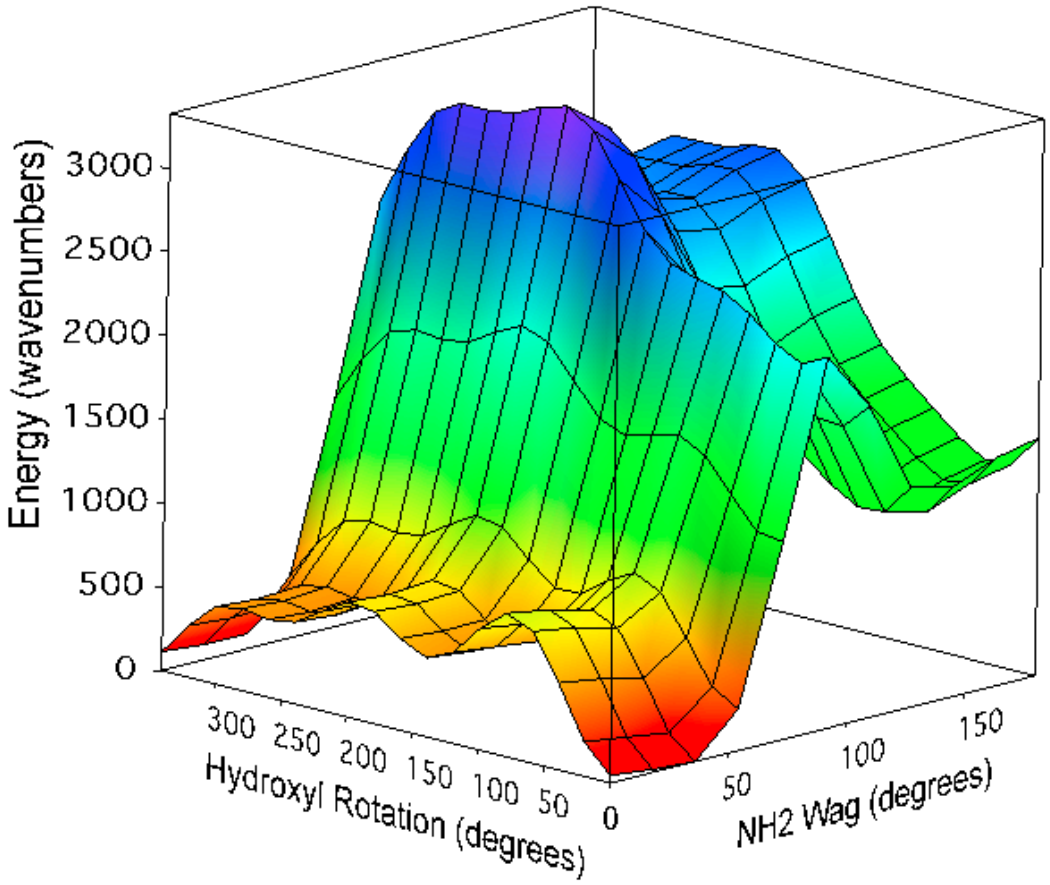

Figure B.3: The torsional potential energy surface of aminomethanol determined using single point calculations where either the methyl group or the amine group was rotated by 20 degrees between each point. Steric hindrance limited the range for the NH_2 wagging motion, and so only a range of 170 degrees was considered.

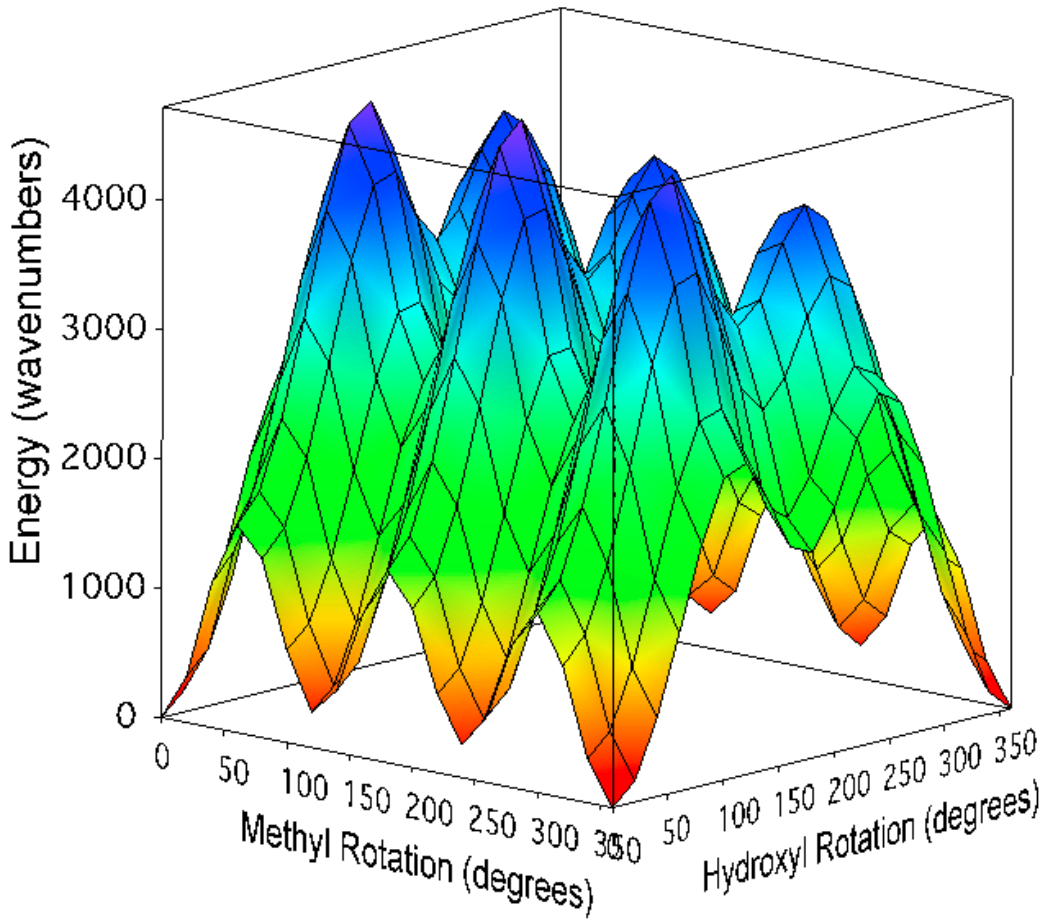

Figure B.4: The torsional potential energy surface for n-methylhydroxylamine determined using single point calculations where either the methyl or the hydroxyl group was rotated by 20 degrees between each point.

B.3 Geometries and Vibrations

Table B.1: Structural information for methanol.

Bond	Ångstroms
C1, O2	1.4232
C1, H4	1.0859
C1, H5	1.0912
C1, H6	1.0912
O2, H3	0.9609
Bond Angle	Degrees
O2, C1, H4	106.5174
O2, C1, H5	111.9051
O2, C1, H6	111.9051
H4, C1, H5	108.6025
H4, C1, H6	108.6025
H5, C1, H6	109.1587
C1, O2, H3	108.0815
Dihedral Angle	Degrees
H4, C1, O2, H3	180.0000
H5, C1, O2, H3	-61.4417
H6, C1, O2, H3	61.4417

Table B.2: Structural information and vibrational frequencies for methanediol.

Bond	Ångstroms	Frequencies (cm^{-1})
C1, O2	1.4063	364.2605
C1, O3	1.4068	378.5913
C1, H4	1.0890	559.9924
C1, H6	1.0890	1016.6886
O2, H5	0.9639	1046.6101
O3, H7	0.9640	1083.9979
Bond Angle	Degrees	1213.5224
O2, C1, H3	112.7323	1372.8495
O2, C1, H4	105.1214	1397.8214
O2, C1, H6	111.8698	1454.2736
O3, C1, H4	111.8293	1552.6344
O3, C1, H6	105.1116	3094.3001
C1, O2, H5	107.4179	3158.1204
C1, O3, H7	107.3914	3825.9488
Dihedral Angle	Degrees	3826.3650
H3, C1, O2, H5	-62.0232	
H4, C1, O2, H5	175.9147	
H6, C1, O2, H5	56.1897	
O2,C1, O3, H7	-61.6279	
H4, C1, O3, H7	56.5697	
H6, C1, O3, H7	176.2667	

Table B.3: Structural information and vibrational frequencies for methylperoxide.

Bond	Ångstroms	Frequencies (cm^{-1})
C1, O2	1.4167	169.9185
C1, H5	1.0884	260.4652
C1, H6	1.0902	446.8944
C1, H7	1.0894	869.6252
O2, H3	1.4559	1059.7153
O3, H4	0.9678	1180.8876
Bond Angle	Degrees	1210.7689
O2, C1, H5	104.4603	1358.6424
O2, C1, H6	111.2225	1463.8601
O2, C1, H7	110.7004	1490.3166
H5, C1, H6	110.2201	1532.1732
H5, C1, H7	110.0292	3061.4367
H6. C1, H7	110.0834	3151.4521
C1, O2, O3	104.9812	3179.1472
O2, O3, H4	99.3250	3777.4473
Dihedral Angle	Degrees	
H5, C1, O2, O3	176.9937	
H6, C1, O2, O3	-64.1219	
H7, C1, O2, O3	58.5979	
C1, O2, O3,H4	119.4986	

Table B.4: Structural information and vibrational frequencies for the methylperoxide association product.

Bond	Ångstroms	Frequencies (cm^{-1})
C1, O2	1.4521	237.5463
C1, H4	1.0815	389.3071
C1, H5	1.0845	813.4002
C1, H6	1.0878	942.0327
O2, H3	0.9714	1017.4553
O2, O7	1.4597	1120.3855
Bond Angle	Degrees	1188.8665
O2,C1,H4	104.4891	1333.5335
O2, C1, H5	108.3713	1459.3584
O2,C1, H6	107.3582	1486.6430
H4, C1, H5	110.8872	1522.7509
H4, C1, H6	111.9969	3101.7367
H5, C1, H6	113.2300	3217.8814
C1, O2, H3	109.2847	3255.5977
C1, O2, O7	107.5099	3715.6577
H3, O2, O7	101.1949	
Dihedral Angle	Degrees	
H4, C1, O2, H3	-175.1867	
H4, C1, O2, O7	-66.1563	
H5, C1, O2, H3	-56.9032	
H5, C1, O2, O7	52.1272	
H6, C1, O2, H3	65.7290	
H6, C1, O2, O7	174.7594	

Table B.5: Structural information and vibrational frequencies for the methylperoxide transition state.

Bond	Ångstroms	Frequencies (cm^{-1})
C1, O2	1.4447	-1388.2944
C1, H5	1.0870	220.4719
C1, H6	1.0840	387.0124
C1, H7	1.0846	862.4006
O2, O3	1.5264	974.5668
O2, H4	1.0338	1041.7644
O3, H4	1.3952	1192.8622
Bond Angle	Degrees	1258.4458
O2, C1, H5	106.1918	1461.4611
O2, C1, H6	105.8839	1491.8584
O2, C1, H7	109.4874	1519.7258
H5, C1, H6	111.8746	3058.2952
H5, C1, H7	112.4150	3103.7724
H6, C1, H7	110.6573	3217.3017
C1, O2, O3	105.7667	3232.9634
C1, O2, H4	112.6995	
O3,O2, H4	62.6053	
O2, O3, H4	41.1402	
Dihedral Angle	Degrees	
H5, C1, O2, O3	173.5567	
H5, C1, O2, H4	107.1439	
H6, C1, O2, O3	-67.3657	
H6, C1, O2, H4	-133.7785	
H7, C1, O2, H3	51.9595	
H7, C1, O2, H4	-14.4533	
C1, O2, O3, H4	-107.7769	

Table B.6: Structural information for the higher energy conformer of methanediol.

Bond	Ångstroms
C1, O2	1.4071
C1, O3	1.4071
C1, H5	1.0846
C1, H6	1.0931
O2, H4	0.9623
O3, H7	0.9623
Bond Angle	Degrees
O2, C1, O3	113.7571
O2, C1, H5	105.8528
O2, C1, H6	110.4817
O3, C1, H5	105.8422
O3, C1, H6	110.4863
H5, C1, H6	110.1911
C1, O2, H4	108.9211
C1, O3, H7	108.919
Dihedral Angle	Degrees
O3, C1, O2, H4	-78.8392
H5, C1, O2, H4	165.3726
H6, C1, O2, H4	46.0925
O2, C1, O3, H7	78.6617
H5, C1, O3, H7	-165.5439
H6, C1, O3, H7	-46.2676

Table B.7: Structural information for methylamine.

Bond	Ångstroms
C1, N2	1.4642
C1, H3	1.0938
C1, H4	1.0881
C1, H5	1.0881
N2, H6	1.0121
N2, H7	1.0121
Bond Angle	Degrees
N2, C1, H3	114.8725
N2, C1, H4	108.9760
N2, C1, H5	108.9760
H3, C1, H4	108.1764
H3, C1, H5	108.1764
H4, C1, H5	107.4153
C1, N2, H6	110.2643
C1, N2, H7	110.2643
H6, N2, H7	106.2772
Dihedral Angle	Degrees
H3, C1, N2, H6	-58.5260
H3, C1, N2, H7	58.5260
H4, C1, N2, H6	63.0083
H4, C1, N2, H7	-179.9396
H5, C1, N2, H6	179.9396
H5, C1, N2, H7	-63.0083

Table B.8: Structural information and vibrational frequencies for aminomethanol.

Bond	Ångstroms	Frequencies (cm^{-1})
N1, C2	1.4358	269.2429
N1, H4	1.0116	389.6262
N1, H5	1.0120	478.1419
C2, O3	1.4304	808.3167
C2, H6	1.0908	913.7363
C2, H7	1.0864	1009.5524
O3, H8	0.9630	1114.4726
Bond Angle	Degrees	1166.7494
C2, N1, H4	111.8136	1369.3947
C2, N1, H5	110.7358	1396.6060
H4, N1, H5	108.1094	1425.9934
N1, C2, O3	116.0949	1528.2146
N1, C2, H6	108.1711	1664.2491
N1, C2, H7	108.8263	3090.5415
O3, C2, H6	110.2645	3172.3069
O3, C2, H7	104.3197	3538.7235
H6, C2, H7	108.9469	3639.1238
C2, O3, H8	108.0436	3833.7639
Dihedral Angle	Degrees	
H4, N1, C2, O3	67.5762	
H4, N1, C2, H6	-56.9421	
H4, N1, C2, O3	-175.1684	
H5, N1, C2, O3	-53.558	
H5, N1, C2, H6	-177.5741	
H5, N1, C2, H7	64.1996	
N1, C2, O3, H8	-69.1395	
H6, C2, O3, H8	54.2959	
H7, C2, O3, H8	171.1331	

Table B.9: Structural information and vibrational frequencies for n-methylhydroxylamine.

Bond	Ångstroms	Frequencies (cm^{-1})
N1, H2	1.0156	272.3795
N1, C3	1.4563	316.8757
N1, O7	1.4455	439.0457
C3, H4	1.0926	862.5445
C3, H5	1.0898	980.8109
C3, H6	1.0869	1072.6385
O7, H8	0.9633	1159.1919
Bond Angle	Degrees	1233.3312
H2, N1, C3	107.9407	1359.9496
H2, N1, O7	102.5564	1449.0287
C3, N1, O7	106.4235	1484.5862
N1, C3, H4	112.6919	1497.0301
N1, C3, H5	107.5608	1535.0797
N1, C3, H6	109.0450	3053.3379
H4, C3, H5	109.5530	3142.8423
H4, C3, H6	109.0740	3177.9268
H5, C3, H6	108.8418	3509.8256
N1, O7, H8	102.0548	3827.4315
Dihedral Angle	Degrees	
H2, N1, C3, H4	59.8525	
H2, N1, C2, H5	-60.9992	
H2, N1, C3, H6	-178.8781	
O7, N1, C3, H4	-49.6391	
O7, N1, C3, H5	-170.4908	
O7, N1, C3, H6	71.6302	
H2, N1, O7, H8	120.9144	
H3, N1, O7, O8	-125.8411	

Table B.10: Structural information and vibrational frequencies for the n-methylhydroxylamine association product.

Bond	Ångstroms	Frequencies (cm^{-1})
C1, N2	1.4827	265.0533
C1, H3	1.0907	441.8763
C1, H4	1.0843	888.8567
C1, H5	1.0843	919.6961
N2, H6	1.0278	1071.8611
N2, H7	1.0278	1191.8143
N2, O8	1.3545	1199.5897
Bond Angle	Degrees	1363.9633
N2, C1, H3	110.3701	1412.9665
N2, C1, H4	106.7256	1436.2526
N2, C1, H5	106.7256	1490.3557
H3, C1, H4	111.5281	1520.8430
H3, C1, H5	111.5281	1665.4721
H4, C1, H5	109.7407	3082.2699
C1, N2, H6	108.2116	3196.2951
C1, N2, H7	108.2116	3231.5217
C1, N2, O8	112.4381	3307.5263
H6, N2, H7	105.7616	3354.0224
H6, N2, H8	110.9697	
H7, N2, H8	110.9697	
Dihedral Angle	Degrees	
H3, C1, N2, H6	-57.0800	
H3, C1, N2, H7	57.0800	
H3, C1, N2, O8	180.0000	
H4, C1, N2, H6	64.2728	
H4, C1, N2, H7	178.4327	
H4, C1, N2, O8	-58.6473	
H5, C1, N2, H6	-178.4327	
H5, C1, N2, H7	-64.2728	
H5, C1, N2, O8	58.6473	

Table B.11: Structural information and vibrational frequencies for the n-methylhydroxylamine transition state.

Bond	Ångstroms	Frequencies (cm^{-1})
N1, H2	1.0131	-1669.1976
N1, C3	1.4485	247.7275
N1, O7	1.4943	387.0110
N1, H8	1.1126	790.5939
C3, H4	1.0895	875.0881
C3, H5	1.0894	1085.1462
C3, H6	1.0847	1158.9226
O7, H8	1.3091	1190.7279
Bond Angle	Degrees	1228.0202
H2, N1, C3	114.6948	1406.0023
H2, N1, O7	107.6797	1452.6525
H2, N1, H8	119.1675	1495.6516
C3, N1, H7	110.7188	1521.3699
C3, N1, H8	125.7748	2810.4018
O7, N1, H8	58.1000	3077.4215
N1, C3, H4	108.6138	3170.1956
N1, C3, H5	109.5358	3208.4513
N1, C3, H6	108.2672	3545.3588
H4, C3, H5	110.9066	
H4, C3, H6	109.1837	
H5, C3, H6	110.2753	
N1, O7, H8	46.1834	
Dihedral Angle	Degrees	
H2, N1, C3, H4	64.6959	
H2, N1, C3, H5	-56.5725	
H2, N1, C3, H6	-176.8595	
O7, N1, C3, H4	-57.3979	
O7, N1, C3, H5	-178.6663	
O7, N1, C3, H6	61.0467	
H8, N1, C3, H4	-122.3218	
H8, N1, C3, H5	116.4098	
H8, N1, C3, H6	-3.8772	
H2, N1, O7, H8	113.8358	
C3, N1, O7, H8	-120.0513	

Table B.12: Structural information and vibrational frequencies for methoxyamine.

Bond	Ångstroms	Frequencies (cm^{-1})
C1, O2	1.4167	261.1686
C1, H6	1.0943	316.9404
C1, H7	1.0874	456.5971
C1, H8	1.0943	892.5891
O2, N3	1.4211	1071.6268
N3, H4	1.0203	1166.2399
N3, H5	1.0203	1178.7636
Bond Angle	Degrees	1245.6064
O2, C1, H6	111.0306	1340.8136
O2, C1, H7	106.4321	1470.1821
O2, C1, H8	111.0315	1504.6082
H6, C1, H7	109.5508	1516.9114
H6, C1, H8	109.1989	1648.0657
H7, C1, H8	109.5510	3024.5797
C1, O2, N3	111.0872	3096.8146
O2, N3, H4	106.2529	3175.1365
O2, N3, H5	106.2592	3410.0561
H4, N3, H5	106.1516	3517.3968
Dihedral Angle	Degrees	
H6, C1, O2, N3	60.8421	
H7, C1, O2, N3	-180.0022	
H8, C1, O2, N3	-60.8458	
C1, O2, N3, H4	56.3693	
C1, O2, N3, H5	-56.3897	
O2, N3, H4, H5	-112.8333	

Table B.13: Structural information and vibrational frequencies for the methoxyamine transition state.

Bond	Ångstroms	Frequencies (cm^{-1})
C1, O2	1.4453	-325.8265
C1, H6	1.0877	261.4611
C1, H7	1.0839	357.4218
C1, H8	1.0871	659.0400
O2, N3	1.5705	820.8142
O2, H4	0.9682	1014.0172
O2, H5	1.9917	1085.7698
N3, H4	1.9597	1182.8771
N3, H5	1.0255	1342.3646
Bond Angle	Degrees	1437.6965
O2, C1, H6	109.3276	1470.6694
O2, C1, H7	105.1961	1504.8538
O2, C1, H8	108.2641	1525.4530
H6, C1, H7	110.9968	3089.2897
H6, C1, H8	111.9526	3195.2892
H7, C1, H8	110.8342	3226.5536
C1, O2, N3	114.2093	3424.2519
C1, O2, H4	108.9422	3766.0190
C1, O2, H5	83.8726	
N3, O2, H4	98.8724	
N3, O2, H5	30.6538	
H4, O2, H5	113.9105	
O2, N3, H4	29.2713	
O2, N3, H5	98.0102	
H4, N3, H5	113.0801	
Dihedral Angle	Degrees	
H6, C1, O2, N3	-51.3910	
H6, C1, O2, H4	57.3119	
H6, C1, O2, H5	-55.8999	
H7, C1, O2, N3	67.8669	
H7, C1, O2, N4	176.5698	
H7, C1, O2, H5	63.3580	
H8, C1, O2, N3	-173.5949	
H8, C1, O2, H4	-64.8920	
H8, C1, O2, H5	-178.1038	
C1, O2, N3, H4	115.1403	
C1, O2, N3, H5	-8.8188	
O2, N3, H4, H5	-63.2880	

Table B.14: Structural information for the first excited conformer of aminomethanol.

Bond	Ångstroms
N1, C2	1.4377
N1, H4	1.0103
N1, H5	1.011
C2, O3	1.4225
C2, H6	1.0926
C2, H7	1.097
C3, H8	0.9629
Bond Angle	Degrees
C2, N1, H4	111.3606
C2, N1, H5	111.6097
H4, N1, H5	108.7602
N1, C2, O3	106.6747
N1, C2, H6	107.7563
N1, C2, H7	114.1481
O3, C2, H6	110.8309
O3, C2, H7	108.8382
H6, C2, H7	108.5948
C2, O3, H8	107.8112
Dihedral Angle	Degrees
H4, N1, C2, O3	160.1654
H4, N1, C2, H6	41.1065
H4, N1, C2, H7	-79.5905
H5, N1, C2, O3	-78.0747
H5, N1, C2, H6	162.8665
H5, N1, C2, H7	42.1695
N1, C2, O3, H8	162.1124
H6, C2, O3, H8	-80.8492
H7, C2, O3 H8	38.5106

Table B.15: Structural information for the second excited conformer of aminomethanol.

Bond	Ångstroms
N1, C2	1.4263
N1, H4	1.0121
N1, H5	1.0121
C2, O3	1.4369
C2, H6	1.0911
C2, H7	1.0911
O3, H8	0.9641
Bond Angle	Degrees
C2, N1, H4	110.2947
C2, N1, H5	110.2948
H4, N1, H5	107.5
N1, C2, O3	110.6374
N1, C2, H6	108.6985
N1, C2, H7	108.6984
O3, C2, H6	109.7871
O3, C2, H7	109.7871
H6, C2, H7	109.2006
C2, O3, H8	108.4547
Dihedral Angle	Degrees
H4, N1, C2, O3	59.2963
H4, N1, C2, H6	-61.3252
H4, N1, C2, H7	179.9176
H5, N1, C2, O3	-59.2969
H5, N1, C2, H6	-179.918
H5, C1, O2, H7	61.3244
N1, C2, O3, H8	-179.998
H6, C2, O3, H8	-60.027
H7, C2, O3, H8	60.031

Table B.16: Structural information for the third excited conformer of aminomethanol.

Bond	Ångstroms
N1, C2	1.448
N1, H4	1.0112
N1, H5	1.0117
C2, O3	1.4132
C2, H6	1.093
C2, H7	1.0912
O3, H8	0.965
Bond Angle	Degrees
C2, N1, H4	111.5823
C2, N1, H5	111.4424
H4, N1, H5	108.4241
N1, C2, O3	110.0289
N1, C2, H6	107.446
N1, C2, H7	114.6502
O3, C2, H6	111.3608
O3, C2, H6	104.6915
H6, C2, H7	108.7081
C2, O3, H8	105.7605
Dihedral Angle	Degrees
H4, N1, C2, O3	160.391
H4, N1, C2, H6	38.9955
H4, N1, C2, H7	-81.9445
H5, N1, C2, O3	-78.2425
H5, N1, C2, H6	160.362
H5, N1, C2, H7	39.4221
N1, C2, O3, H8	-44.2781
H6, C2, O3, H8	74.7488
H7, C2, O3, H8	-167.955

Table B.17: Structural information for first excited conformer of n-methylhydroxylamine.

Bond	Ångstroms
N1, H2	1.0161
N1, C3	1.4522
N1, O7	1.4298
C3, H4	1.0981
C3, H5	1.0892
C3, H6	1.0867
O7, H8	0.9706
Bond Angle	Degrees
H2, N1, C3	109.5312
H2, N1, O7	105.6153
C3, N1, O7	109.1912
N1, C3, H4	113.313
N1, C3, H5	108.0239
N1, C3, H6	108.7354
H4, C3, H5	108.7835
H4, C3, H6	108.8745
H5, C3, H6	109.0369
N1, O7, H8	106.5117
Dihedral Angle	Degrees
H2, N1, C3, H4	59.774
H2, N1, C3, H5	-60.8187
H2. N1, C3, H6	-179.019
O7, N1, C3, H4	-55.4327
O7, N1, C3, H5	-176.026
O7, N1, C3, H6	65.7739
H2, N1, O7, H8	-65.9432
C3, N1, O7, H8	51.7566

Table B.18: Structural information for dimethylether.

Bond	Ångstroms
C1, O2	1.4122
C1, H4	1.095
C1, H5	1.0864
C1, H6	1.095
O2, C3	1.4122
C3, H7	1.095
C3, H8	1.095
C3, H9	1.0864
Bond Angle	Degrees
O2, C1, H4	111.1016
O2, C1, H5	107.4291
O2, C1, H6	111.1016
H4, C1, H5	109.2879
H4, C1, H6	108.6007
H5, C1, H6	109.2879
C1, O2, C3	110.7228
O2, C3, H7	111.1016
O2, C3, H8	111.1016
O2, C3, H9	107.4291
H7, C3, H9	108.6007
H7, C3, H9	109.2879
H8, C3, H9	109.2879
Dihedral Angle	Degrees
H4, C1, O2, C3	60.5118
H5, C1, O2, C3	180.0
H6, C1, O2, C3	-60.5118
C1, O2, C3, H7	-60.5118
C1, O2, C3, H8	60.5118
C1, O2, C3, H9	180.0

Table B.19: Structural information and vibrational frequencies for methoxymethanol.

Bond	Ångstroms	Frequencies (cm^{-1})
C1, O2	1.3987	138.0816
C1, O3	1.4091	203.5355
C1, H5	1.0895	356.4675
C1, H6	1.0926	393.2570
O2, C4	1.4226	588.0993
O3, H10	0.9639	952.5048
C4, H7	1.0856	1037.8078
C4, H8	1.0937	1069.3492
C4, H9	1.0897	1162.0133
Bond Angle	Degrees	1187.1601
O2, C1, O3	113.2563	1215.2168
O2, C1, H5	105.495	1311.2149
O2, C1, H6	110.8969	1387.2748
O3, C1, H5	111.5654	1439.7246
O3, C1, H6	105.0661	1484.1279
H5, C1, H6	110.6742	1511.1105
C1, O2, C4	112.1398	1532.1849
C1, O3, H10	107.3191	1537.7881
O2, C4, H7	106.799	3047.4580
O2, C4, H8	110.4084	3068.0749
O2, C4, H9	111.2858	3133.8867
H7, C4, H8	109.4349	3141.8814
H7, C4, H9	109.7638	3191.7246
H8, C4, H9	109.1133	3826.5370
Dihedral Angle	Degrees	
O3, C1, O2, C4	67.4385	
H5, C1, O2, C4	-170.265	
H6, C1, O2, C4	-50.3964	
O2, C1, O3, H10	64.7163	
H5, C1, O3, H10	-54.134	
H6, C1, O3, H10	-174.103	
C1, O2, C4, H7	177.9081	
C1, O2, C4, H8	59.0153	
C1, O2, C4, H9	-62.3102	

Table B.20: Structural information and vibrational frequencies for dimethylperoxide.

Bond	Ångstroms	Frequencies (cm^{-1})
C1, O2	1.4145	38.8833
C1, H5	1.0902	217.1057
C1, H6	1.0902	270.9136
C1, H10	1.088	304.7779
O2, O3	1.4653	483.3889
O3, C4	1.4144	830.8182
C4, H7	1.0879	1067.6101
C4, H8	1.0902	1082.9486
C4, H9	1.0902	1176.1646
Bond Angle	Degrees	1180.2149
O2, C1, H5	110.8242	1185.3125
O2, C1, H6	110.8295	1261.0593
O2, C1, H10	104.6382	1456.8276
H5, C1, H6	110.1248	1462.9087
H5, C1, H10	110.1532	1486.0992
H6, C1, H10	110.1523	1486.9781
C1, O2, O3	103.4401	1532.2919
O2, O3, C4	103.4391	1537.7629
O3, C4, H7	104.6393	3059.8659
O3, C4, H8	110.8296	3061.3126
O3, C4, H9	110.8278	3147.4435
H7, C4, H8	110.1491	3147.6109
H7, C4, H9	110.1517	3181.9295
H8, C4, H9	110.1247	3182.1647
Dihedral Angle	Degrees	
H5, C1, O2, O3	61.2619	
H6, C1, O2, O3	-61.3237	
H10, C1, O2, O3	179.9683	
C1, O2, O3, C4	180.0298	
O2, O3, C4, H7	-179.989	
O2, O3, C4, H8	-61.2841	
O2, O3, C4, H9	61.304	

Table B.21: Structural information and vibrational frequencies for the dimethylperoxide association product.

Bond	Ångstroms	Frequencies (cm^{-1})
C1, O2	1.4469	232.0881
C1, H4	1.088	278.6304
C1, H5	1.0818	391.4397
C1, H6	1.0869	413.3364
O2, C3	1.4469	415.5668
O2, O10	1.4453	820.3072
C3, H7	1.088	977.0942
C3, H8	1.0869	1015.5273
C3, H9	1.0818	1153.7999
Bond Angle	Degrees	1211.7711
O2, C1, H4	107.3847	1215.6672
O2, C1, H5	104.97	1257.4164
O2, C1, H6	107.9396	1439.8939
H4, C1, H5	112.188	1470.4930
H4, C1, H6	112.8682	1475.1071
H5, C1, H6	111.0169	1489.5920
C1, O2, C3	112.2101	1504.5338
C1, O2, O10	106.4868	1524.3761
C3, O2, O10	106.4868	3088.5818
O2, C3, H7	107.3847	3093.4924
O2, C3, H8	107.9396	3199.6843
O2, C3, H9	104.97	3202.5251
H7, C3, H8	112.8682	3249.1678
H7, C3, H9	112.188	3250.2286
H8, C3, H9	111.0169	
Dihedral Angle	Degrees	
H4, C1, O2, C3	62.5903	
H4, C1, O2, O10	178.7276	
H5, C1, O2, C3	-177.849	
H5, C1, O2, O10	-61.7119	
H6, C1, O2, C3	-59.3738	
H6, C1, O2, O10	56.7635	
C1, O2, C3, H7	-62.5903	
C1, O2, C3, H8	59.3737	
C1, O2, C3, H9	177.8492	
O10, O2, C3, H7	-178.728	
O10, O2, C3, H8	-56.7635	
O10, O2, C3, H9	61.7119	

Table B.22: Structural information and vibrational frequencies for the dimethylperoxide transition state.

Bond	Ångstroms	Frequencies (cm^{-1})
C1, O2	1.4302	-1055.0993
C1, H5	1.0885	167.7517
C1, H6	1.0872	222.4717
C1, H7	1.0881	244.0774
O2, O3	1.4886	413.6270
O2, C4	1.7325	643.8061
C4, H8	1.0958	902.9224
C4, H9	1.0829	1018.3456
C4, H10	1.0786	1090.0620
O3, C4	1.869	1100.1556
Bond Angle	Degrees	1190.2128
O2, C1, H5	106.4071	1197.8073
O2, C1, H6	106.6653	1392.8226
O2, C1, H7	110.1804	1453.9514
H5, C1, H6	111.5335	1472.0380
H5, C1, H7	111.6776	1485.5785
H6, C1, H7	110.187	1509.0287
C1, O2, O3	105.8051	1539.9095
C1, O2, C4	115.3476	3014.6317
O3, O2, C4	70.4697	3074.6988
O2, C4, H8	91.138	3171.0334
O2, C4, H9	125.1777	3184.5387
O2, C4, H10	102.9216	3193.6298
H8, C4, H9	110.4973	3285.7479
H8, C4, H10	111.468	
H9, C4, H10	113.4518	
O2, O3, C4	60.8855	
O3, C4, H8	136.4263	
O3, C4, H9	87.0198	
O3, C4, H10	95.7249	
Dihedral Angle	Degrees	
H5, C1, O2, O3	177.5385	
H5, C1, O2, C4	102.0373	
H6, C1, O2, O3	-63.282	
H6, C1, O2, C4	-138.7832	
H7, C1, O2, O3	56.3088	
H7, C1, O2, C4	-19.1925	
C1, O2, C4, H8	-62.6921	
C1, O2, C4, H9	53.5707	

Table B.23: Structural information and vibrational frequencies for the dimethylperoxide transition state.

Bond	Ångstroms	Frequencies (cm^{-1})
C1, O2	1.4302	-1055.0993
C1, H5	1.0885	167.7517
C1, H6	1.0872	222.4717
C1, H7	1.0881	244.0774
O2, O3	1.4886	413.6270
O2, C4	1.7325	643.8061
C4, H8	1.0958	902.9224
C4, H9	1.0829	1018.3456
C4, H10	1.0786	1090.0620
O3, C4	1.869	1100.1556
Bond Angle	Degrees	1190.2128
O2, C1, H5	106.4071	1197.8073
O2, C1, H6	106.6653	1392.8226
O2, C1, H7	110.1804	1453.9514
H5, C1, H6	111.5335	1472.0380
H5, C1, H7	111.6776	1485.5785
H6, C1, H7	110.187	1509.0287
C1, O2, O3	105.8051	1539.9095
C1, O2, C4	115.3476	3014.6317
O3, O2, C4	70.4697	3074.6988
O2, C4, H8	91.138	3171.0334
O2, C4, H9	125.1777	3184.5387
O2, C4, H10	102.9216	3193.6298
H8, C4, H9	110.4973	3285.7479
H8, C4, H10	111.468	
H9, C4, H10	113.4518	
O2, O3, C4	60.8855	
O3, C4, H8	136.4263	
O3, C4, H9	87.0198	
O3, C4, H10	95.7249	
Dihedral Angle	Degrees	
H5, C1, O2, O3	177.5385	
H5, C1, O2, C4	102.0373	
H6, C1, O2, O3	-63.282	
H6, C1, O2, C4	-138.7832	
H7, C1, O2, O3	56.3088	
H7, C1, O2, C4	-19.1925	
C1, O2, C4, H8	-62.6921	
C1, O2, C4, H9	53.5707	
C1, O2, C4, H10	-175.0333	
O3, O2, C4, H8	-161.4203	
O3, O2, C4, H9	-45.1575	

Table B.23: Structural information and vibrational frequencies for the dimethylperoxide transition state – continued.

Dihedral Angle	Degrees
O3, O2, C4, H10	86.2385
C1, O2, O3, C4	-111.8195
O2, O3, C4, H8	27.5266
O2, O3, C4, H9	144.5256
O2, O3, C4, H10	-102.19

Table B.24: Structural information for the first excited conformer of methoxymethanol.

Bond	Ångstroms
C1, O2	1.3992
C1, O3	1.4094
C1, H5	1.0852
C1, H6	1.0972
O2, C4	1.4162
O3, H10	0.9617
C4, H7	1.0857
C4, H8	1.0957
C4, H9	1.0921
Bond Anglev Degrees	
O2, C1, O3	113.8441
O2, C1, H5	105.8695
O2, C1, H6	109.6035
O3, C1, H5	106.563
O3, C1, H6	110.117
H5, C1, H6	110.7248
C1, O2, C4	112.4451
C1, O3, H10	108.9099
O2, C4, H7	107.1106
O2, C4, H8	110.809
O2, C4, H9	111.4946
H7, C4, H8	109.1535
H7, C4, H9	108.8603
H8, C1, H9	109.3456
Dihedral Angle	Degrees
O3, C1, O2, C4	68.6637
H5, C1, O2, C4	-174.614
H6, C1, O2, C4	-55.1559
O2, C1, O3, H10	-86.3434
H5, C1, O3, H10	157.3386
H6, C1, O3, H10	37.198
C1, O2, C4, H7	171.8162
C1, O2, C4, H8	52.8533
C1, O2, C4, H9	-69.1881

Table B.25: Structural information for the second excited conformer of methoxymethanol.

Bond	Ångstroms
C1, O2	1.4099
C1, O3	1.39
C1, H5	1.0992
C1, H6	1.0933
O2, C4	1.416
O3, H10	0.9638
C4, H7	1.0855
C4, H8	1.0941
C4, H9	1.0945
Bond Angle	Degrees
O2, C1, O3	109.2426
O2, C1, H5	108.867
O2, C1, H6	110.6122
O3, C1, H5	111.9955
O3, C1, H6	106.5361
H5, C1, H6	109.5798
C1, O2, C4	110.7082
C1, O3, H10	107.4625
O2, C4, H7	107.1068
O2, C4, H8	111.1705
O2, C4, H9	111.2844
H7, C4, H8	109.1965
H7, C4, H9	109.2753
H8, C4, H9	108.7642
Dihedral Angle	Degrees
O3, C1, O2, C4	-178.5838
H5, C1, O2, C4	-56.0015
H6, C1, O2, C4	64.456
O2,C1, O3, H10	59.3219
H5, C1, O3, H10	-61.3683
H6, C1, O3, H10	178.8334
C1, O2, C4, H7	179.4238
C1, O2, C4, H8	-61.359
C1, O2, C4, H9	60.0457

C

Appendix C

C.1 Vinyl Alcohol

The CALPGM/SPFIT output file in the .fit file format for vinyl alcohol is presented below.

C.1.1 fit file

```
syn-vinyl alcohol                                    Mon Feb  2 23:50:58 2015
LINES REQUESTED=  111 NUMBER OF PARAMETERS=  8 NUMBER OF ITERATIONS=  5
  MARQUARDT PARAMETER = 0.0000E+00 max (OBS-CALC)/ERROR =1.0000E+02
                              PARAMETERS - A.PRIORI ERROR
     1      1         10000   5.9660782610220E+04    1.000000E+18 A
     2      2         20000   1.0561605286859E+04    1.000000E+18 B
     3      3         30000   8.9658420981262E+03    1.000000E+18 C
     4      4           200  -7.4978891818088E-03    1.000000E+18 -DJ
     5      5          1100   5.9867009677285E-02    1.000000E+18 -DJK
```

```
     6      6          2000  -9.1480002948176E-01    1.000000E+18 -DK
     7      7         40100  -1.6657445338922E-03    1.000000E+18 d1
     8      8         50000  -1.1579010731859E-04    1.000000E+18 d2
8 parameters read, 8 independent parameters
ENERGY SORT OF WANG SUB-BLOCKS
PROLATE ROTOR
    V KMIN KMAX WTPL WTMN ESYMWT NSYM SPINS
    0    0   23    1    1    999    2
BLOCK - WT - SYM - V - TSP - N  -  other quanta  (rel. to F=0 )
    1    1    x    0    0
    2    1    c    0    0
    3    1    b    0    0
    4    1    a    0    0
Maximum Dimension for Hamiltonian = 12
                          EXP.FREQ.  -  CALC.FREQ. -  DIFF.  - EXP.ERR.- EST.ERR.-AVG. CALC.FREQ. -  DIFF. - WT.
    1:   3  1  2  3  1  3                    9573.50000    9573.52585   -0.02585    0.07000   0.00000
    2:   1  1  1  2  0  2                   10081.92000   10082.00306   -0.08306    0.07000   0.00000
    3:   3  0  3  2  1  2                   10887.37000   10887.42639   -0.05639    0.07000   0.00000
    4:   9  2  7 10  1 10                   12549.33000   12549.33403   -0.00403    0.02000   0.00000
    5:  16  3 13 16  3 14                   14022.07000   14022.08413   -0.01413    0.02000   0.00000
    6:  14  2 12 15  1 15                   15083.91000   15083.90478    0.00522    0.02000   0.00000
    7:   4  1  3  4  1  4                   15952.29000   15952.28620    0.00380    0.02000   0.00000
    8:   5  2  4  6  1  5                   16254.94000   16254.97369   -0.03369    0.02000   0.00000
    9:  10  3  8 11  2  9                   16331.36000   16331.35225    0.00775    0.02000   0.00000
   10:  16  4 12 17  3 15                   16344.18000   16344.14715    0.03285    0.02000   0.00000
   11:  15  2 14 14  3 11                   16509.22000   16509.22595   -0.00595    0.02000   0.00000
   12:   8  2  6  9  1  9                   19252.11000   19252.11061   -0.00061    0.02000   0.00000
   13:  17  3 14 17  3 15                   19465.27000   19465.27502   -0.00502    0.02000   0.00000
   14:   1  0  1  0  0  0                   19527.42000   19527.41739    0.00261    0.02000   0.00000
   15:  19  3 17 18  4 14                   19653.40000   19653.40299   -0.00299    0.02000   0.00000
   16:  15  4 12 16  3 13                   20609.74000   20609.69593    0.04407    0.02000   0.00000
   17:  15  2 13 16  1 16                   23064.74000   23064.73639    0.00361    0.02000   0.00000
   18:  23  4 19 22  5 18                   23389.29000   23389.32123   -0.03123    0.02000   0.00000
   19:   5  1  4  5  1  5                   23917.42500   23917.40949    0.01551    0.02000   0.00000
   20:  20  5 16 21  4 17                   23920.54000   23920.60348   -0.06348    0.02000   0.00000
   21:  11  2  9 11  2 10                   24602.24000   24602.24315   -0.00315    0.02000   0.00000
   22:  11  3  8 12  2 11                   25593.31000   25593.30764    0.00236    0.02000   0.00000
   23:  18  3 15 18  3 16                   26337.33000   26337.32290    0.00710    0.02000   0.00000
   24:  16  2 15 15  3 12                   27536.51500   27536.52690   -0.01190    0.02000   0.00000
   25:   7  2  5  8  1  8                   28043.31000   28043.32728   -0.01728    0.02000   0.00000
   26:  18  3 15 17  4 14                   29695.75000   29695.75818   -0.00818    0.02000   0.00000
   27:  20  5 15 21  4 18                   31107.22000   31107.24278   -0.02278    0.02000   0.00000
   28:   4  0  4  3  1  3                   32449.23000   32449.20647    0.02353    0.02000   0.00000
   29:  12  2 10 12  2 11                   33276.24000   33276.25164   -0.01164    0.02000   0.00000
   30:  16  2 14 17  1 17                   33414.96000   33414.96535   -0.00535    0.02000   0.00000
   31:   6  1  5  6  1  6                   33457.09000   33457.09028   -0.00028    0.02000   0.00000
   32:   8  1  7  7  2  6                   33841.19000   33841.15643    0.03357    0.02000   0.00000
   33:  19  3 16 19  3 17                   34797.32000   34797.30292    0.01708    0.02000   0.00000
   34:  15  4 11 16  3 14                   35155.25000   35155.21257    0.03743    0.02000   0.00000
   35:  13  2 11 12  3 10                   36108.97000   36108.99905   -0.02905    0.02000   0.00000
   36:  20  3 18 19  4 15                   36530.02000   36529.99679    0.02321    0.02000   0.00000
   37:  17  2 16 16  3 13                   36667.97000   36667.97295   -0.00295    0.02000   0.00000
   38:   2  1  2  1  1  1                   37459.19000   37459.18442    0.00558    0.02000   0.00000
   39:   6  2  4  7  1  7                   38713.67000   38713.68668   -0.01668    0.02000   0.00000
   40:   2  0  2  1  0  1                   39016.31000   39016.38586   -0.07586    0.07000   0.00000
   41:   2  1  1  1  1  0                   40650.65000   40650.60419    0.04581    0.07000   0.00000
   42:   7  1  6  7  1  7                   44551.00000   44551.00104   -0.00104    0.07000   0.00000
   43:   1  1  0  1  0  1                   50694.22000   50694.13878    0.08122    0.07000   0.00000
   44:   2  1  1  2  0  2                   52328.36000   52328.35712    0.00288    0.07000   0.00000
   45:   5  0  5  4  1  4                   54481.75000   54481.71628    0.03372    0.07000   0.00000
   46:   3  1  2  3  0  3                   54850.91000   54850.88697    0.02303    0.07000   0.00000
   47:   3  1  3  2  1  2                   56164.74000   56164.78751   -0.04751    0.07000   0.00000
   48:   8  1  7  8  1  8                   57167.17000   57167.11268    0.05732    0.07000   0.00000
   49:   4  1  3  4  0  4                   58345.45000   58345.48678   -0.03678    0.07000   0.00000
   50:   3  0  3  2  0  2                   58428.60000   58428.61387   -0.01387    0.07000   0.00000
   51:   3  2  2  2  2  1                   58583.00000   58582.98031    0.01969    0.07000   0.00000
   52:   3  2  1  2  2  0                   58735.84000   58735.87658   -0.03658    0.07000   0.00000
   53:   3  1  2  2  1  1                   60951.08000   60951.14373   -0.06373    0.07000   0.00000
```

```
  54:   5  1  4  5  0  5          62919.79000   62919.72723    0.06277    0.07000   0.00000
  55:   1  1  1  0  0  0          68625.75000   68625.80631   -0.05631    0.07000   0.00000
  56:   6  1  5  6  0  6          68699.14000   68699.07103    0.06897    0.07000   0.00000
  57:   7  1  6  7  0  7          75817.04000   75817.10881   -0.06881    0.07000   0.00000
  58:   6  0  6  5  1  5          76840.85000   76840.76450    0.08550    0.07000   0.00000
  59:   9  1  8  9  0  9          94557.79000   94557.85566   -0.06566    0.07000   0.00000
  60:   7  0  7  6  1  6          99366.69000   99366.80315   -0.11315    0.07000   0.00000
  61:   3  1  3  2  0  2         103706.07000  103705.97500    0.09500    0.07000   0.00000
  62:  10  1  9 10  0 10         106350.75000  106350.72441    0.02559    0.07000   0.00000
  63:   4  2  2  4  1  3         142348.06000  142348.05884    0.00116    0.02000   0.00000
  64:   3  2  1  3  1  2         145107.92000  145107.94660   -0.02660    0.02000   0.00000
  65:   2  2  0  2  1  1         147323.23000  147323.21374    0.01626    0.02000   0.00000
  66:   8  1  8  7  1  7         149130.33000  149130.35019   -0.02019    0.02000   0.00000
  67:   6  1  6  5  0  5         151085.05000  151085.06299   -0.01299    0.02000   0.00000
  68:   2  2  1  2  1  2         152072.13000  152072.11995    0.01005    0.02000   0.00000
  69:   8  0  8  7  0  7         153161.84000  153161.90431   -0.06431    0.02000   0.00000
  70:   3  2  2  3  1  3         154490.28000  154490.31275   -0.03275    0.02000   0.00000
  71:   4  2  3  4  1  4         157727.94000  157727.94557   -0.00557    0.02000   0.00000
  72:   5  2  4  5  1  5         161794.81000  161794.80922    0.00078    0.02000   0.00000
  73:   7  1  7  6  0  6         165874.89000  165874.89167   -0.00167    0.02000   0.00000
  74:   9  0  9  8  0  8         171507.44000  171507.35138    0.08862    0.02000   0.00000
  75:   8  1  8  7  0  7         180396.52000  180396.45796    0.06204    0.02000   0.00000
  76:  10  1 10  9  1  9         185958.06000  185958.03073    0.02927    0.02000   0.00000
  77:   2  2  1  1  1  0         187935.56000  187935.55451    0.00549    0.02000   0.00000
  78:  10  0 10  9  0  9         189665.50000  189665.41305    0.08695    0.02000   0.00000
  79:   9  1  9  8  0  8         194806.97000  194806.97428   -0.00428    0.02000   0.00000
  80:  10  1  9  9  1  8         201458.34000  201458.28180    0.05820    0.02000   0.00000
  81:   3  2  2  2  1  1         205867.92000  205867.93063   -0.01063    0.02000   0.00000
  82:  10  1 10  9  0  9         209257.55000  209257.65364   -0.10364    0.02000   0.00000
  83:   4  2  3  3  1  2         222996.83000  222996.82677    0.00323    0.04000   0.00000
  84:   4  2  2  3  1  3         233142.75000  233142.75209   -0.00209    0.04000   0.00000
  85:   5  2  4  4  1  3         239326.55000  239326.55703   -0.00703    0.04000   0.00000
  86:   7  3  4  7  2  5         246130.31000  246130.32572   -0.01572    0.04000   0.00000
  87:   7  3  4  7  2  5         246130.36000  246130.32572    0.03428    0.04000   0.00000
  88:   6  3  3  6  2  4         247546.31000  247546.40317   -0.09317    0.04000   0.00000
  89:   5  3  2  5  2  3         248458.84000  248458.82801    0.01199    0.04000   0.00000
  90:   5  3  2  5  2  3         248458.90000  248458.82801    0.07199    0.04000   0.00000
  91:   4  3  1  4  2  2         248991.83000  248991.64617    0.18383    0.04000   0.00000
  92:   4  3  2  4  2  3         249559.94000  249560.03256   -0.09256    0.04000   0.00000
  93:   5  3  3  5  2  4         249773.68000  249773.59051    0.08949    0.04000   0.00000
  94:   6  3  4  6  2  5         250143.89000  250143.81950    0.07050    0.04000   0.00000
  95:   7  3  5  7  2  6         250727.75000  250727.78133   -0.03133    0.04000   0.00000
  96:   6  2  5  5  1  4         254866.44000  254866.45798   -0.01798    0.04000   0.00000
  97:   5  2  3  4  1  4         256609.64000  256609.64566   -0.00566    0.04000   0.00000
  98:   7  2  6  6  1  5         269632.08000  269632.12708   -0.04708    0.04000   0.00000
  99:   6  2  4  5  1  5         281429.34000  281429.34285   -0.00285    0.04000   0.00000
 100:   8  2  7  7  1  6         283646.97000  283647.00167   -0.03167    0.04000   0.00000
 101:   7  2  5  6  1  6         307806.54000  307806.58839   -0.04839    0.04000   0.00000
 102:  10  2  9  9  1  8         309569.00000  309569.02653   -0.02653    0.04000   0.00000
 103:   4  3  2  3  2  1         327448.90000  327448.91273   -0.01273    0.04000   0.00000
 104:   4  3  1  3  2  2         327644.18000  327644.08552    0.09448    0.04000   0.00000
 105:   8  2  6  7  1  7         335954.84000  335954.88142   -0.04142    0.04000   0.00000
 106:   5  3  3  4  2  2         346752.00000  346752.08870   -0.08870    0.04000   0.00000
 107:   5  3  2  4  2  3         347340.53000  347340.52809    0.00191    0.04000   0.00000
 108:   6  3  4  5  2  3         365801.97000  365802.07533   -0.10533    0.04000   0.00000
 109:   6  3  3  5  2  4         367180.91000  367180.93681   -0.02681    0.04000   0.00000
 110:   5  4  2  4  3  1         446783.08000  446783.09052   -0.01052    0.04000   0.00000
 111:   5  4  1  4  3  2         446787.13000  446787.16776   -0.03776    0.04000   0.00000
NORMALIZED DIAGONAL:
   1  1.00000E+00   2  8.78222E-01   3  1.80216E-01   4  6.06317E-01   5  6.67398E-02   6  2.69532E-01
    7   2.41071E-01    8   9.98900E-01
MARQUARDT PARAMETER = 0, TRUST EXPANSION = 1.00
                                NEW PARAMETER (EST. ERROR) -- CHANGE THIS ITERATION
   1         10000          A      59660.78243(199)         -0.00018
   2         20000          B      10561.60521( 49)         -0.00007
   3         30000          C       8965.84204( 44)         -0.00006
   4           200        -DJ         -7.49749(278)E-03      0.00040E-03
   5          1100       -DJK         0.059876( 38)         0.000009
```

```
  6          2000        -DK        -0.914853(129)        -0.000053
  7         40100         d1        -1.665723(297)E-03     0.000021E-03
  8         50000         d2        -0.115784( 67)E-03     0.000006E-03
MICROWAVE AVG =       -0.002483 MHz, IR AVG =        0.00000
MICROWAVE RMS =        0.048245 MHz, IR RMS =        0.00000
END OF ITERATION  1 OLD, NEW RMS ERROR=        1.44291         1.44219
                              EXP.FREQ.  -  CALC.FREQ. -  DIFF.  - EXP.ERR.- EST.ERR.-AVG. CALC.FREQ. -  DIFF. - WT.
   1:   3  1  2  3  1  3                    9573.50000    9573.52577   -0.02577    0.07000   0.00151
   2:   1  1  1  2  0  2                   10081.92000   10082.00317   -0.08317    0.07000   0.00158
   3:   3  0  3  2  1  2                   10887.37000   10887.42613   -0.05613    0.07000   0.00219
   4:   9  2  7 10  1 10                   12549.33000   12549.33460   -0.00460    0.02000   0.00818
   5:  16  3 13 16  3 14                   14022.07000   14022.08380   -0.01380    0.02000   0.00418
   6:  14  2 12 15  1 15                   15083.91000   15083.90505    0.00495    0.02000   0.00921
   7:   4  1  3  4  1  4                   15952.29000   15952.28608    0.00392    0.02000   0.00244
   8:   5  2  4  6  1  5                   16254.94000   16254.97383   -0.03383    0.02000   0.00496
   9:  10  3  8 11  2  9                   16331.36000   16331.35221    0.00779    0.02000   0.00733
  10:  16  4 12 17  3 15                   16344.18000   16344.14686    0.03314    0.02000   0.00602
  11:  15  2 14 14  3 11                   16509.22000   16509.22490   -0.00490    0.02000   0.00611
  12:   8  2  6  9  1  9                   19252.11000   19252.11107   -0.00107    0.02000   0.00735
  13:  17  3 14 17  3 15                   19465.27000   19465.27448   -0.00448    0.02000   0.00553
  14:   1  0  1  0  0  0                   19527.42000   19527.41726    0.00274    0.02000   0.00089
  15:  19  3 17 18  4 14                   19653.40000   19653.40195   -0.00195    0.02000   0.00804
  16:  15  4 12 16  3 13                   20609.74000   20609.69519    0.04481    0.02000   0.00726
  17:  15  2 13 16  1 16                   23064.74000   23064.73645    0.00355    0.02000   0.01092
  18:  23  4 19 22  5 18                   23389.29000   23389.32031   -0.03031    0.02000   0.01457
  19:   5  1  4  5  1  5                   23917.42500   23917.40931    0.01569    0.02000   0.00351
  20:  20  5 16 21  4 17                   23920.54000   23920.60133   -0.06133    0.02000   0.01109
  21:  11  2  9 11  2 10                   24602.24000   24602.24287   -0.00287    0.02000   0.00487
  22:  11  3  8 12  2 11                   25593.31000   25593.30776    0.00224    0.02000   0.00594
  23:  18  3 15 18  3 16                   26337.33000   26337.32206    0.00794    0.02000   0.00741
  24:  16  2 15 15  3 12                   27536.51500   27536.52573   -0.01073    0.02000   0.00690
  25:   7  2  5  8  1  8                   28043.31000   28043.32758   -0.01758    0.02000   0.00645
  26:  18  3 15 17  4 14                   29695.75000   29695.75692   -0.00692    0.02000   0.00804
  27:  20  5 15 21  4 18                   31107.22000   31107.24031   -0.02031    0.02000   0.01143
  28:   4  0  4  3  1  3                   32449.23000   32449.20607    0.02393    0.02000   0.00289
  29:  12  2 10 12  2 11                   33276.24000   33276.25126   -0.01126    0.02000   0.00577
  30:  16  2 14 17  1 17                   33414.96000   33414.96516   -0.00516    0.02000   0.01520
  31:   6  1  5  6  1  6                   33457.09000   33457.09005   -0.00005    0.02000   0.00467
  32:   8  1  7  7  2  6                   33841.19000   33841.15579    0.03421    0.02000   0.00617
  33:  19  3 16 19  3 17                   34797.32000   34797.30171    0.01829    0.02000   0.01011
  34:  15  4 11 16  3 14                   35155.25000   35155.21151    0.03849    0.02000   0.00690
  35:  13  2 11 12  3 10                   36108.97000   36108.99804   -0.02804    0.02000   0.00802
  36:  20  3 18 19  4 15                   36530.02000   36529.99525    0.02475    0.02000   0.01138
  37:  17  2 16 16  3 13                   36667.97000   36667.97181   -0.00181    0.02000   0.00864
  38:   2  1  2  1  1  1                   37459.19000   37459.18422    0.00578    0.02000   0.00159
  39:   6  2  4  7  1  7                   38713.67000   38713.68679   -0.01679    0.02000   0.00557
  40:   2  0  2  1  0  1                   39016.31000   39016.38561   -0.07561    0.07000   0.00172
  41:   2  1  1  1  1  0                   40650.65000   40650.60396    0.04604    0.07000   0.00169
  42:   7  1  6  7  1  7                   44551.00000   44551.00076   -0.00076    0.07000   0.00584
  43:   1  1  0  1  0  1                   50694.22000   50694.13863    0.08137    0.07000   0.00165
  44:   2  1  1  2  0  2                   52328.36000   52328.35698    0.00302    0.07000   0.00165
  45:   5  0  5  4  1  4                   54481.75000   54481.71576    0.03424    0.07000   0.00350
  46:   3  1  2  3  0  3                   54850.91000   54850.88687    0.02313    0.07000   0.00174
  47:   3  1  3  2  1  2                   56164.74000   56164.78724   -0.04724    0.07000   0.00226
  48:   8  1  7  8  1  8                   57167.17000   57167.11238    0.05762    0.07000   0.00696
  49:   4  1  3  4  0  4                   58345.45000   58345.48673   -0.03673    0.07000   0.00201
  50:   3  0  3  2  0  2                   58428.60000   58428.61353   -0.01353    0.07000   0.00244
  51:   3  2  2  2  2  1                   58583.00000   58582.98018    0.01982    0.07000   0.00196
  52:   3  2  1  2  2  0                   58735.84000   58735.87646   -0.03646    0.07000   0.00197
  53:   3  1  2  2  1  1                   60951.08000   60951.14341   -0.06341    0.07000   0.00240
  54:   5  1  4  5  0  5                   62919.79000   62919.72724    0.06276    0.07000   0.00254
  55:   1  1  1  0  0  0                   68625.75000   68625.80604   -0.05604    0.07000   0.00224
  56:   6  1  5  6  0  6                   68699.14000   68699.07111    0.06889    0.07000   0.00330
  57:   7  1  6  7  0  7                   75817.04000   75817.10897   -0.06897    0.07000   0.00427
  58:   6  0  6  5  1  5                   76840.85000   76840.76389    0.08611    0.07000   0.00396
  59:   9  1  8  9  0  9                   94557.79000   94557.85601   -0.06601    0.07000   0.00661
  60:   7  0  7  6  1  6                   99366.69000   99366.80250   -0.11250    0.07000   0.00422
  61:   3  1  3  2  0  2                  103706.07000  103705.97463    0.09537    0.07000   0.00332
```

```
   62:  10  1  9 10  0 10                106350.75000  106350.72488    0.02512    0.07000   0.00789
   63:   4  2  2  4  1  3                142348.06000  142348.05833    0.00167    0.02000   0.00374
   64:   3  2  1  3  1  2                145107.92000  145107.94584   -0.02584    0.02000   0.00408
   65:   2  2  0  2  1  1                147323.23000  147323.21280    0.01720    0.02000   0.00446
   66:   8  1  8  7  1  7                149130.33000  149130.35013   -0.02013    0.02000   0.00386
   67:   6  1  6  5  0  5                151085.05000  151085.06287   -0.01287    0.02000   0.00420
   68:   2  2  1  2  1  2                152072.13000  152072.11897    0.01103    0.02000   0.00456
   69:   8  0  8  7  0  7                153161.84000  153161.90413   -0.06413    0.02000   0.00384
   70:   3  2  2  3  1  3                154490.28000  154490.31191   -0.03191    0.02000   0.00425
   71:   4  2  3  4  1  4                157727.94000  157727.94493   -0.00493    0.02000   0.00401
   72:   5  2  4  5  1  5                161794.81000  161794.80884    0.00116    0.02000   0.00402
   73:   7  1  7  6  0  6                165874.89000  165874.89177   -0.00177    0.02000   0.00448
   74:   9  0  9  8  0  8                171507.44000  171507.35145    0.08855    0.02000   0.00449
   75:   8  1  8  7  0  7                180396.52000  180396.45834    0.06166    0.02000   0.00505
   76:  10  1 10  9  1  9                185958.06000  185958.03122    0.02878    0.02000   0.00613
   77:   2  2  1  1  1  0                187935.56000  187935.55334    0.00666    0.02000   0.00555
   78:  10  0 10  9  0  9                189665.50000  189665.41345    0.08655    0.02000   0.00595
   79:   9  1  9  8  0  8                194806.97000  194806.97501   -0.00501    0.02000   0.00614
   80:  10  1  9  9  1  8                201458.34000  201458.28232    0.05768    0.02000   0.00699
   81:   3  2  2  2  1  1                205867.92000  205867.92956   -0.00956    0.02000   0.00557
   82:  10  1 10  9  0  9                209257.55000  209257.65479   -0.10479    0.02000   0.00792
   83:   4  2  3  3  1  2                222996.83000  222996.82589    0.00411    0.04000   0.00542
   84:   4  2  2  3  1  3                233142.75000  233142.75113   -0.00113    0.04000   0.00571
   85:   5  2  4  4  1  3                239326.55000  239326.55644   -0.00644    0.04000   0.00526
   86:   7  3  4  7  2  5                246130.31000  246130.32442   -0.01442    0.04000   0.00601
   87:   7  3  4  7  2  5                246130.36000  246130.32442    0.03558    0.04000   0.00601
   88:   6  3  3  6  2  4                247546.31000  247546.40119   -0.09119    0.04000   0.00566
   89:   5  3  2  5  2  3                248458.84000  248458.82544    0.01456    0.04000   0.00631
   90:   5  3  2  5  2  3                248458.90000  248458.82544    0.07456    0.04000   0.00631
   91:   4  3  1  4  2  2                248991.83000  248991.64313    0.18687    0.04000   0.00737
   92:   4  3  2  4  2  3                249559.94000  249560.02951   -0.08951    0.04000   0.00737
   93:   5  3  3  5  2  4                249773.68000  249773.58793    0.09207    0.04000   0.00631
   94:   6  3  4  6  2  5                250143.89000  250143.81749    0.07251    0.04000   0.00564
   95:   7  3  5  7  2  6                250727.75000  250727.77999   -0.02999    0.04000   0.00598
   96:   6  2  5  5  1  4                254866.44000  254866.45778   -0.01778    0.04000   0.00541
   97:   5  2  3  4  1  4                256609.64000  256609.64493   -0.00493    0.04000   0.00577
   98:   7  2  6  6  1  5                269632.08000  269632.12739   -0.04739    0.04000   0.00629
   99:   6  2  4  5  1  5                281429.34000  281429.34246   -0.00246    0.04000   0.00624
  100:   8  2  7  7  1  6                283646.97000  283647.00260   -0.03260    0.04000   0.00816
  101:   7  2  5  6  1  6                307806.54000  307806.58843   -0.04843    0.04000   0.00752
  102:  10  2  9  9  1  8                309569.00000  309569.02906   -0.02906    0.04000   0.01470
  103:   4  3  2  3  2  1                327448.90000  327448.90956   -0.00956    0.04000   0.00816
  104:   4  3  1  3  2  2                327644.18000  327644.08234    0.09766    0.04000   0.00816
  105:   8  2  6  7  1  7                335954.84000  335954.88200   -0.04200    0.04000   0.00987
  106:   5  3  3  4  2  2                346752.00000  346752.08605   -0.08605    0.04000   0.00711
  107:   5  3  2  4  2  3                347340.53000  347340.52544    0.00456    0.04000   0.00712
  108:   6  3  4  5  2  3                365801.97000  365802.07334   -0.10334    0.04000   0.00661
  109:   6  3  3  5  2  4                367180.91000  367180.93481   -0.02481    0.04000   0.00664
  110:   5  4  2  4  3  1                446783.08000  446783.08289   -0.00289    0.04000   0.01591
  111:   5  4  1  4  3  2                446787.13000  446787.16012   -0.03012    0.04000   0.01591
NORMALIZED DIAGONAL:
   1  1.00000E+00   2  8.78222E-01   3  1.80216E-01   4  6.06317E-01   5  6.67398E-02   6  2.69532E-01
    7   2.41071E-01    8   9.98900E-01
MARQUARDT PARAMETER = 0, TRUST EXPANSION = 1.00
                              NEW PARAMETER (EST. ERROR) -- CHANGE THIS ITERATION
   1         10000          A      59660.78243(199)         -0.00000
   2         20000          B      10561.60521( 49)          0.00000
   3         30000          C       8965.84204( 44)          0.00000
   4           200        -DJ         -7.49749(278)E-03     -0.00000E-03
   5          1100       -DJK          0.059876( 38)        -0.000000
   6          2000        -DK         -0.914853(129)         0.000000
   7         40100         d1         -1.665723(297)E-03     0.000000E-03
   8         50000         d2         -0.115784( 67)E-03    -0.000000E-03
 MICROWAVE AVG =       -0.001766 MHz, IR AVG =        0.00000
 MICROWAVE RMS =        0.048279 MHz, IR RMS =        0.00000
 END OF ITERATION  2 OLD, NEW RMS ERROR=        1.44219         1.44219
 1 2 0.686811 1 3 0.681554 1 4 -0.676433 1 5 -0.577696 1 6 -0.194085 1 7 -0.426727 1 8 -0.136143 2 1 0.686811
 2 3 0.845845 2 4 -0.795106 2 5 -0.689521 2 6 0.131210 2 7 -0.660887 2 8 -0.080477 3 1 0.681554 3 2 0.845845
```

```
 3  4 -0.820751  3  5 -0.690980  3  6  0.114752  3  7 -0.226774  3  8 -0.245424  4  1 -0.676433  4  2 -0.795106  4  3 -0.820751
 4  5  0.948653  4  6 -0.282915  4  7  0.531246  4  8  0.260616  5  1 -0.577696  5  2 -0.689521  5  3 -0.690980  5  4  0.948653
 5  6 -0.531219  5  7  0.525023  5  8  0.279087  6  1 -0.194085  6  2  0.131210  6  3  0.114752  6  4 -0.282915  6  5 -0.531219
 6  7 -0.110076  6  8 -0.192448  7  1 -0.426727  7  2 -0.660887  7  3 -0.226774  7  4  0.531246  7  5  0.525023  7  6 -0.110076
 7  8 -0.216156  8  1 -0.136143  8  2 -0.080477  8  3 -0.245424  8  4  0.260616  8  5  0.279087  8  6 -0.192448  8  7 -0.216156
syn-vinyl alcohol                                    Mon Feb  2 23:50:58 2015
```

References

[1] Herbst, E.; van Dishoeck, E. *Ann. Rev. Astron. & Astrophys.* **2009**, *47*, 427.

[2] Garrod, R. T.; Weaver, S. L. W.; Herbst, E. *Astrophysical Journal* **2008**, *682*, 283–302.

[3] Charnley, S. Interstellar Organic Chemistry. 2001.

[4] Wrobel, R.; Sander, W.; Kraka, E.; Cremer, D. *Journal of Physical Chemistry A* **1999**, *103*, 3693–3705.

[5] Huang, C.-K.; Xu, Z.-F.; Nakajima, M.; Nguyen, H. M. T.; Lin, M. C.; Tsuchiya, S.; Lee, Y.-P. *The Journal of Chemical Physics* **2012**, *137*, 164307–14.

[6] Lugez, C.; Schriver, A.; Levant, R.; Schriver-Mazzuoli, L. *Chemical Physics* **1994**, *181*, 129 – 146.

[7] Lin, J.; Harich, S.; Lee, Y.; Yang, X. *Journal of Chemical Physics* **1999**, *110*, 10821–10830.

[8] Basco, N.; Norrish, R. G. W. *Proceedings of the Royal Society of London. Series A. Mathematical and Physical Sciences* **1961**, *260*, 293.

[9] Greenberg, R. I.; Heicklen, J. *International Journal of Chemical Kinetics* **1972**, *4*, 417–432.

[10] Lin, C.; DeMore, W. *Journal of Physical Chemistry* **1973**, *77*, 863–869.

[11] Tsang, W. *International Journal of Chemical Kinetics* **1976**, *8*, 193–203.

[12] Casavecchia, P.; Buss, R.; Sibner, S.; Lee, Y. *Journal of Chemical Physics* **1980**, *73*, 6351–6352.

[13] Luntz, A. *Journal of Chemical Physics* **1980**, *73*, 1143–1152.

[14] Aker, P.; O'Brien, J.; Sloan, J. *Journal of chemical Physics* **1986**, *84*, 745–749.

[15] Cheskis, S.; Iogansen, A.; Kulakov, P.; Razuvaev, I.; Sarkisov, O.; Titov, A. *Chemical Physics Letters* **1989**, *155*, 37–42.

[16] Satyapal, S.; Park, J.; Bersohn, R.; Katz, B. *Journal of Chemical Physics* **1989**, *91*, 6873–6879.

[17] Park, C.; Wiesenfeld, J. *Journal of Chemical Physics* **1991**, *95*, 8166–8177.

[18] Rudich, Y.; Hurwitz, Y.; Frost, G.; Vaida, V.; Naaman, R. *Journal of Chemical Physics* **1993**, *99*, 4500–4508.

[19] Parnis, J. M.; Hoover, L. E.; Fridgen, T. D.; Lafleur, R. D. *The Journal of Physical Chemistry* **1993**, *97*, 10708–10711.

[20] Matsumi, Y.; Tonokura, K.; Inagaki, Y.; Kawasaki, M. *Journal of Physical Chemistry* **1993**, *97*, 6816–6821.

[21] Hurwitz, Y.; Rudich, Y.; Naaman, R. *Chemical Physics Letters* **1993**, *215*, 674–680.

[22] Brouard, M.; Duxon, S.; Enriquez, P.; Simons, J. *Journal of the Chemical Society – Faraday Transactions* **1993**, *89*, 1435–1442, NATO Advanced Research Workshop on Orientation and Polarisation Effects in Chemical Reaction Dynamics, Assisi, Italy, Nov. 20-25, 1992.

[23] Schlutter, J.; Schott, R.; Kleinermanns, K. *Chemical Physics Letters* **1993**, *213*, 262–268.

[24] Suzuki, T.; Hirota, E. *Journal of Chemical Physics* **1993**, *98*, 2387–2398.

[25] Brouard, M.; Duxon, S.; Simons, J. *Israel Journal of Chemistry* **1994**, *34*, 67–75.

[26] Vanzee, R.; Stephenson, J.; Casassa, M. *Chemical Physics Letters* **1994**, *223*, 167–172.

[27] Schott, R.; Schlutter, J.; Olzmann, M.; Kleinermanns, K. *Journal of Chemical Physics* **1995**, *102*, 8371–8377.

[28] Hack, W.; Thiesemann, H. *Journal of Physical Chemistry* **1995**, *99*, 17364–17371.

[29] Vanzee, R.; Stephenson, J. *Journal of Chemical Physics* **1995**, *102*, 6946–6948.

[30] Wada, S.-i.; Obi, K. *The Journal of Physical Chemistry A* **1998**, *102*, 3481–3491.

[31] Gonzalez, M.; Puyuelo, M.; Hernando, J.; Sayos, R.; Enriquez, P.; Guallar, J.; Banos, I. *Journal of Physical Chemistry A* **2000**, *104*, 521–529.

[32] Lin, J.; Shu, J.; Lee, Y.; Yang, X. *Journal of Chemical Physics* **2000**, *113*, 5287–5301.

[33] Ausfelder, F.; Hippler, H.; Striebel, F. *Zeitschrift fur Physikalische Chemie-International Journal of Research in Physical Chemistry and Chemical Physics* **2000**, *214*, 403–417.

[34] Miller, C.; van Zee, R.; Stephenson, J. *Journal of Chemical Physics* **2001**, *114*, 1214–1232.

[35] Chen, H.; Thweatt, W.; Wang, J.; Glass, G.; Curl, R. *Journal of Physical Chemistry A* **2005**, *109*, 2207–2216.

[36] Hancock, G.; Morrison, M.; Saunders, M. *Journal of Photochemistry and Photobiology A – Chemistry* **2005**, *176*, 191–198.

[37] Atkinson, R.; Baulch, D. L.; Cox, R. A.; Crowley, J. N.; Hampson, R. F.; Hynes, R. G.; Jenkin, M. E.; Rossi, M. J.; Troe, J. *Atmospheric Chemistry and Physics* **2006**, *6*, 3625–4055.

[38] Yang, X. *Physical Chemistry Chemical Physics* **2006**, *8*, 205–215.

[39] Vranckx, S.; Peeters, J.; Carl, S. *Physical Chemistry Chemical Physics* **2008**, *10*, 5714–5722.

[40] Shuai, Q.; Pan, H.; Yang, J.; Zhang, D.; Jiang, B.; Dai, D.; Yang, X. *Journal of Chemical Physics* **2012**, *137*.

[41] Shuai, Q.; Pan, H.; Yang, J.; Zhang, D.; Jiang, B.; Dai, D.; Yang, X. *Journal of Physical Chemistry Letters* **2012**, *3*, 1310–1314.

[42] Arai, H.; Kato, S.; Koda, S. *Journal of Physical Chemistry* **1994**, *98*, 12–16.

[43] Brownsword, R.; Hillenkamp, M.; Schmiechen, P.; Volpp, H.; Upadhyaya, H. *Journal of Physical Chemistry A* **1998**, *102*, 4438–4443.

[44] Gonzalez, M.; Hernando, J.; Banos, I.; Sayos, R. *Journal of Chemical Physics* **1999**, *111*, 8913–8924.

[45] Gonzalez, M.; Hernando, J.; Puyuelo, M.; Sayos, R. *Journal of Chemical Physics* **2000**, *113*, 6748–6759.

[46] Chang, A.; Lin, S. *Chemical Physics Letters* **2002**, *363*, 175–181.

[47] Chang, A.; Lin, S. *Chemical Physics Letters* **2004**, *384*, 229–235.

[48] Yu, H.; Muckerman, J. *Journal of Physical Chemistry A* **2004**, *108*, 8615–8623.

[49] Liu, X.; Lin, J. J.; Harich, S.; Schatz, G. C.; Yang, X. *Science* **2000**, *289*, 1536–1538.

[50] Córdova, J. F.; Rettner, C. T.; Kinsey, J. L. *The Journal of Chemical Physics* **1981**, *75*, 2742–2748.

[51] Walker, F. *Formaldeyde*; Reinhold: New York, 1964.

[52] Kent, D. R.; Widicus, S. L.; Blake, G. A.; Goddard, W. A. *The Journal of Chemical Physics* **2003**, *119*, 5117–5120.

[53] Laas, J. C.; Garrod, R. T.; Herbst, E.; Widicus Weaver, S. L. *Astrophysical Journal* **2011**, *728*, 71.

[54] Nielsen, A. T.; Moore, D. W.; Ogan, M. D.; Atkins, R. L. *The Journal of Organic Chemistry* **1979**, *44*, 1678–1684.

[55] Feldmann, M. T.; Widicus, S. L.; Blake, G. A.; Kent, D. R.; Goddard, W. A. *The Journal of Chemical Physics* **2005**, *123*, 034304–.

[56] Bossa, J. B.; Theule, P.; Duvernay, F.; Chiavassa, T. *The Astrophysical Journal* **2009**, *707*, 1524.

[57] Puzzarini, C.; Stanton, J. F.; Gauss, J. *International Reviews in Physical Chemistry* **2010**, *29*, 273–367.

[58] Hays, B. M.; Widicus Weaver, S. L. *The Journal of Physical Chemistry A* **2013**, *117*, 7142–7148.

[59] Frisch, M. J. et al. Gaussian 09. 2009.

[60] CFOUR, Coupled-Cluster techniques for Computational Chemistry, a quantum-chemical program package by. J.F. Stanton, J. Gauss, M.E. Harding, P.G. Szalay with contributions from A.A. Auer, R.J. Bartlett, U. Benedikt, C. Berger, D.E. Bernholdt, Y.J. Bomble, L. Cheng, O. Christiansen, M. Heckert, O. Heun, C. Huber, T.-C. Jagau, D. Jonsson, J. Jusélius, K. Klein, W.J. Lauderdale, D.A. Matthews, T. Metzroth, L.A. Mück, D.P. O'Neill, D.R. Price, E. Prochnow, C. Puzzarini, K. Ruud, F. Schiffmann, W. Schwalbach, C. Simmons, S. Stopkowicz, A. Tajti, J. Vázquez, F. Wang, J.D. Watts and the integral packages MOLECULE (J. Almlöf and P.R. Taylor), PROPS (P.R. Taylor), ABACUS (T. Helgaker, H.J. Aa. Jensen, P. Jørgensen, and J. Olsen), and ECP routines by A. V. Mitin and C. van Wüllen. For the current version, see http://www.cfour.de.

[61] Hetzer, G.; Pulay, P.; Werner, H.-J. *Chemical Physics Letters* **1998**, *290*, 143 – 149.

[62] Schütz, M.; Hetzer, G.; Werner, H.-J. *The Journal of Chemical Physics* **1999**, *111*, 5691–5705.

[63] Dunning, T. H. *The Journal of Chemical Physics* **1989**, *90*, 1007–1023.

[64] Gross, R. L.; Liu, X.; Suits, A. G. *Chemical Physics Letters* **2003**, *376*, 710 – 716.

[65] Hampel, C.; Werner, H. *The Journal of Chemical Physics* **1996**, *104*, 6286–6297.

[66] Hampel, C.; Peterson, K. A.; Werner, H.-J. *Chemical Physics Letters* **1992**, *190*, 1 – 12.

[67] Pickett, H. M.; Poynter, R. L.; Cohen, E. A.; Delitsky, M. L.; Pearson, J. C.; Müller, H. S. P. *Journal of Quantitative Spectroscopy and Radiative Transfer* **1998**, *60*, 883–890.

[68] `http://slater.chemie.uni-mainz.de/xaces2/aces2man/node29.html`.

[69] Schalley, C. A.; Harvey, J. N.; Schröder, D.; Schwarz, H. *The Journal of Physical Chemistry A* **1998**, *102*, 1021–1035.

[70] Scuseria, G. E.; Lee, T. J. *The Journal of Chemical Physics* **1990**, *93*, 5851–5855.

[71] Fong, M. Y.; Johnson, L. J.; Harmony, M. D. *Journal of Molecular Spectroscopy* **1974**, *53*, 45 – 56.

[72] Haas, B.; Oberhammer, H. *Journal of the American Chemical Society* **1984**, *106*, 6146–6149.

[73] M. Tyblewski, R. M. A. B., T. K. Ha; Blom, C. E. *The Journal of Chemical Physics* **1992**, *97*, 6168–6180.

[74] Tonmunphean, S.; Parasuk, V.; Karpfen, A. *The Journal of Physical Chemistry A* **2002**, *106*, 438–446.

[75] Sung, E.-M.; Harmony, M. D. *Journal of Molecular Spectroscopy* **1979**, *74*, 228 – 241.

[76] Pollack, I. B.; Konen, I. M.; Li, E. X. J.; Lester, M. I. *The Journal of Chemical Physics* **2003**, *119*, 9981–9984.

[77] Konen, I. M.; Pollack, I. B.; Li, E. X. J.; Lester, M. I.; Varner, M. E.; Stanton, J. F. *The Journal of Chemical Physics* **2005**, *122*, 094320.

[78] Hays, B. M.; Wehres, N.; DePrince, B. A.; Roy, A. M.; Widicus Weaver, S. L. *Chem. Phys. Letters* **2015**, *in revision.*

[79] Kolbe, W. F.; Leskovar, B. *Rev. Sci. Instrum.* **1985**, *56*, 1577–1581.

[80] Duffy, L. M. *Rev. Sci. Instrum.* **2005**, *76*, 093104.

[81] Schmuttenmaer, C. A.; Cohen, R. C.; Heath, N. P. J. R.; Cooksy, A. L.; Busarow, K. L.; Saykally, R. J. *Science* **1990**, *249*, 897–900.

[82] Abeysekera, C.; Zack, L. N.; Park, G. B.; Joalland, B.; Oldham, J. M.; Prozument, K.; Ariyasingha, N. M.; Sims, I. R.; Field, R. W.; Suits, A. G. *The Journal of Chemical Physics* **2014**, *141*, 214203–.

[83] Prozument, K.; Shaver, R. G.; Ciuba, M. A.; Muenter, J. S.; Park, G. B.; Stanton, J. F.; Guo, H.; Wong, B. M.; Perry, D. S.; Field, R. W. *Faraday Discuss.* **2013**, *163*, 33–57.

[84] Beames, J. M.; Liu, F.; Lu, L.; Lester, M. I. *Journal of the American Chemical Society* **2012**, *134*, 20045.

[85] Takahashi, K.; Hayashi, S.; Matsumi, Y.; Taniguchi, N.; Hayashida, S. *Journal of Geophysical Research: Atmospheres* **2002**, *107*, ACH 11–1–ACH 11–8.

[86] Laas, J. C.; Hays, B. M.; Widicus Weaver, S. L. *The Journal of Physical Chemistry A* **2013**, *117*, 9548–9554.

[87] Müller, H. S. P.; Schlöder, F.; Stutzki, J.; Winnewisser, G. *Journal of Molecular Structure* **2005**, *742*, 215–227.

[88] Honma, K. *The Journal of Chemical Physics* **1993**, *99*, 7677–7686.

[89] Gonzalez, M.; Puyuelo, M. P.; Hernando, J.; Martinez, R.; Sayos, R.; Enriquez, P. A. *Chemical Physics Letters* **2001**, *346*, 69 – 80.

[90] Lee, S.-H.; Chen, W.-K.; Huang, W.-J. *The Journal of Chemical Physics* **2009**, *130*, 054301–.

[91] Nguyen, T. L.; Vereecken, L.; Hou, X. J.; Nguyen, M. T.; Peeters, J. *The Journal of Physical Chemistry A* **2005**, *109*, 7489–7499, PMID: 16834118.

[92] Clubb, A. E.; Jordan, M. J. T.; Kable, S. H.; Osborn, D. L. *The Journal of Physical Chemistry Letters* **2012**, *3*, 3522–3526.

[93] Andrews, D. U.; Heazlewood, B. R.; Maccarone, A. T.; Conroy, T.; Payne, R. J.; Jordan, M. J. T.; Kable, S. H. *Science* **2012**, *337*, 1203–1206.

[94] Rodler, M.; Bauder, A. *Journal of the American Chemical Society* **1984**, *106*, 4025–4028.

[95] Rodler, M. *Journal of Molecular Spectroscopy* **1985**, *114*, 23 – 30.

[96] Saito, S. *Chemical Physics Letters* **1976**, *42*, 399 – 402.

[97] Turner, B. E.; Apponi, A. J. *The Astrophysical Journal Letters* **2001**, *561*, L207.

[98] Belloche, A.,; Müller, H. S. P.,; Menten, K. M.,; Schilke, P.,; Comito, C., *Astron. & Astrophys.* **2013**, *559*, A47.

[99] Neill, J. L. et al. *The Astrophysical Journal* **2014**, *789*, 8.

[100] Rodler, M. Ph.D. thesis, ETH Zurich, 1983.

[101] Pickett, H. M. *Journal of Molecular Spectroscopy* **1991**, *148*, 371 – 377.

[102] Brown, G. G.; Dian, B. C.; Douglass, K. O.; Geyer, S. M.; Shipman, S. T.; Pate, B. H. *Review of Scientific Instruments* **2008**, *79*, 053103–.

[103] Zaleski, D. P.; Neill, J. L.; Muckle, M. T.; Seifert, N. A.; Carroll, P. B.; Weaver, S. L. W.; Pate, B. H. *Journal of Molecular Spectroscopy* **2012**, *280*, 68 – 76.

[104] Park, G. B.; Steeves, A. H.; Kuyanov-Prozument, K.; Neill, J. L.; Field, R. W. *The Journal of Chemical Physics* **2011**, *135*, –.

[105] Steber, A. L.; Harris, B. J.; Neill, J. L.; Pate, B. H. *Journal of Molecular Spectroscopy* **2012**, *280*, 3 – 10.

[106] Gerecht, E.; Douglass, K. O.; Plusquellic, D. F. *Opt. Express* **2011**, *19*, 8973–8984.

[107] Neill, J. L.; Harris, B. J.; Steber, A. L.; Douglass, K. O.; Plusquellic, D. F.; Pate, B. H. *Opt. Express* **2013**, *21*, 19743–19749.

[108] Petkie, D. T.; Goyette, T. M.; Bettens, R. P. A.; Belov, S. P.; Albert, S.; Helminger, P.; De Lucia, F. C. *Review of Scientific Instruments* **1997**, *68*, 1675–1683.

[109] Medvedev, I.; Winnewisser, M.; Lucia, F. C. D.; Herbst, E.; Białkowska-Jaworska, E.; Pszczółkowski, L.; Kisiel, Z. *Journal of Molecular Spectroscopy* **2004**, *228*, 314 – 328.

[110] Fortman, S. M.; Medvedev, I. R.; Neese, C. F.; Lucia, F. C. D. *The Astrophysical Journal* **2010**, *714*, 476.

[111] Medvedev, I. R.; Neese, C. F.; Plummer, G. M.; Lucia, F. C. D. *Opt. Lett.* **2010**, *35*, 1533–1535.

[112] McCarthy, M. C.; Cheng, L.; Crabtree, K. N.; Martinez, O.; Nguyen, T. L.; Womack, C. C.; Stanton, J. F. *The Journal of Physical Chemistry Letters* **2013**, *4*, 4133–4139.

[113] Endo, Y.; Nakajima, M. *Journal of Molecular Spectroscopy* **2014**, *301*, 15 – 19.

[114] Finneran, I. A.; Holland, D. B.; Carroll, P. B.; Blake, G. A. *Review of Scientific Instruments* **2013**, *84*, 083104–.

[115] Rissanen, M. P.; Eskola, A. J.; Nguyen, T. L.; Barker, J. R.; Liu, J.; Liu, J.; Halme, E.; Timonen, R. S. *The Journal of Physical Chemistry A* **2014**, *118*, 2176–2186, PMID: 24592923.

[116] Levine, I. N. *Journal of Molecular Spectroscopy* **1962**, *8*, 276 – 284.

[117] Coffey, D.; Britt, C. O.; Boggs, J. E. *The Journal of Chemical Physics* **1968**, *49*, 591–600.

[118] Turner, P. H.; Cox, A. P. *J. Chem. Soc., Faraday Trans. 2* **1978**, *74*, 533–559.

[119] Valehi, S.; Vahedpour, M. *Journal of Chemical Sciences* **2014**, *126*, 1173–1180.

[120] Gauss, J.; Stanton, J. F. *Chemical Physics Letters* **1997**, *276*, 70 – 77.